

POLITECNICO DI TORINO

Collegio di Ingegneria Chimica e dei Materiali

**Corso di Laurea Magistrale
in Ingegneria Chimica e dei Processi Sostenibili**

Tesi di Laurea Magistrale

Elaboration of aqueous dispersions of conjugated polymer nanoparticles for organic photovoltaic cells



Relatori

prof. Fissore Davide
prof.ssa Hèbraud Anne

Candidato

Chimienti Claudia

Marzo 2021

*Alla mia famiglia, ai miei amici, a Jordi,
ai compagni di Torino, ai colleghi di Strasburgo.*

Grazie.

Index of content

Riassunto	I
Abstract	1
1. Introduction	3
1.1. Organic photovoltaic cells	3
1.2. Photoactive materials.....	4
1.2.1. PTQ10	4
1.2.2. ITIC-4F.....	5
1.3. Synthesis of nanoparticles	6
1.4. Aim of the work.....	8
2. Materials and methods.....	10
2.1. Synthesis.....	10
<i>Synthesis of 5,8-dibromo-6,7-difluoro-2-(2-hexyldecyloxy) quinoxaline</i>	10
<i>Synthesis of 2,5-Bis(trimethylstannyl)thiophene</i>	11
<i>Polymerization of Poly[(thiophene)-alt-(6,7-difluoro-2-(2-hexyldecyloxy)quinoxaline] (PTQ10)</i>	11
2.2. NMR	13
2.3. SEC.....	13
2.4. DLS.....	13
2.5. UV visible spectrophotometry	14
2.6. Ultrasonication.....	14
2.7. SEM	14
2.8. Dialysis	14
2.9. Tensiometry	15
2.10. Fluorescence	15
2.11. Procedure for nanoprecipitation of PTQ10 and ITIC-4F in water.....	16
2.12. Spin-coating	17
2.13. Profilometry	17
2.14. Efficiency measurement.....	17
3. Experimental part	19
3.1. Synthesis results	19
3.2. PTQ10 characterization	20

3.3.	Solubility of PTQ10 and ITIC-4F	22
3.4.	Nanoparticles elaboration	24
3.4.1.	<i>Influence of the solubilization temperature of PTQ10 in THF</i>	24
3.4.2.	<i>Influence of ratio between organic solvent and aqueous solution (Vorg:Vaq)..</i> 25	
3.4.3.	<i>Influence of surfactant</i>	27
3.4.4.	<i>Influence of sonication</i>	29
3.4.5.	<i>Influence of temperature of nanoprecipitation</i>	31
3.4.6.	<i>Influence of the evaporation procedure</i>	32
3.4.7.	<i>Influence of ultrasonication time</i>	34
3.4.8.	<i>Variation of nanoprecipitation temperature</i>	35
3.5.	Composite nanoparticles.....	36
3.5.1.	<i>Stability of suspension</i>	39
3.5.2.	<i>Stability of surfactant free suspension</i>	40
3.5.3.	<i>Increase in concentration</i>	40
3.6.	Microscope images	41
3.7.	Fluorescence	45
3.8.	Surfactant removal.....	48
3.9.	Active layer thickness measurement	51
3.10.	OPV devices efficiency measurement	53
4.	Conclusions	56
5.	List of abbreviations and symbols	57
6.	Bibliography.....	59

Riassunto

L'obiettivo di questo lavoro di Tesi è la preparazione e lo studio di nanoparticelle di materiale polimerico foto-attivo per l'impiego in celle fotovoltaiche organiche. La produzione di nanoparticelle mediante nanoprecipitazione in mezzo acquoso è una tecnica innovativa, attualmente sperimentata solo su scala di laboratorio, con interessanti possibili applicazioni nella produzione su larga scala di dispositivi fotovoltaici. In particolare la coppia donatore/accettore per il materiale foto-attivo è data in questo studio da PTQ10/ITIC-4F.

Il primo capitolo è rivolto ad introdurre il tema trattato, iniziando con una breve descrizione del funzionamento delle celle fotovoltaiche organiche: il materiale foto-attivo è formato da un donatore e da un accettore; il donatore assorbe un fotone formando un eccitone (in un materiale semiconduttore, l'eccitone è dato dalla coppia elettrone e lacuna), quest'ultimo, una volta arrivato all'interfaccia con il materiale accettore, si dissocia in due cariche libere, che si muovono verso i rispettivi elettrodi della cella. In figura 0.1 si illustra tale meccanismo. È fondamentale la modulazione dei livelli energetici HOMO e LUMO dei due materiali foto-attivi (mediante modificazione di gruppi chimici delle molecole) in modo da permettere tale meccanismo di trasporto di energia ed ottenere una alta efficienza di produzione di corrente elettrica. È altresì determinante la morfologia interna del materiale: la conformazione ideale è una compenetrazione tra i domini di donatore ed accettore, in quanto la distanza entro la quale l'eccitone decade è dell'ordine di 20 nm.

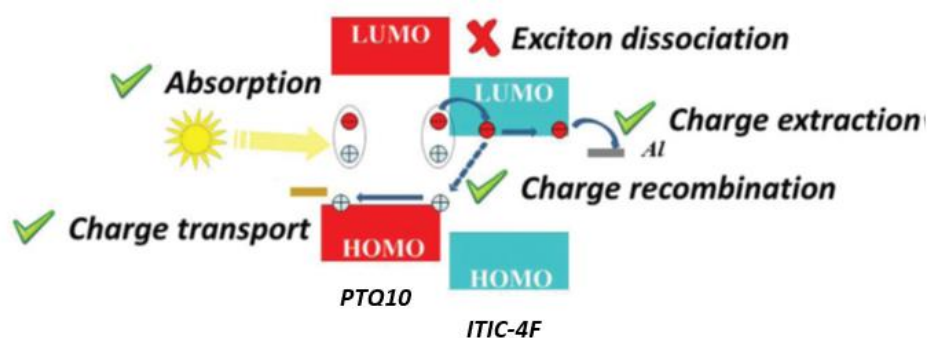


Figura 0.1: illustrazione schematica del meccanismo che porta alla conversione di energia solare a corrente elettrica nelle celle OPV.

Per questa ragione, l'impiego di un materiale nanostrutturato per formare lo strato attivo della cella fotovoltaica è una strategia fruttuosa, accompagnata alla tecnica standard di dissoluzione del materiale foto-attivo. La preparazione di nanoparticelle contenenti una coppia donatore/accettore viene effettuata secondo due tecniche principali: miniemulsione e nanoprecipitazione. Il processo di miniemulsione consiste nel solubilizzare il materiale foto-attivo in un buon solvente (affine alle molecole foto-attive) e miscelare tale soluzione con un solvente che sia immiscibile sia con il materiale foto-attivo che con il primo solvente. La miscelazione avviene in presenza di un surfattante e con ultrasonicazione. Questa tecnica viene impiegata ampiamente perché non complessa, presenta tuttavia lo svantaggio di fornire

nanoparticelle ricoperte di surfattante, che portano alla produzione di dispositivi fotovoltaici con efficienze altamente inferiori rispetto a quelli dati dagli stessi materiali foto attivi con il processo standard di dissoluzione.

La seconda tecnica è la nanoprecipitazione, essa consiste nel dissolvere la miscela di donatore/accettore all'interno di un buon solvente (generalmente un solvente organico), il quale viene messo a contatto con un solvente immiscibile con il materiale foto attivo ma miscibile con il primo solvente, in presenza o meno di surfattante. A causa della rapida diminuzione di solubilità del materiale foto attivo all'interno della miscela solvente/non-solvente, avviene la formazione di nanoparticelle, ed il solvente organico viene fatto evaporare con diverse possibili procedure. Il vantaggio di questa tecnica è la possibilità di rimuovere il surfattante presente, nonostante ciò possa portare alla riduzione della stabilità della sospensione. In figura 0.2 viene riportato uno schema della procedura.

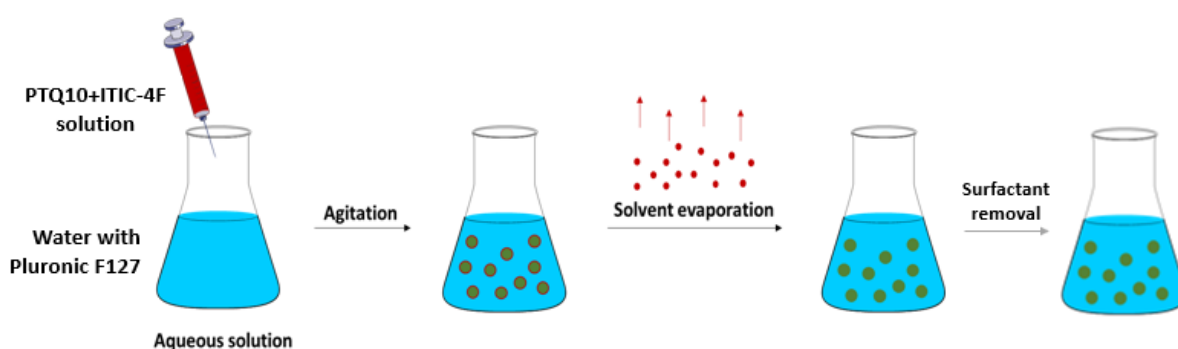


Figura 0.2: Elaborazione di nanoparticelle mediante nanoprecipitazione.

In questo lavoro è stato scelto di impiegare la tecnica della nanoprecipitazione in quanto permette la rimozione del surfattante. L'assenza di surfattante nello strato attivo aumenta la mobilità delle cariche e porta all'ottenimento di dispositivi fotovoltaici con efficienze maggiori.

Ci si concentra, all'interno di questo lavoro, su un'unica coppia donatore/accettore. Il donatore di elettroni è il polimero coniugato PTQ10, mentre l'accettore di elettroni è la molecola ITIC-4F, con struttura non-fullerenica. Le strutture chimiche dei due composti vengono mostrate in figura 0.3.

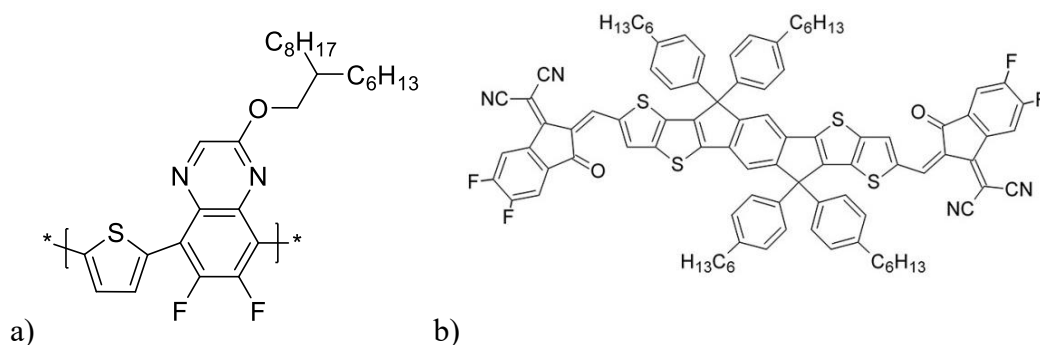


Figura 0.3: a) struttura chimica del polimero PTQ10. b) struttura chimica di ITIC-4F.

Una caratteristica fondamentale del PTQ10 è la presenza di anelli planari lungo lo scheletro della catena polimerica, che danno luogo alla cosiddetta impilazione π - π (π - π *stacking*), ovvero gli anelli si sovrappongono formando legami π e fornendo una struttura ordinata al dominio polimerico, che favorisce la percolazione delle cariche. La seconda importante caratteristica è data dalla presenza di un gruppo alcossilico che garantisce solubilità in diversi solventi organici. ITIC-4F è stato individuato come possibile accettore per PTQ10 sulla base dei suoi livelli energetici HOMO e LUMO.

La nanoprecipitazione viene effettuata in acqua mediante l'aggiunta del surfattante Pluronic F127, un composto non ionico appartenente al gruppo dei polossameri. La sua efficacia è stata riscontrata in letteratura, così come la dipendenza della sua micellizzazione dalla temperatura; ciò evidenzia la particolare importanza del controllo della temperatura al momento della nanoprecipitazione e della rimozione del surfattante stesso.

Nel secondo capitolo di questo lavoro si descrive il processo di sintesi dei due monomeri componenti il polimero PTQ10, in particolare il monomero 5,8-dibromo-6,7-difluoro-2-(2-esildecil-ossi) chinoxalina era stato previamente sintetizzato mediante la reazione illustrata in figura 0.4 mentre il 2,5-bis(trimetilstannil)tiofene è stato sintetizzato all'interno di questo lavoro con la reazione di figura 0.5.

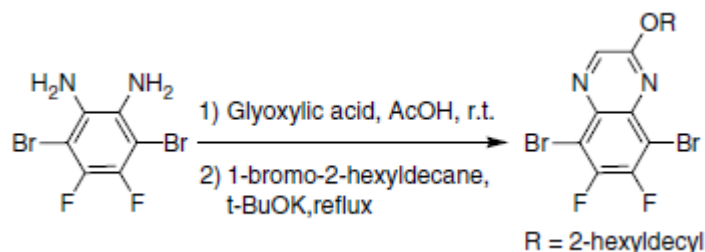


Figura 0.4: reazione di sintesi del composto 5,8-dibromo-6,7-difluoro-2-(2-esildecil-ossi) chinoxalina.¹

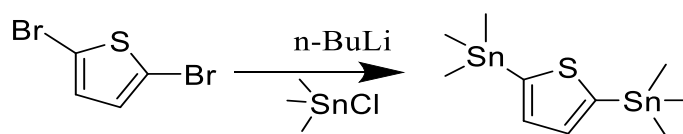


Figura 0.5: reazione di sintesi del composto 2,5-bis(trimetilstannil)tiofene.

Il polimero PTQ10 è stato successivamente polimerizzato mediante reazione di poli condensazione di Stille tra i due monomeri, in atmosfera di Argon. La reazione è rappresentata in figura 0.6. Il prodotto è stato estratto con estrattore Soxhlet e purificato in forma di film solido in un evaporatore rotante.

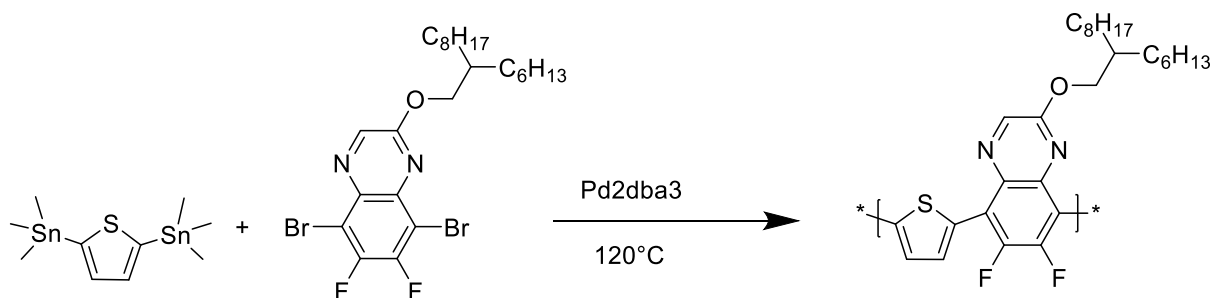


Figura 0.6: reazione di polimerizzazione di PTQ10 mediante meccanismo di poli condensazione di Stille.

Il secondo capitolo prosegue con la descrizione delle apparecchiature e tecniche analitiche.

¹H NMR:

La risonanza magnetica nucleare del protone è stata effettuata con lo spettrometro Bruker Advance 400 MHz. Gli spostamenti sono stati riferiti al solvente cloroformio-*d*, con valore $\delta = 7,26$ ppm. I campioni sono stati preparati dissolvendo una piccola quantità di sostanza da esaminare in cloroformio deuterato (CDCl₃), le analisi sono state effettuate a 298K.

SEC:

La cromatografia ad esclusione dimensionale è stata svolta in una colonna PSS con 1,2,4 triclorobenzene, a 150 °C, con portata 1 ml/min. (Sistema GPC-HT, colonna PSS).

DLS:

Per la DLS si è utilizzato il sistema ALV/CGS-3 Compact goniometer di ALV-GmbH ed il software ALV-7004 per la correlazione. Le misurazioni sono state eseguite con angolo di 90°. Indice di rifrazione: 1.33200, viscosità: 0.89000 cP, lunghezza d'onda: 632.8 nm, durata: 30 s. I campioni sono stati preparati per diluizione delle sospensioni con acqua, con concentrazione finale 0.003 mg/ml. La provetta di vetro viene immersa in toluene, allo scopo di attenuare fenomeni di rifrazione e riflessione all'interfaccia tra aria e vetro.

Spettrofotometria UV visibile:

Lo spettro di assorbimento delle soluzioni e sospensioni analizzate è stato rilevato usando lo spettrofotometro UV-visibile modello UV-2600 240V IVDD di Shimadzu Corporation. Per solventi organici sono state impiegate provette in quarzo, mentre per soluzioni acquose provette in plastica, e vetro per film solidi. Le misurazioni sono state effettuate nel range di lunghezza d'onda di 300-1000 nm.

Ultrasonificazione:

È stato utilizzato l'apparato Digital sonicator by Branson, modello 450. Per ciascun campione sono stati utilizzati i seguenti parametri: tempo di ultrasonificazione da 1 a 3 minuti, ampiezza 40%, 3 s di ultrasonificazione intervallati da 2 s di pausa. Un bagno di acqua e ghiaccio è stato usato per rimuovere il calore prodotto.

SEM:

Le dimensioni e la morfologia delle nanoparticelle sono state valutate mediante microscopio elettronico a scansione, modello Vega3 Tescan, 5 kV, distanza 5 mm. I campioni sono stati preparati diluendo la sospensione di nanoparticelle, raggiungendo una concentrazione di 0.05 mg/ml, e depositandone una goccia su alluminio. Prima dell'osservazione al microscopio, i campioni sono stati rivestiti utilizzando il dispositivo di rivestimento a polverizzazione di oro Quorum Technologies Q150RS.

Rimozione del surfattante:

Per rimuovere il surfattante Pluronic F127, ci si è serviti della centrifuga refrigerata SIGMA modello 3-16KL, a 0°C. I filtri utilizzati sono: VIVASPIN 20 (Sartorius) con filtro in PES, 30000 MW cut-off e filtro Amicon® Ultra-15 con filtro in cellulosa, 100000 MW cut-off.

Tensiometro:

La tensione superficiale delle soluzioni analizzate è stata Misurata con le tecnica dell'analisi di una goccia pendente, utilizzando il tensiometro TECLIS TRACKER™.

Fluorescenza:

Si è utilizzato lo spettrofluorometro FluoroMax-4 di Horiba Scientific, ed il software FluorEssence è stato impiegato per esaminare i dati. I campioni sono stati preparati diluendo le sospensioni in mezzo acquoso a 0.002 mg/ml. Gli esperimenti sono stati svolti con eccitazione alla lunghezza d'onda di 500 nm (4 nm slit) ed emissione da 530 nm a 850 nm (4 nm slit). Prima dell'analisi a fluorescenza, la sospensione di nanoparticelle di PTQ10 e di ITIC-4F sono state analizzate, separatamente, mediante spettrofotometria UV-visibile (da 350 nm a 1000 nm), allo scopo di rivelare le lunghezze d'onda di picco e poter determinare i *range* per l'analisi di fluorescenza.

Il secondo capitolo si conclude con la procedura per la nanoprecipitazione di PTQ10 e ITIC-4F in soluzione acquosa:

Vengono preparate le soluzioni di *stock*: la soluzione di Pluronic F127 20 mg/ml in acqua viene preparata usando acqua MilliQ filtrata 0.2 µm. La soluzione di PTQ10 in THF 1 mg/ml viene preparata e solubilizzata per un minimo di 4 ore a 45°C. Con lo stesso procedimento si prepara la soluzione di ITIC-4F 1 mg/ml.

Nella nanoprecipitazione, viene preparata la miscela donatore/accettore in THF unendo 0.5 ml di soluzione di PTQ10 e 0.5 ml di soluzione di ITIC-4F, tale miscela viene aggiunta rapidamente sotto agitazione a 2 ml di soluzione acquosa di Pluronic F127. Il processo è svolto a temperatura ambiente o a temperature più elevate a seconda dell'esperimento.

Il campione viene poi sottoposto a ultrasonificazione, viene misurato il peso totale e viene fatto evaporare il THF mediante soffiaggio di una corrente di gas inerte (Argon). L'ago dal quale viene fatto fuoriuscire l'Argon è posizionato all'esterno della sospensione, perpendicolarmente alla sua superficie. Una seconda misura del peso permette di verificare la completa evaporazione del THF.

Nel terzo capitolo di questo studio vengono riportati gli esperimenti di nanoprecipitazione con i relativi risultati, nonché i risultati dell'analisi delle nanoparticelle mediante microscopio e fluorescenza, e della rimozione del surfattante.

Nei primi esperimenti, la preparazione di nanoparticelle contenenti PTQ10 portava alla produzione di particelle di dimensioni troppi grandi per il loro utilizzo, in alcuni casi visibili ad occhio nudo e non misurabili mediante *dynamic light scattering*. All'interno degli esperimenti di seguito riepilogati si è ottimizzata la procedura generale della nanoprecipitazione, rendendola adeguata al materiale utilizzato ed ai solventi, in particolare all'acqua impiegata come non-solvente per il materiale foto-attivo. Per prima cosa, è stata verificata la temperatura adeguata alla solubilizzazione di PTQ10 in THF, che si è rivelata essere 45°C. Si è studiata in seguito l'influenza del rapporto tra quantità di solvente organico e solvente acquoso, si è scelto di lavorare con un rapporto 1:2 in quanto ottimale per la successiva concentrazione della sospensione ed anche per la dimensione delle nanoparticelle. Si è verificata la bontà della scelta di Pluronic F127 come surfattante e della concentrazione di 20 mg/ml in acqua, come riportato nella pubblicazione di Xie et al.²

Poiché la dimensione delle nanoparticelle superava ancora i 1000 nm di diametro, si è scelto di introdurre un passaggio di ultrasonificazione (emissione di onde ad alta frequenza), confrontando in primo luogo gli effetti di sonicazione ed ultrasonificazione come riportato nella tabella 0.1. I risultati ottenuti con ultrasonificazione sono risultati convenienti.

Tabella 0.1: effetto della sonicazione ed ultrasonificazione. Parametri chiave della nanoprecipitazione dei campioni da CC045 a CC049.

Sample	T nanoprecip. (°C)	T evaporation (°C)	Average diameter (nm)	Dispersion (nm)	Notes
CC045	Tamb	66	2839	1988	no sonication
CC046			2368	8363	sonication bath during nanoprecipitation
CC047			363	108	sonication bath during nanoprecipitation and then ultrasonication
CC048			2753	9126	sonication bath after nanoprecipitation
CC049			384	215	sonication bath after nanoprecipitation and then ultrasonication

In figura 0.7 si possono confrontare le diverse distribuzioni della dimensione delle nanoparticelle, rappresentate dalle curve ottenute mediante DLS. In tale figura, i campioni CC047 e CC049 mostrano avere una distribuzione spostata verso valori di raggio inferiori, grazie all'aggiunta della fase di ultrasonificazione.

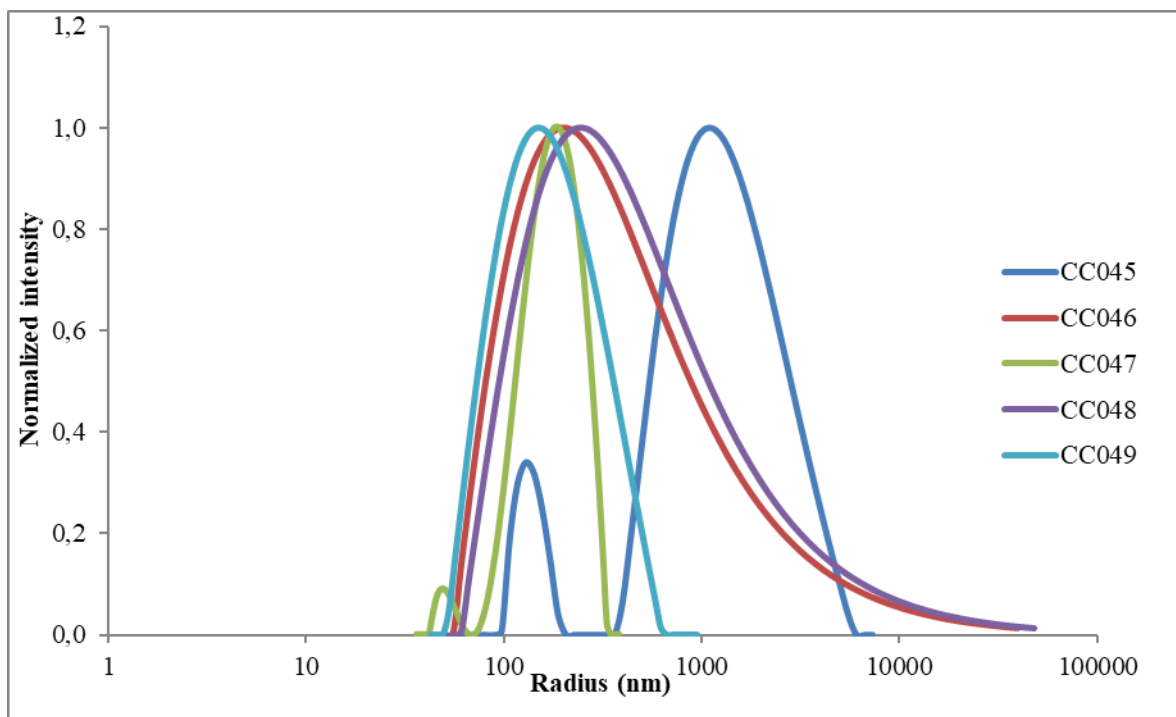


Figura 0.7: effetto della sonicazione ed ultrasonicazione. Curve di distribuzione del raggio dai risultati della DLS dei campioni da CC045 a CC049.

In seguito, si è variata la temperatura di nanoprecipitazione, per verificare se fosse più favorevole una temperatura elevata o meno. Come si evince dalla tabella 0.2, la combinazione di ultrasonicazione e bassa temperatura di nanoprecipitazione (campione CC051) porta a dimensioni inferiori delle nanoparticelle.

Tabella 0.2: effetto della temperatura di nanoprecipitazione. Parametri chiave della nanoprecipitazione dei campioni da CC045 a CC049.

Sample	T nanoprecip. (°C)	T nanoprecip. measured (°C)	Average diameter (nm)	Dispersion (nm)	Notes
CC050	Tamb	22,3	536	27	ultrasonication
CC051	Tamb	22,4	381	43	sonication bath during nanoprecipitation, ultrasonication
CC052	66°C	59	516	81	ultrasonication
CC053	66°C	59	529	21	sonication bath after nanoprecipitation, ultrasonication

Lo stesso risultato è osservabile anche in figura 0.8.

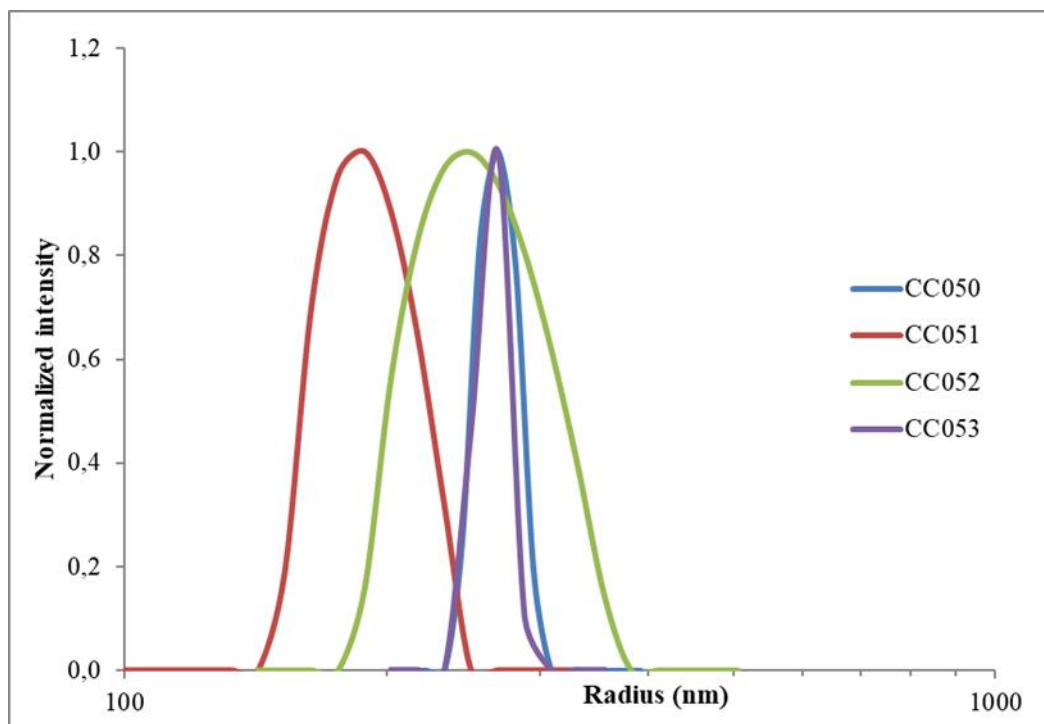


Figura 0.8: effetto della temperatura di nanoprecipitazione. Curve di distribuzione del raggio dai risultati della DLS dei campioni da CC050 a CC053.

Infine, la procedura di evaporazione è stata modificata, sperimentando l'evaporazione mediante bagno di sabbia a 66°C ed a 27°C e altresì l'evaporazione mediante soffiaggio di Argon (tabella 0.3). Quest'ultimo metodo si è rivelato più efficace, è probabile che ciò sia dovuto al fatto che l'incremento di temperatura destabilizzi il surfattante, portando a fenomeni di aggregazione.

Tabella 0.3: effetto del metodo di evaporazione. Parametri chiave della nanoprecipitazione dei campioni da CC050 a CC057.

Sample	T nanoprecip. (°C)	Evaporation	Average diameter (nm)	Dispersion (nm)	Notes
CC050	Tamb	66°C	536	27	evaporation with heat (66°C)
CC052	66°C	66°C	516	81	evaporation with heat (66°C)
CC055	Tamb	Argon	407	94	evaporation with Argon
CC056	Tamb	Argon	352	54	evaporation with Argon
CC057	Tamb	27°C	542	27	evaporation with heat (27°C)

In figura 0.9 si può osservare come il campione CC056, sottoposto a nanoprecipitazione a temperatura ambiente e ad evaporazione con Argon, presenti raggi delle particelle inferiori.

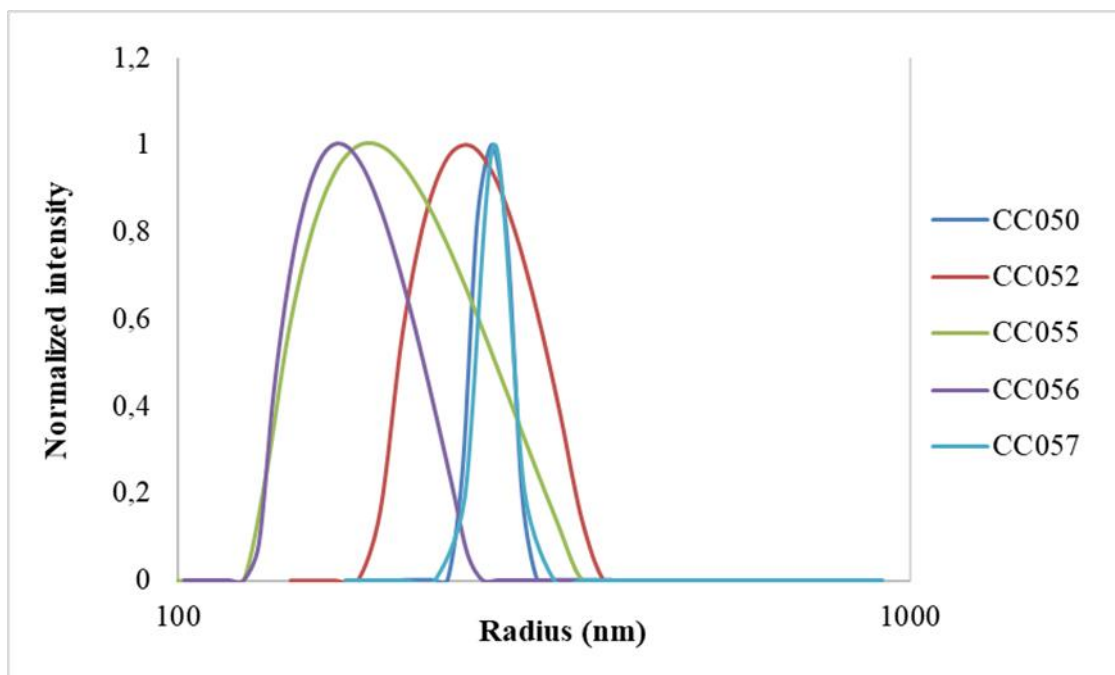


Figura 0.9: effetto del metodo di evaporazione. Curve di distribuzione del raggio dai risultati della DLS dei campioni da CC050 a CC057.

Un diametro medio delle nanoparticelle di 352 nm (tabella 0.3) è un risultato soddisfacente, perciò si è passati all'elaborazione di nanoparticelle composite contenenti PTQ10 ed ITIC-4F. In tabella 0.4 vengono riportati i risultati ottenuti negli esperimenti svolti con diverse proporzioni tra i due composti.

Tabella 0.4: preparazione di nanoparticelle composite. Parametri chiave della nanoprecipitazione dei campioni da CC062 a CC070.

Sample	Ratio PTQ10:ITIC-4F	PTQ10 (mg/ml)	ITIC-4F (mg/ml)	Average diameter(nm)	Dispersion (nm)
CC062	1 : 0	1	0	598	410
CC063	8 : 2	0,8	0,2	503	349
CC064	7 : 3	0,7	0,3	333	102
CC065	6 : 4	0,6	0,4	330	86
CC066	5 : 5	0,5	0,5	300	70
CC067	4 : 6	0,4	0,6	322	176
CC068	3 : 7	0,3	0,7	268	93
CC069	2 : 8	0,2	0,8	244	114
CC070	0 : 1	0	1	149	69

Come si può osservare dalla figura 0.10, il diametro medio e l'ampiezza della distribuzione diminuiscono all'aumentare della quantità di ITIC-4F: ciò è dovuto alla differenza di dimensione tra il polimero PTQ10 e la molecola ITIC-4F. Il rapporto che si sceglie di utilizzare per la preparazione dello strato attivo è il rapporto 1:1 in peso, in quanto ritenuto favorevole al meccanismo foto-attivo.

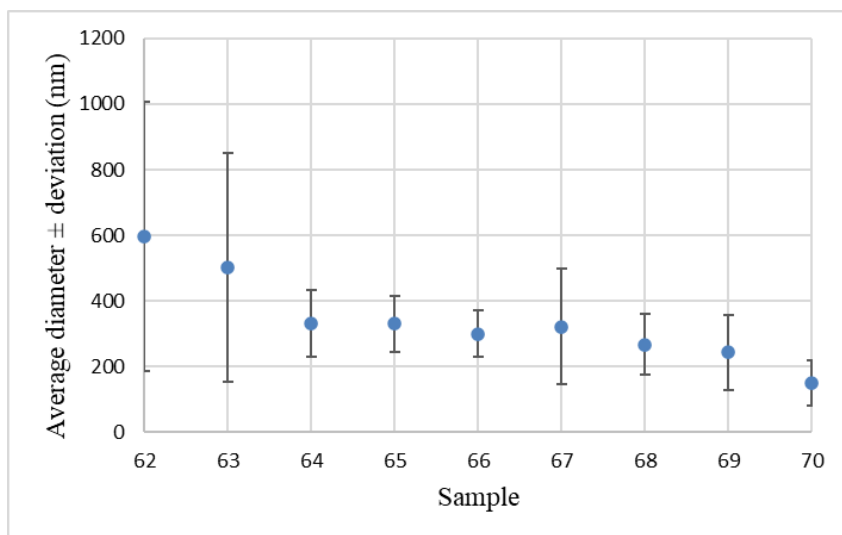


Figura 0.10: preparazione di nanoparticelle composite. Risultati della DLS: diametro medio e deviazione standard dei campioni da CC062 a CC070.

Le particelle composite vengono inoltre osservate al TEM ed al SEM: nella figura 0.11 viene riportato un esempio di immagini ottenute con entrambe le tecniche microscopiche. Nella figura 0.11a si può osservare una singola nanoparticella al TEM, mentre nella figura 0.11b, prodotta con SEM con un campo di vista di 10 μm , si può osservare uno strato di nanoparticelle.

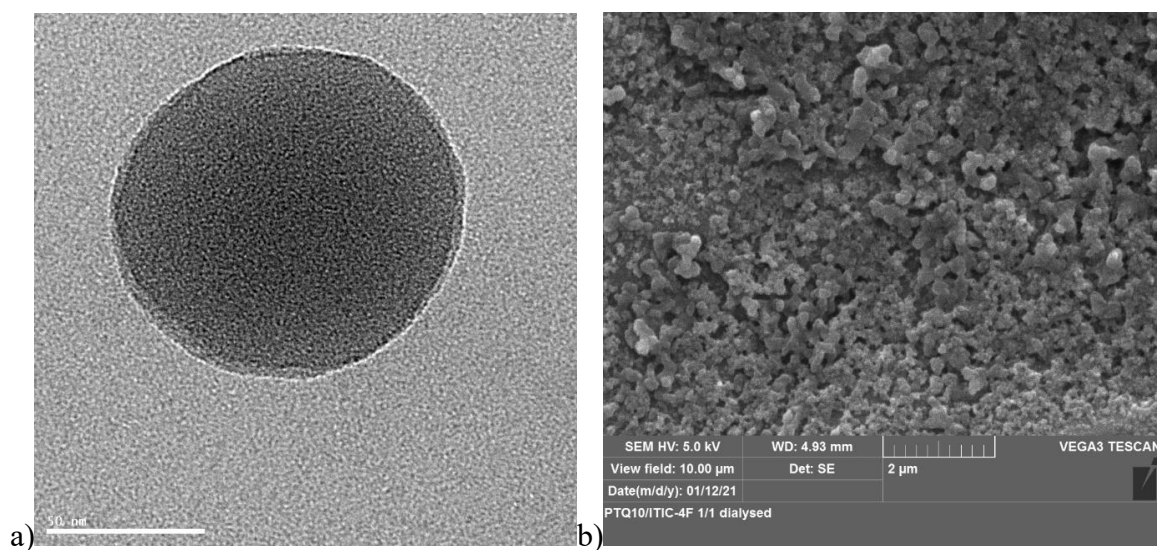


Figura 0.11: a) immagine al TEM di nanoparticella di PTQ10:ITIC-4F (1:1). b) immagine al SEM di nanoparticelle di PTQ10:ITIC-4F (1:1), campo visivo 10 μm .

Nell'ultima sezione sono presentati i risultati della fluorescenza, tali risultati sono volti a dimostrare la presenza, all'interno di una singola nanoparticella, di entrambi i materiali foto-attivi. In figura 0.12 sono riportati i risultati della fluorescenza su una miscela di nanoparticelle contenenti solo un tipo di materiale foto-attivo. Le curve non mostrano effetti di trasferimento di energia. In figura 0.13, invece, i risultati sono dati dall'analisi a fluorescenza di nanoparticelle composite, elaborate con una miscela di donatore ed accettore. Si può osservare un'attenuazione delle curve (*quenching*) dato dal fenomeno di trasferimento

di energia: tale fenomeno è conosciuto come FRET e può avvenire se la distanza tra i due materiali è sufficientemente piccola. Si dimostra così la compresenza e la compenetrazione di entrambi i materiali all'interno delle nanoparticelle prodotte.

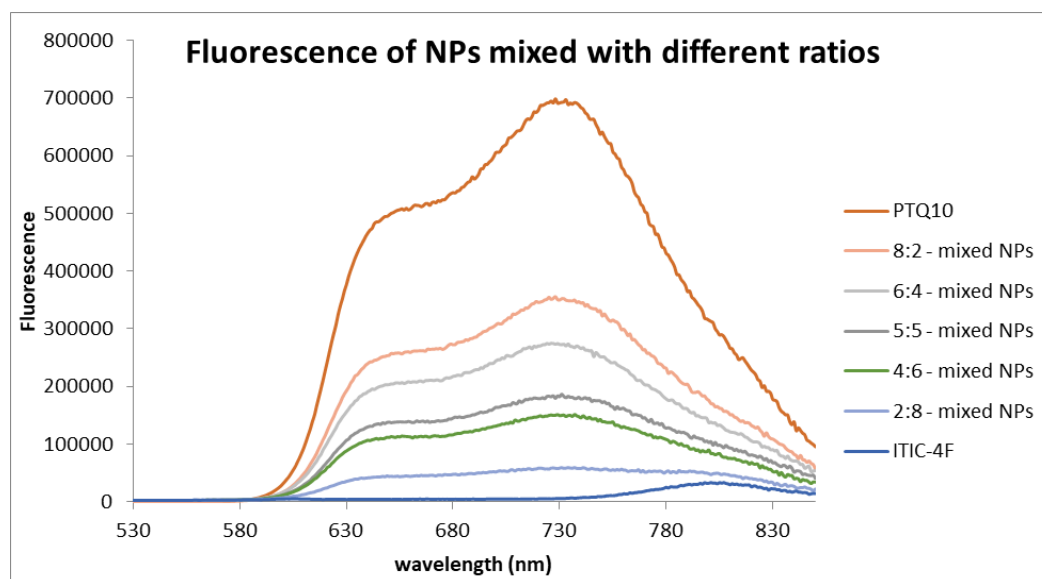


Figura 0.12: fluorescenza di sospensioni contenenti miscele di nanoparticelle di PTQ10 ed ITIC-4F con diverse proporzioni.

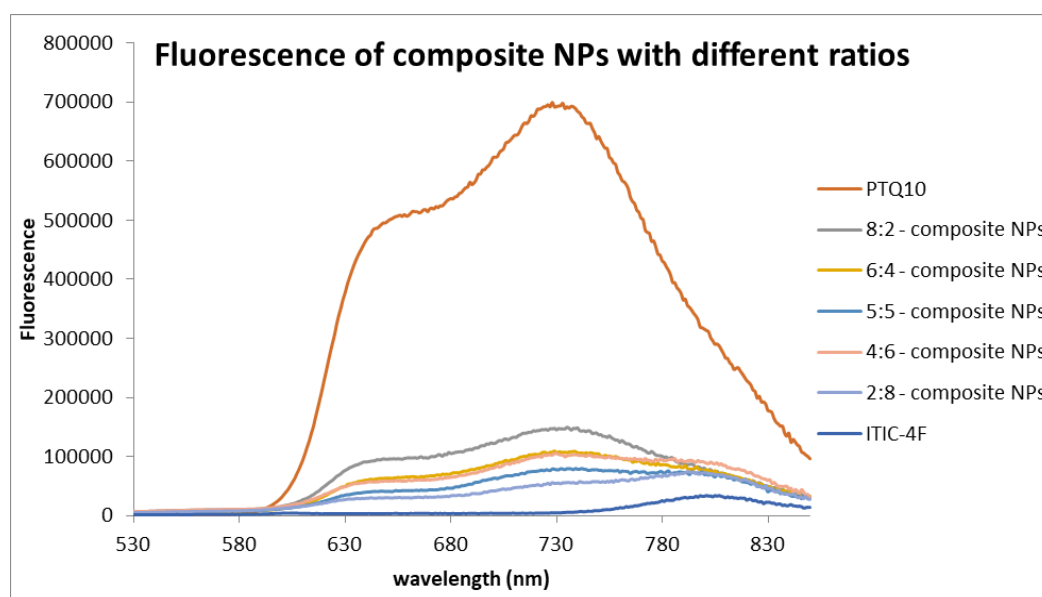


Figura 0.13: fluorescenza di sospensioni contenenti nanoparticelle composite di PTQ10 ed ITIC-4F, con diverse proporzioni.

In conclusione, è stata verificata la possibilità di produrre PTQ10, un polimero promettente come donatore di elettroni, con una sintesi ad alta resa e con costi contenuti.

L'elaborazione di nanoparticelle disperse in mezzo acquoso ha dato buoni risultati, una volta risolte le problematiche riguardanti i parametri della nanoprecipitazione in termini di solvente, temperatura, ultrasonificazione, metodo di evaporazione, rapporto tra solvente e non solvente, rapporto tra i due materiali foto-attivi.

È stata dimostrata la stabilità delle nanoparticelle in seguito a rimozione del solvente e concentrazione, una volta individuate le condizioni ottimali per compiere questi procedimenti.

Infine, il calcolo dell'efficienza del dispositivo fotovoltaico ottenuto per deposizione della sospensione mediante *spin-coating* ha dato un risultato esiguo, dell'ordine di $10^{-4}\%$.

I risultati ottenuti risultano ad ogni modo promettenti e incoraggiano ulteriori studi su questa tecnica innovativa di preparazione dello strato attivo di celle fotovoltaiche organiche. Lo studio relativo al raggiungimento di una efficienza elevata per le celle fotovoltaiche basate su PTQ10 e ITIC-4F è aperto e il margine di miglioramento è certamente ampio. Questo studio verrà proseguito nel laboratorio del CNRS di Strasburgo.

Abstract

Conjugated polymer nanoparticles are versatile functional nanostructured materials that can find applications in various fields, among them Organic Photovoltaic Cells (OPV) and Organic Light Emitting Diode (OLED). Several organic molecules and solvents are used for the preparation of these nanoparticles, with the intention of reaching a high efficiency, a favourable preparation of the devices on industrial scale and attractive applications. Latest studies have demonstrated that it is possible to finely tune the active-layer morphology using nanoparticles and achieve high power conversion efficiencies. Recently, the use of conjugated polymer nanoparticle dispersions in water or alcohols has emerged as a possible solution to avoid toxic solvents.

The objective of the Master Thesis is to study the preparation of composite nanoparticles containing PTQ10, a conjugated electron-donor polymer, and ITIC-4F, a non-fullerene molecule electron-acceptor, using the nanoprecipitation technique. Organic photovoltaic devices are currently prepared from hot solutions in toxic chlorinated solvent. The aqueous dispersion of the synthesized nanoparticles enables an eco-friendly preparation of these devices, since the chlorinated solvents are substituted by water. The work encloses and focuses on the study of the influence of process parameters on the size and morphology of the particles, aiming to an optimization of the nanoprecipitation procedure, along with the procedure of dialysis and concentration of the suspension. The particles will be characterized by Dynamic Light Scattering (DLS), fluorescence, SEM, TEM.

The results of the experiments led to the obtainment of a composite nanoparticles water suspension, with an adequate dimension of the particles. Furthermore, with the spin-coating technique, a solid layer was prepared using this suspension, for the preparation of a laboratory scale OPV device.

Versione italiana:

Le nanoparticelle di polimeri coniugati sono un interessante e versatile nanomateriale, che trova applicazione in diversi campi, tra i quali le celle fotovoltaiche e i diodi basati su polimeri organici (OPV e OLED). Recenti studi dimostrano che le celle OPV possono raggiungere efficienze comparabili a quelle delle celle fotovoltaiche a base di Silicio; in quest'ottica, vengono attualmente investigate diverse specie di accettori e donatori funzionalizzati chimicamente e differenti metodi di preparazione dello strato attivo, la cui morfologia può essere finemente modulata modificando il nanomateriale e la sua deposizione in strato solido, al fine di raggiungere efficienze sempre più soddisfacenti.

L'obiettivo di questa Tesi è la preparazione di nanoparticelle composite contenenti un donatore, il polimero coniugato PTQ10, ed un accettore: ITIC-4F, una molecola accettrice non fullerenica. Le nanoparticelle vengono preparate utilizzando la tecnica della nanoprecipitazione, sostituendo i solventi organici comunemente usati con una fase acquosa; ciò ha il vantaggio di evitare l'impiego di solventi tossici, che verrebbero poi rimossi

mediante evaporazione, sfruttando l'acqua che è priva di tossicità e dando una alternativa *eco-friendly* per la preparazione delle celle fotovoltaiche. Per la preparazione delle nanoparticelle ci si avvale della tecnica di nanoprecipitazione, il cui procedimento viene sperimentato ed ottimizzato all'interno di questo lavoro di tesi, modulando numerosi parametri, tra i quali: concentrazione delle soluzioni, temperatura di nanoprecipitazione e di evaporazione, tempo di ultrasonicazione. L'obiettivo è l'ottenimento di nanoparticelle di dimensioni ottimali; la distribuzione di tali dimensioni viene analizzata tramite Dynamic Light Scattering (DLS). Le particelle vengono inoltre analizzate tramite TEM, SEM e fluorescenza.

I risultati di questi esperimenti hanno permesso di ottenere una sospensione in mezzo acquoso di nanoparticelle composite di diametro adeguato. Inoltre, tale sospensione è stata impiegata per la preparazione di uno stato solido mediante *spin-coating*, preparando una *OPV cell* su scala di laboratorio, al fine di misurarne l'efficienza.

1.Introduction

In this historical period, characterized by a world population of 7,8 billion people and growing fast, and by a proven global warming issue, the reduction of CO₂ emissions and the enhancement of renewable energy sources is a troublesome priority. The transition from fossil and non-renewable energy sources, to sustainable and low impact solutions is challenging and still requires the work and the progress of science. In this context, major efforts are being made to increase the performance of photovoltaic panels and improve their applications. Among the different photovoltaic technologies, organic photovoltaics (OPVs) look appealing and are a subject of innovative studies. OPV performances are promising at laboratory scale, although they are still below those of mono- and poly-crystalline based silicon photovoltaics. One of the central objectives of OPVs production, to effectively enter the market, is the low-cost and eco-friendly processing through industrial printing techniques; this scale up, for mass production, requires the replacement of environmental toxic and hazardous solvents with non-halogenated solvents.³ High power conversion efficiencies (PCE) have been achieved with chlorinated solvents, while PCE lowers drastically when replacing them with more eco-compatible solvents.⁴ A smart strategy to address this issue is the synthesis of organic nanoparticles in eco-friendly solvents, such as alcohol or water. Several works strive for the optimization of this strategy and the reaching of high PCE in OPVs prepared with this technique is a challenge for future works.

1.1.Organic photovoltaic cells

The field of organic solar cells includes all those devices whose photoactive part is based on organic carbon compounds. The basic structure of an organic cell can be called "sandwich" as it is composed of a substrate, glass or flexible plastic, and one or more films containing the photoactive materials, sandwiched between two conductive electrodes. The variety of organic solar cells is wide and in different stages of research and technological maturation: it includes the "dye sensitized" cells (whose photoelectrically active part is made up of a pigment, titanium oxide and an electrolyte), organic (whose active part is totally organic or polymeric), organic/inorganic hybrid and biological hybrid.

The working principle of photovoltaic solar cells is the production of electricity using the energy of the photons coming from light. In OPVs two organic materials are present in the active layer: the donor and the acceptor. In the donor material there is the formation of an exciton, which moves to the interface giving the electron to the acceptor material, the hole and the electron go then in opposite directions through the electrodes, therefore, applying a potential, there is production of electric current. The main characteristic according to which the donors and acceptors are coupled are the HOMO and LUMO energies: they behave as semiconductor materials, so the efficiency of electrons displacement depends on the differences between these energy levels.

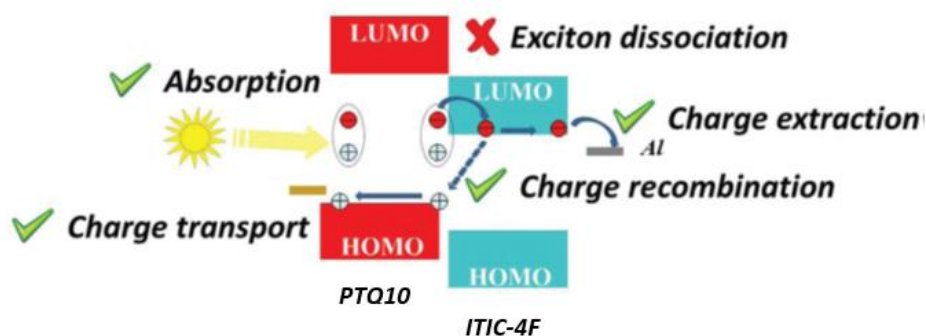


Figure 1.1: Schematic illustration of the different mechanisms leading to power conversion in bulk heterojunction solar cells. Adapted with permission from ⁵.

The domains of the two materials must be small enough to permit the exciton to get to the interface, where it dissociates into free charges: this separation has to occur rapidly, otherwise the exciton will disappear, it has to reach the interface with the acceptor material within a distance of 10-20 nm (average exciton diffusion length),⁶ furthermore, the material configuration must permit and favor the percolation of the electron to the electrode. The morphology of the phase separation is a critical variable because it simultaneously enables the exciton dissociation and the free-charge collection. The ideal structure is an interpenetrating blend of the two phases with a typical length scale of the order of the exciton diffusion length. The morphological organization of the active-layer depends on the materials' physico-chemical properties (solubility, planarity, etc.) and on the film preparation process.⁵

At the present time, the best OPV performances can reach a conversion of 18% (at laboratory scale)⁷, which almost approaches the conversion obtained with mono- and polycrystalline silicon-based photovoltaics, that is 20%. The increase of the Power Conversion Efficiencies (PCE) of OPV devices has been achieved thanks to the evolution of photoactive material design: the development of more performing donors and acceptors, and the improvement of configuration and morphology of the active layer. The OPV field experiences a recent and rapid development of photoactive materials with properties increasingly more appropriate for photon harvesting and charge carrier transport, such as low band-gap (LBG) polymers and non-fullerene acceptors (NFA).⁵

1.2. Photoactive materials

1.2.1. PTQ10

Poly [(thiophene)-alt-(6,7-difluoro-2-(2-hexyldecyloxy) quinoxaline)], known as PTQ10 in an abbreviated form, is a conjugated polymer currently experimented in organic photovoltaic cells. Its chemical structure can be observed in figure 1.2.

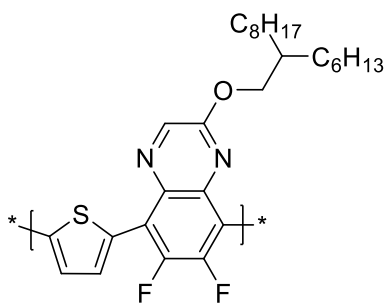


Figure 1.2: PTQ10 chemical structure.

The molecular design strategy of PTQ10 is based on the donor–acceptor copolymerization concept, using thiophene ring as donor unit and difluorine substituted quinoxaline as acceptor unit. The alkoxy side chain on quinoxaline unit ensures good solubility in organic solvents and enhances absorption of the polymer, while the difluorine substituents have the effect of downshifting the highest occupied molecular orbital (HOMO) energy level and increasing hole mobility.⁸

It is known from literature that PTQ10 possesses good solubility in some common organic solvents. Its thermal decomposition temperature (T_d) at 5% weight loss is 383 °C, indicating its good thermal stability for the application in photovoltaic solar cells. The E_{HOMO} and E_{LUMO} of PTQ10 are -5.54 eV and -2.98 eV.¹ PTQ10 possesses a quite simple molecular structure and can be synthesized with low cost and high overall yield from cheap raw materials. Furthermore, the optimized OPV cells with PTQ10 as donor and non-fullerene acceptors already demonstrated high PCE among the single junction photovoltaic cells.¹ The results indicate that PTQ10 is a promising polymer donor for commercial products, and it will make the application of OPV cells highly auspicious.

PTQ10 is a conjugated polymer: the aromatic nature of its monomer gives a planar structure to the chain and enables interaction of neighboring aromatic rings with π bonds, which is called π -stacking. This rearrangement in space gives an ordered 3-D organization and permits the formation of lamellar regions. The overlap between π - π orbitals can create pathways for electrons to pass from one molecule to another; therefore, short π -stacking distances are usually beneficial for the charge transport properties. The polymeric chain can organize in space by mixed stacking or segregated stacking. Taking into consideration PTQ10, in the first case a quinoxaline ring forms a π -bond with a thiophene ring, the bond has a certain obliquity and movement in space is permitted. In the second case, a quinoxaline ring forms a bond with another quinoxaline ring (and so for the thiophene) and the stacking is perfectly perpendicular to the chain, with no possible movement.

1.2.2. ITIC-4F

The acceptor molecule that will be used in this work, in the active layer of the OPV cell, is ITIC-4F. It is an indacenodithienothiophene (IDTT)-based post-fullerene electron acceptor, of high interest in OPV development. The complete name is 3,9-bis(2-methylene-((3-(1,1-dicyanomethylene)-6,7-difluoro)-indanone))-5,5,11,11-tetrakis(4-hexylphenyl)-dithieno[2,3-d':2',3'-d']-s-indaceno[1,2-b:5,6-b']dithiophene, the same molecule is also

known with the names IT-4F, ITIC-2F, ITIC-DF3. Its chemical structure shows an Acceptor-Donor-Acceptor arrangement⁶ (figure 1.3).

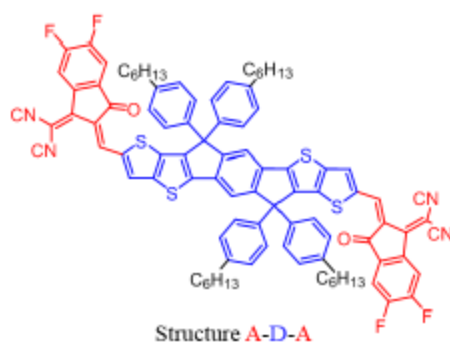


Figure 1.3: ITIC-4F chemical structure.⁶

In the past years, designing molecules with the donor-acceptor (D-A) approach has proved to be successful. It is a viable route to finely control both HOMO and LUMO levels, respectively governed by the D and A units.⁹ Its structure also promotes intermolecular π -stacking interactions for better charge transport. In the latest years, non-fullerene acceptors (NFAs) showed a rapid development and NFA-based solar cells rapidly outperformed the fullerene-based OPV.⁶ The E_{HOMO} and E_{LUMO} of ITIC-4F are -5.66 eV and -4.14 eV, its band gap is 1.52 eV. HOMO and LUMO energy levels of PTQ10 and ITIC-4F are showed in figure 1.4.

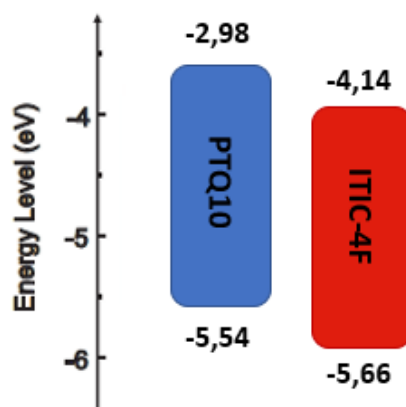


Figure 1.4: PTQ10 and ITIC-4F HOMO and LUMO energy levels.

1.3.Synthesis of nanoparticles

Two principal methods have been reported for the formation of donor/acceptor nanoparticle dispersions: miniemulsion and nanoprecipitation.

Preparation of aqueous dispersions of semiconducting polymer nanoparticles by the miniemulsion process was first demonstrated by Landfester et al.¹⁰ The miniemulsion method involves intermixing a photoactive blend solution where the materials are in a good solvent, and an immiscible nonsolvent (a solvent that the organic semiconductors are not soluble in) by ultrasonication in the presence of a surfactant¹¹ (figure 1.5). The presence of the surfactant is necessary to stabilize the interface between the solution of the materials and the non-

solvent. Dialysis is commonly required in these type of process, in order to reduce the amount of the surfactant in the dispersion.¹¹ Due to its simplicity and wide applicability, the miniemulsion method is very used. However, the disadvantage of a surfactant-containing nanoparticle dispersion is that the yield of the obtained OPV device reaches moderate power conversion efficiencies (PCE), well below those of the standard solution-processed devices using the same materials.



Figure 1.5: Elaboration of nanoparticles (NP) of organic semiconductors (OSC) via the miniemulsion process.⁵

The second method is nanoprecipitation, according to this technique nanoparticles are formed by adding a good solvent containing the donor and acceptor to a miscible nonsolvent, this gives rise to efficient organic solar cells while avoiding the use of surfactants. The good solvent is an organic solvent, which is emulsified in an aqueous solution (with or without a surfactant). Then, the organic solvent is removed with different possible procedures, and this process allows nanoparticle formation. The procedure is schematized in figure 1.6. This nanoparticle precipitation is fast due to the rapidly decreased solubility of the donor/acceptor blend in the good solvent/nonsolvent mixture.¹² From a practical perspective, a disadvantage of this process is that the surfactant-free nanoparticle dispersions can aggregate over time. However, by careful choice of material combinations, it is possible to form stable surfactant-free nanoparticles.

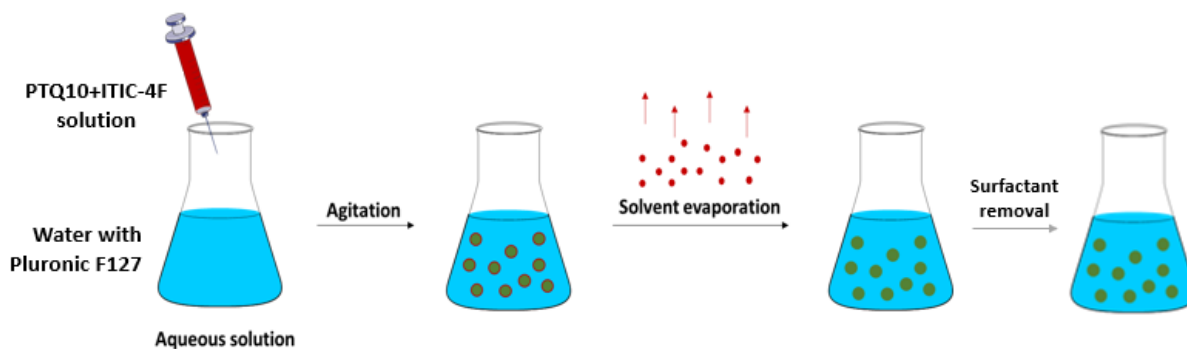
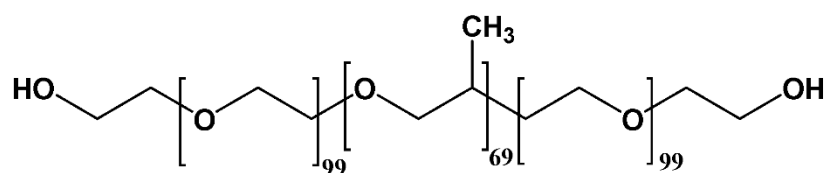


Figure 1.6: Elaboration of nanoparticles via the nanoprecipitation process. Adapted with permission from⁵.

The poloxamers, particularly Pluronic 127, have been exploited for use in the preparation of nanoparticles as emulsifying or stabilizing agent. Pluronic F127 is the BASF trade name for the compound Poloxamer 407 (general name). It is a hydrophilic non-ionic surfactant of the more general class of copolymers known as poloxamers. Pluronic F127 is a triblock copolymer consisting of a central hydrophobic block of polypropylene glycol flanked by two hydrophilic blocks of polyethylene glycol (PEG) (figure 1.7). The approximate lengths of the two PEG blocks is 99 repeat units, while the approximate length of the propylene glycol block is 69 repeat units.¹³ It is in the form of white powder, very soluble in water. Common uses of Pluronic F127 are related to its surfactant properties, as it forms micelles and can solubilize hydrophobic compounds; an example of common application is in cosmetics for dissolving oily ingredients in water.



Pluronic F127

Figure 1.7: Pluronic F127 chemical structure.

In comparison to low-molecular-weight nonionic surfactants, the aggregation behavior of Pluronic surfactants like F127 is complex. It has been reported that aggregation of Pluronics occurs over a range of concentrations, rather than at a unique cmc (critical micelle concentration). As a result, cmc values defined for a copolymer can be widely different depending on the experimental technique used. In Pluronic F127 molecule conformation depends strongly on temperature, as described by Bohorquez et al,¹⁴ therefore, the aggregation behavior of Pluronics is most appropriately characterized by a cmc and a cmt (critical micellization temperature). Since phenomena of micellization and destabilization of suspension are regulated by temperature, this is a critical parameter for the preparation of nanoparticles via nanoprecipitation. As showed from Xie et al. ² the surface stripping of Pluronic F127, for the production of surfactant-free nanoparticles, is effective at 0°C, temperature at which the micelles of Pluronic F127 convert to linear poloxamers in water, and enable the removal by centrifugal filtration, leaving the retentate with rather pure nanoparticles.

1.4.Aim of the work

The objective of the work is the elaboration of composite nanoparticles containing PTQ10 and ITIC-4F, using the nanoprecipitation technique: in the experiments the photoactive materials will be solubilized in an organic solvent, THF, and water will be used as non-solvent. This method enables an eco-friendly preparation of the OPV devices thanks to the aqueous dispersion. The work encloses the synthesis of polymer PTQ10 and focuses on the study of the influence of process parameters on the size of the nanoparticles, aiming to an optimization of the nanoprecipitation procedure. Then, dialysis and concentration of the

suspension will be performed and optimized for the preparation of a laboratory scale OPV device, with the spin-coating technique.

2. Materials and methods

2.1. Synthesis

Pluronic F127 was purchased from SIGMA-ALDRICH (CAS 9003-11-6, batch # 095K0016).

THF was purchased from VWR PROLABO chemicals, 0,2 μm filtered, and distilled for the reactions.

Chloroform anhydrous was purchased from SIGMA-ALDRICH.

ITIC-4F was purchased from SIGMA-ALDRICH (CAS 2097998-59-7, lot# MKCM1455).

The synthesis steps described below have been adapted from known literature.^{1,15}

Synthesis of 5,8-dibromo-6,7-difluoro-2-(2-hexyldecyloxy) quinoxaline

5,8-dibromo-6,7-difluoro-2-(2-hexyldecyloxy)quinoxaline was synthesized with the following procedure: To a two-necked, round-bottom flask, 3,6-dibromo-4,5-difluorobenzene-1,2-diamine (906 mg, 3 mmol), glyoxylic acid (222 mg, 3 mmol), and acetic acid (30 mL) are added. The mixture is warmed to 40 °C for 10 min, and then the solution is stirred at room temperature for 3 h. The precipitate is collected by filtration and dried to get a white solid without further purification. The white solid (1 g, 2.94 mmol), potassium *tert*-butanolate (395 mg, 3.53 mmol), and 1-bromo-2-hexyldecane (897 mg, 2.94 mmol) are dissolved in methanol (30 mL). The mixture is refluxed for 12 h, then cooled to room temperature. Then, the reaction mixture is poured into saturated NH_4Cl solution, extracted with dichloromethane, and washed with water. The organic extraction is dried over anhydrous MgSO_4 , and the solvent is evaporated under reduced pressure. The final product is obtained as colorless oil (1.54 g, 2.73 mmol) from the product through column chromatography on silica gel.

^1H NMR (400 MHz, Chloroform- d) δ 8.51 (s, 1H), 4.49 (d, $J = 5.7$ Hz, 2H), 1.90 (p, $J = 5.9$ Hz, 1H), 1.51 – 1.18 (m, 24H), 0.88 (td, $J = 6.9, 2.5$ Hz, 6H).

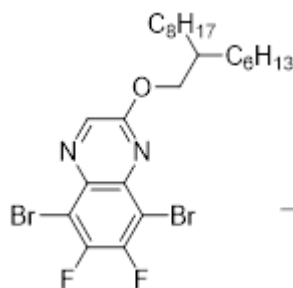


Figure 2.1: chemical structure of 5,8-dibromo-6,7-difluoro-2-(2-hexyldecyloxy)quinoxaline.

Synthesis of 2,5-Bis(trimethylstannyl)thiophene

2,5-Bis(trimethylstannyl)thiophene was synthesized with the following procedure: a spherical flask is put in anhydrous conditions and filled with Argon. The solution of 2,5-dibromothiophene in THF is introduced and maintained at -78°C using a dry ice bath. The catalyst *n*-BuLi 2.5 M is added dropwise with a syringe while stirring, it is added in a time of 20 min in order to maintain the temperature at -78°C . After stirring for 1h at -78°C to let react, SnMe_3Cl is slowly added. The reaction mixture is stirred at for 30 min, maintaining the temperature constant and then it is gradually warmed to room temperature. The mixture is added with water and diethyl-ether in a separatory funnel, it is agitated and decanted, water is removed, and the operation is repeated. Na_2SO_4 is added for the formation of crystals (24 h), the solution is poured in a glass filter and washed with methanol. Crystals are heated in pure methanol and let recrystallize. The operation is repeated three times, to obtain a high purity. Purified crystals are put in a vial and dried in the oven (50°C).

^1H NMR (400 MHz, Chloroform-*d*) δ 7.38 (s, 2H), 0.37 (s, 18H).

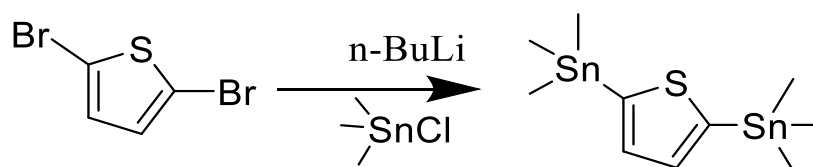


Figure 2.2: synthesis reaction for 2,5-Bis(trimethylstannyl)thiophene.



Figure 2.3: photo of 2,5-Bis(trimethylstannyl)thiophene after purification.

Polymerization of Poly[(thiophene)-alt-(6,7-difluoro-2-(2-hexyldecyloxy)quinoxaline)] (PTQ10)

The polymer PTQ10 is synthesized according to Stille-coupling poly condensation between 5,8-dibromo-6,7-difluoro-2-(2-hexyldecyloxy)quinoxaline (compound 1) and 2,5-bis(trimethylstannyl)thiophene (compound 2) under Argon. Compound 1 (173.3 mg) and compound 2 (126 mg) are transferred into a Schlenk tube, previously heated, put under

vacuum and filled with Argon three times, to remove air and humidity. A stirrer is added, the Schlenk is put under vacuum while the compounds are stirring. Through a rubber stopper, 20 ml of anhydrous toluene are added. The flask is flushed with argon for 20 min, then, 5.87 mg of Pd₂dba₃ catalyst and 7.47 mg of P(o-tolyl)₃ ligand are added. The Schlenk is heated at 120°C through an oil bath for 24 h, while the reaction takes place, and the Schlenk is externally covered with Aluminum foil to protect the reactants from light. In order to quench the reaction, 2-trimethyltinthiophene and 2-bromothiophene end-cappers are added at one hour apart. Then, the solution is cooled down to room temperature, and extracted by Soxhlet extractor with ethanol, cyclohexane, and chloroform one by one. The polymer dissolved in chloroform is added with a water solution of Sodium Diethyl-thiocarbamate, at 60°C 1 h, to remove Pd residues. The water solution is removed using a separatory funnel. Chloroform is evaporated in a rotatory evaporator, a film of polymer is obtained attached to the walls of the flask, it is detached with ethanol, separated using a glass filter, finally washed with acetone and then water, which are then evaporated.

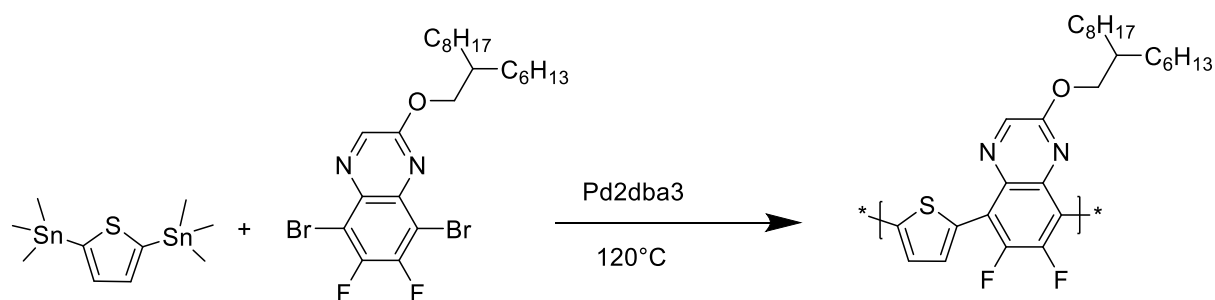


Figure 2.4: polymerization of PTQ10 via Stille coupling poly condensation.

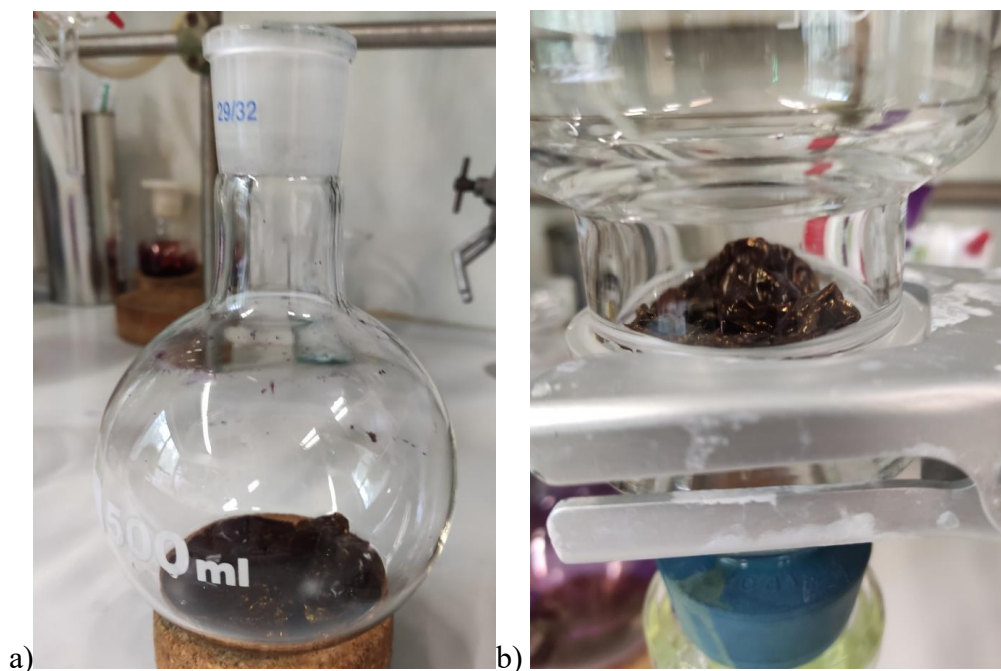


Figure 2.5: a), b) PTQ10 foil at the end of Soxhlet extraction.

2.2.NMR

^1H NMR was performed using a Bruker Advance 400 MHz spectrometer. Chemical shifts were referenced to the solvent value: $\delta = 7.26$ ppm for Chloroform-*d*. The analyses were performed at 298K. The samples were prepared by introducing in the tubes for the NMR a small amount of the examined substance, dissolved in deuterated chloroform (CDCl_3).

2.3.SEC

Size Exclusion Chromatography (SEC) was performed in 1,2,4 TCB at 150 °C with a flow rate of 1 ml/min using a PSS column. System GPC-HT column PSS (measurement performed at LCPP laboratories).

2.4.DLS

Dynamic Light Scattering was performed using ALV/CGS-3 Compact goniometer system by ALV-GmbH and ALV-7004 Correlator Software, ALV/LSE-5004 Light scattering electronics and multiple tau digital correlator. All the measurements were done with a 90° angle, since the samples contained water suspension, Viscosity 0.89000 cP, Refractive Index: 1.33200, Wavelength: 632.8 nm, Duration: 30 s.



Figure 2.6: example of DLS measurement: on top left the correlation function curve, on top right the count rate trace, on bottom left the residuals and on bottom right the result of the distribution function, after fitting of the data.

All the samples for the DLS are prepared by dilution of the water suspension with MilliQ water, reaching a concentration of 0.003 mg/ml; 3 ml of diluted suspension are transferred to a tall glass vial. During the analysis the vial is immersed in toluene, because its refractive index is much closer to the refractive index of glass than air, thus decreasing the reflections and refractions phenomena at the vial wall.

The data from DLS (radius R_i and intensity n_i) are analyzed using the following equations, to calculate the average diameter and the dispersion. The average diameter is the double of the average radius calculated with the equation:

$$R_m = \frac{\sum(R_i \cdot n_i)}{\sum n_i}$$

The dispersion of the diameter distribution is the double of the dispersion calculated for the radii:

$$\sigma = \sqrt{\frac{\sum(R_i - R_m)^2 n_i}{\sum n_i}}$$

2.5. UV visible spectrophotometry

The absorption spectrum of the solutions and suspensions was acquired using a Shimadzu Corporation UV-vis spectrophotometer, model: UV-2600 240V IVDD. Using quartz cuvettes for organic solvents, plastic cuvettes for aqueous solutions (pathlength of 1 cm) and glass for the solid films (200 Deckglaser by Roth 24x24mm). Spectra were measured in the wavelength range 300-1000 nm.

2.6. Ultrasonication

For the ultrasonication of all the samples we used Digital sonicator, model 450, Branson. Settings: time from 1 to 3 minutes, amplitude 40%, 3 seconds on, 2 seconds off. The samples were placed in a cold-water bath, to absorb the heat produced by sonication.

2.7. SEM

The size and the shape of the nanoparticles was evaluated by Scanning Electron Microscopy on Vega3 Tescan, 5 kV, 5 mm of working distance, on a SE detector. Before imaging the nanoparticles, the samples were gold sputtered using Quorum Technologies Q150RS gold sputter coater. Samples are prepared by diluting the dialyzed suspension to 0,1 mg/ml and 0.05 mg/ml, depositing a drop on Aluminum foil, and let dry. The foils are then attached to the SEM supports and gold sputtered. The deposition of a monoatomic layer of gold permits the electrons to displace on the sample surface.

2.8. Dialysis

For the removal of the surfactant we used a cooling centrifuge SIGMA model 3-16KL, at 0°C. Two types of centrifuge filter were used: VIVASPIN 20 (brand Sartorius) with a PES (polyether sulfone), 30000 MW cut-off; filter Amicon Ultra-15 with a cellulose filter with 100000 MW cutoff.

2.9. Tensiometry

Surface tension was measured using the drop shape analysis technique on a pendant drop tensiometer: TECLIS TRACKER™. After performing the required calibrations and testing the surface tension of distilled water, which has to approach the value of 72 mN/m, the measurement of the surface tension of each solution was obtained rinsing the syringe and the needle, filling the syringe with the sample solution and analyzing angles and shape of the pendant drop. For each sample, two values were measured: an instantaneous value and the evolution of the surface tension value with time.

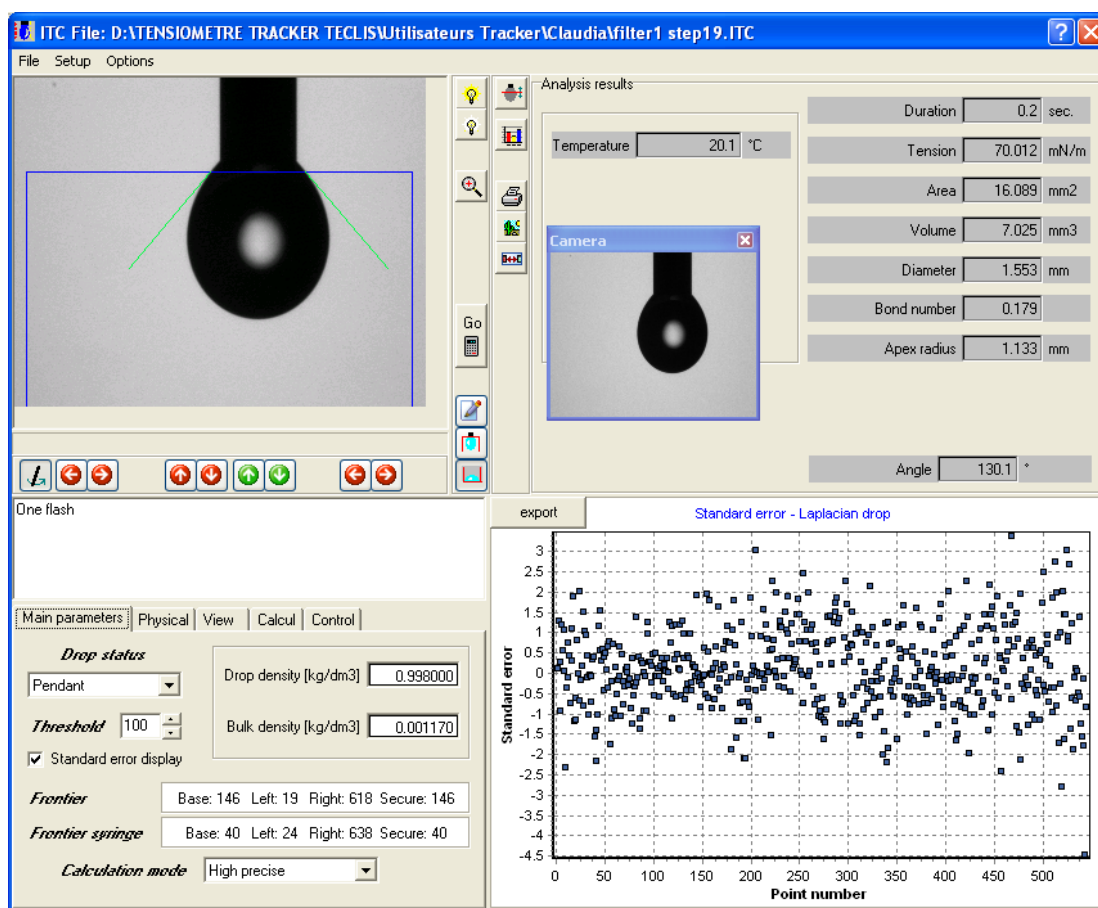


Figure 2.7: example of surface tension measurement, with tensiometer tracker TECLIS, pendant drop method.

2.10. Fluorescence

All the samples were analyzed with FluoroMax-4 Spectrofluorometer by Horiba Scientific, and the data examined with FluorEssence software. The samples, in plastic square based cuvettes, have a concentration of 0.002 mg/ml. The experiments were performed with excitation at 500 nm (4 nm front entrance slit) and emission from 530 nm to 850 nm (4 nm

front exit slit), for the comparison of composite nanoparticles and mixed nanoparticles. For PTQ10 emission 730 nm, slit 4, with filter 450 nm. For ITIC-4F emission 820 nm, slit 4, with filter 495 nm. Before analyzing the samples with the fluorescence, the UV-visible spectrum of the two substances present in the nanoparticles is analyzed (from 1000nm to 350 nm), to measure the peak wavelengths. The two samples are prepared by diluting the water NP suspensions of PTQ10 and ITIC-4F, separately, to 0.002 mg/ml. These values are used to determine the range of the fluorescence analysis and to interpret the results.

2.11. Procedure for nanoprecipitation of PTQ10 and ITIC-4F in water.

Preparation of stock solutions

20 mL of a Pluronic F127 solution at 20 mg/ml in water was prepared using 0.2 μ m-filtered MilliQ water.

PTQ10 solution in THF at 1 mg/ml was prepared. The total weight of the vial was measured, and the solution was stirred with a magnetic stirrer at 250 rpm in a sand bath at 45°C overnight or for a minimum of 4 hours. If solid residues of polymer attached to the walls, sonication bath was used for few seconds. After solubilization, when necessary, THF was added up to the initial total weight.

10 mL of ITIC-4F solution in 0.2 μ m-filtered THF 1 mg/ml was prepared using the same procedure as for PTQ10 solution.

Nanoprecipitation

For each experiment, a donor/acceptor mixture in THF was first prepared by mixing 0.5 ml of PTQ10 solution and 0.5 ml of ITIC-4F solution. This mixture was then added rapidly under magnetic stirring to a 2 ml of Pluronic F127 aqueous solution. The two solutions were either heated or kept at room temperature depending on the experiments. Temperature was measured before and after nanoprecipitation phenomenon with a probe thermometer.

Ultrasonication and evaporation

After removal of the stirrer, the sample was ultrasonicated (time: 2 min, amplitude: 40%, 3 s ON and 2 s OFF), in a cold-water bath to cool down the suspension during ultrasonication. The weight of the vial was measured again before evaporation of the THF. A needle connected with an Argon conduit is placed inside the vial, above the suspension surface, after 30 minutes of Argon blowing, evaporation is finalized. Weighting the vial allowed to ensure the complete evaporation of THF. A total weight lower than expected meant the evaporation of water together with THF. Then eventual missing weight was completed with MilliQ water.

Surfactant removal

After THF evaporation, the nanoparticles stabilized by Pluronic F127 are cooled down to 4°C. Then the dispersion is placed into Amicon® ultra-15 centrifuge filter (cutoff 100000MW) and centrifuged in a cooled centrifuge at 0°C. Parameters: 1500 rpm (236xg), 15 min, 0°C, acceleration 5, deceleration 5. After every centrifugation the retentate is raised to 15 ml with MilliQ filtered water and the permeate is collected in a different vial for every

step. This process is repeated for several times, depending on the amount of surfactant present in the filter. The surface tension is calculated for the permeate with a pendant drop tensiometer, when surface tension stops increasing between consecutive steps of centrifugation, the removal of all the Pluronic molecules is finalized.

2.12. Spin-coating

The surfactant free suspension was concentrated until obtainment of 1.1 ml of suspension with a concentration of 17.5 mg/ml. For the preparation of the solid active layer the spin coater SPIN 150 by SPS-Europe was used. Parameters: speed 1000 rpm, acceleration 100 radius/s², time 60 s. The substrate was put on the support and blocked with vacuum; it was cleaned from dust with a Nitrogen gun. 50 µl of suspension were dropped with an automatic pipette and spread uniformly with the point of the same. After 1 min of drying, the operation was repeated for cells with more than 1 layer. The substrate was previously prepared, it is made of glass 2 cm x 2 cm covered with ITO layer, on the top of which PEDOT-PSS layer is deposited. After the deposition of the active layer, Al electrodes were added through evaporation of Al. In total, 9 devices were prepared, named from PV1 to PV9.

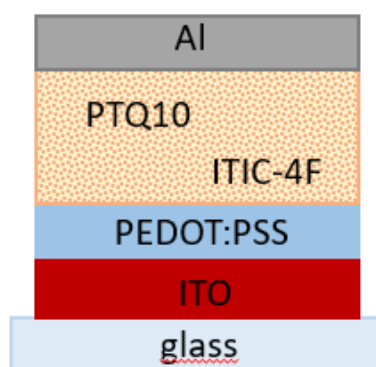


Figure 2.8: scheme of layers in OPV cell.

2.13. Profilometry

Profilometry was used to measure the active layer surface profile and its average thickness. The apparatus Veeco Dektak 150 was used, with the following parameters: radius 12.5 µm, stylus force 1 mg, mass range 6.5 µm.

2.14. Efficiency measurement

Efficiency of photovoltaic devices produced was measured simulating sun light in a Nitrogen protected atmosphere inside a glove box. Cells from PV1 to PV9 were positioned in a circuit and exposed to light with a power of 100 mW/cm². Tension (Vm), current (Im), open-circuit voltage (Voc), short circuit current (Isc), short circuit current density (Jsc) and resistance were measured. Produced power (Pm) and efficiency were calculated considering an area of 0.12 cm².

3. Experimental part

3.1. Synthesis results

Synthesis and purification of the monomers led to the obtainment of the desired compounds, with an adequate purity, as can be observed from the NMR result for the quinoxaline derivative compound (Figure 3.1) and for the thiophene derivative (Figure 3.2): the peaks of the ^1H NMR are in the expected position. The procedure for NMR is described in chapter 2.2.

^1H NMR (400 MHz, Chloroform- d) δ 8.51 (s, 1H), 4.49 (d, $J = 5.7$ Hz, 2H), 1.90 (p, $J = 5.9$ Hz, 1H), 1.51 – 1.18 (m, 24H), 0.88 (td, $J = 6.9, 2.5$ Hz, 6H).

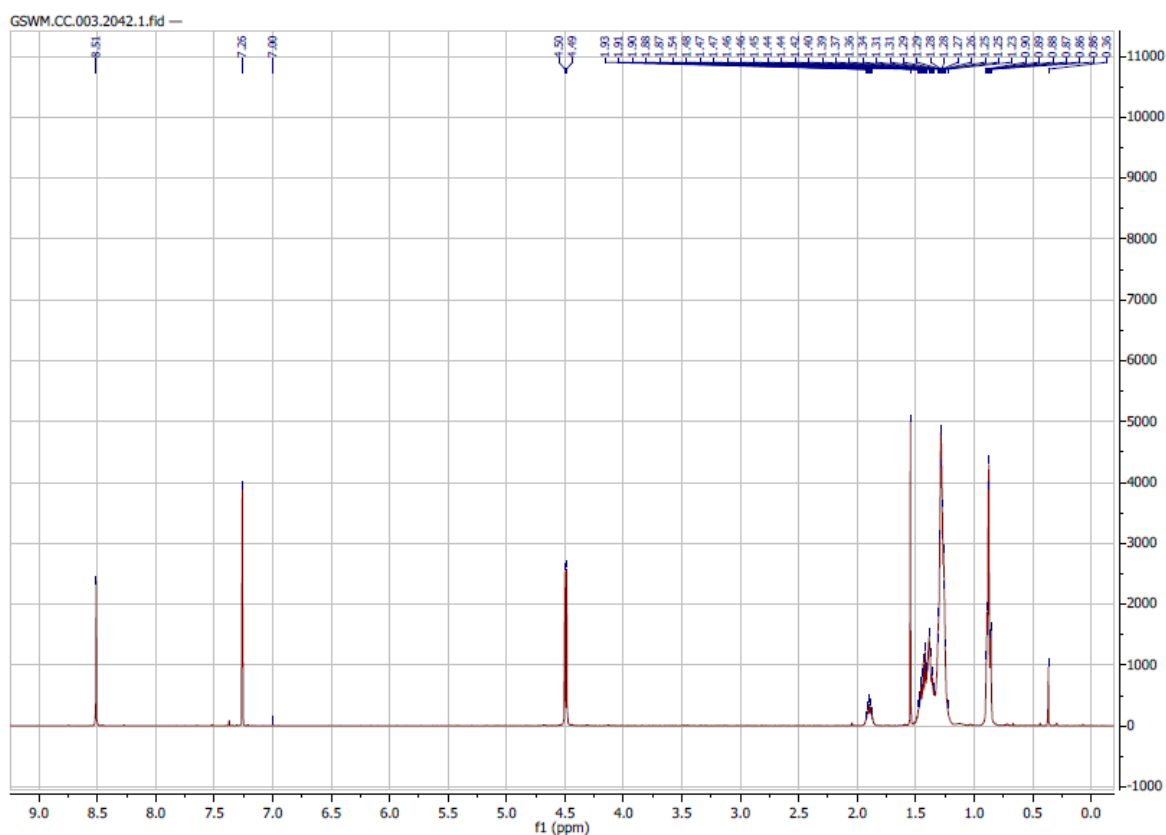


Figure 3.2: NMR of 5,8-dibromo-6,7-difluoro-2-(2-hexyldecyloxy) quinoxaline.

^1H NMR (400 MHz, Chloroform- d) δ 7.38 (s, 2H), 0.37 (s, 18H).

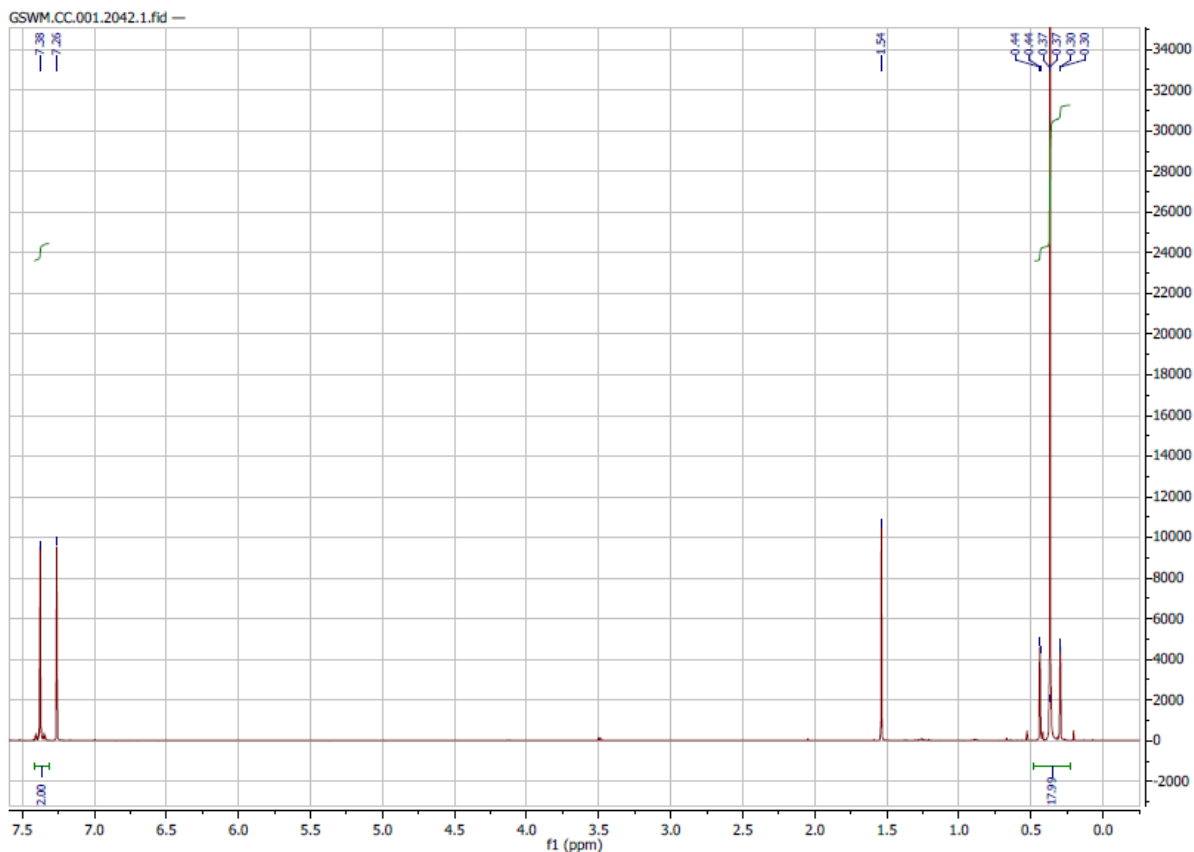


Figure 3.3: NMR of 2,5-Bis(trimethylstannyl)thiophene.

From the polymerization reaction 150 mg of PTQ10 were purified. It is a golden colored thin foil, as shown in figure 3.4.



Figure 3.4: picture of solid foil of PTQ10.

3.2. PTQ10 characterization

Chemical properties and molecular weights of PTQ10 have been analyzed with different techniques. Size Exclusion Chromatography (SEC) was performed to a sample of the polymer, the curves of refractive index detected at the exit of the column and of molecular weight are reported in figures 3.5 and 3.6.

Chromatogrammes

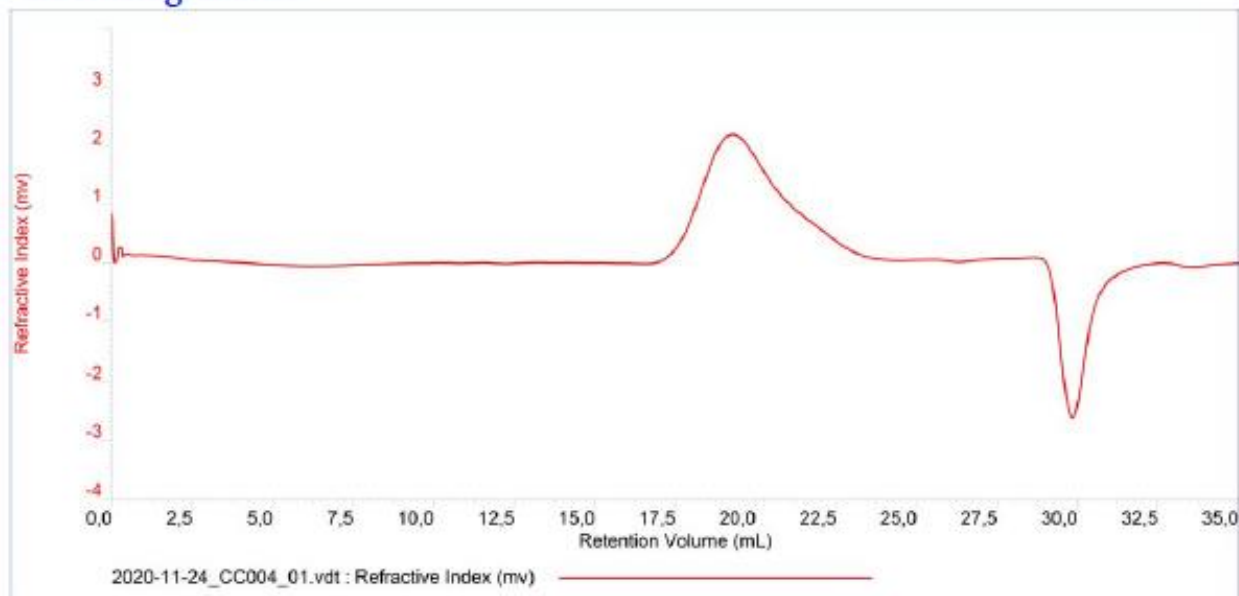
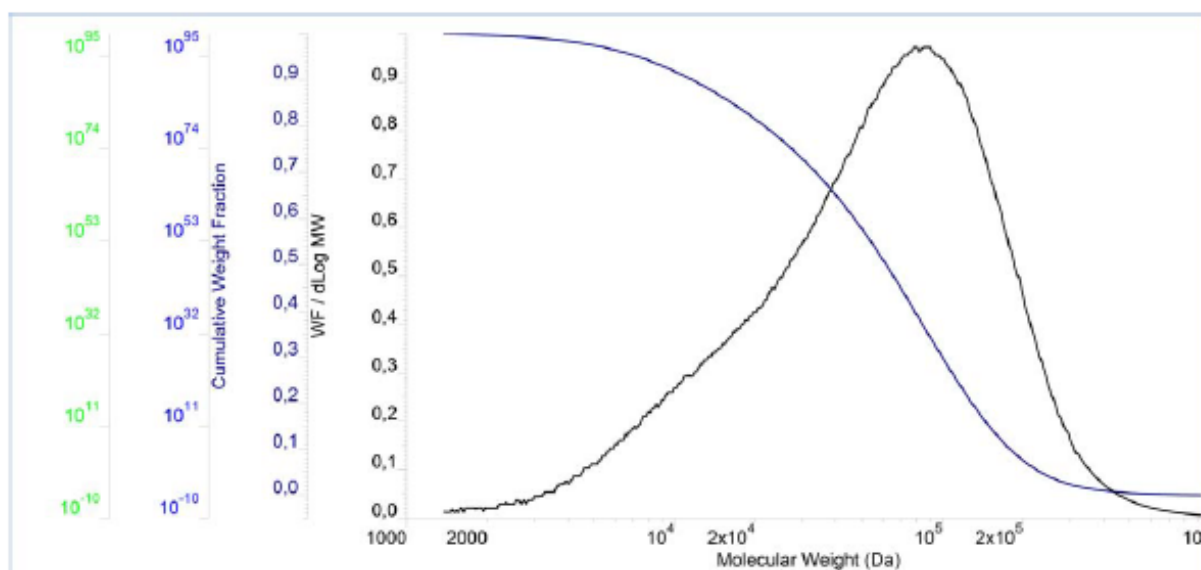


Figure 3.5: Chromatography result, refractive index at exit of the column.



Résultats

Peak	Ret Vol (mL)	Mp (Da)	Mn (Da)	Mw (Da)	Mz (Da)	Mw/Mn	IV (dL/g)	Rh(w) (nm)	Rg(w) (nm)
1	19.347	77 828	27 576	83 589	164 549	3.031	0.0000	0.00	0.00
2	29.783	0	0	0	0	0.000	0.0000	0.00	0.00

Figure 3.6: Chromatography result, molecular weight of PTQ10 polymeric chains.

Table 3.1: results of SEC, molecular weight of PTQ10 polymeric chains.

Mp (Da)	Mn (Da)	Mw (Da)	Mz (Da)	Mw/Mn
77828	27576	83589	164549	3,031

3.3. Solubility of PTQ10 and ITIC-4F

It is known from literature that PTQ10 possesses good solubility in some common organic solvents. The most interesting solvent for the nanoprecipitation experiments is THF, or another solvent miscible with water. Solubility of the polymer was tested in six different solvents: chloroform, THF, DMF, o-DCB, methanol and ethanol. As expected, the polymer turned out to be insoluble in methanol, ethanol and DMF, while it appeared soluble in chloroform, THF and o-DCB. (Figure 3.7)

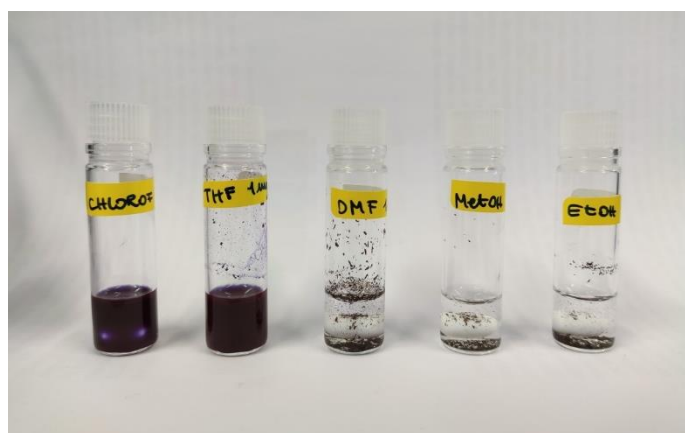


Figure 3.7: solubility experiment of PTQ10 in CHCl_3 , THF, DMF, MeOH, EtOH.

The UV-visible absorption spectrum of PTQ10 was analyzed, both in solid film form and in solution; the curves are shown in Figure 3.8.

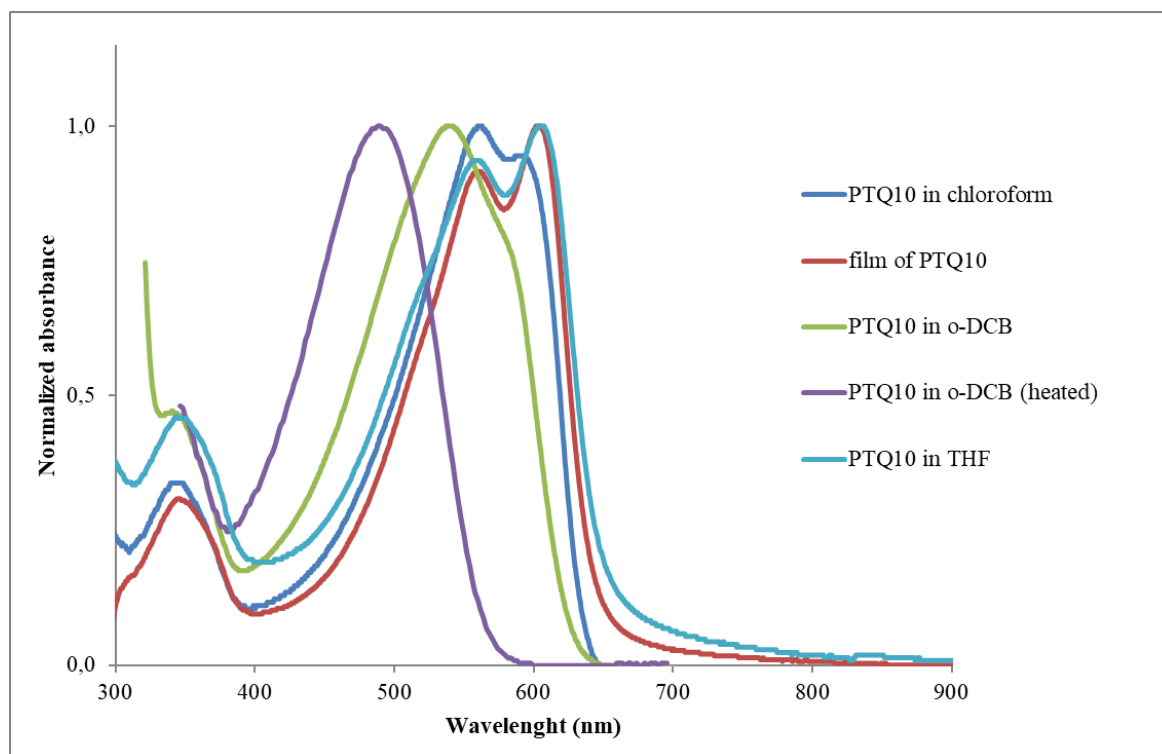


Figure 3.8: Normalized absorption spectra of PTQ10 in CHCl_3 , o-DCB and in solid film.

When the polymer is not solubilized, two peaks can be observed in the spectrum. This happens, in our case, for the film and for the chloroform solution and THF solution at room temperature; therefore, the polymer appears to be not completely soluble in these two solvents (at room temperature). Solubility could be enhanced by the heat, as in the case of *o*-DCB: the two curves of the polymer in *o*-DCB show a shift to the left and a single peak, this effect is enhanced by a higher temperature. It can be observed that the peaks of the polymeric film are different from the ones of the polymer in chloroform, this is because of the different forms of π -stacking of the molecules: mixed or segregated. It is known that polymer PTQ10 is a composite polymer formed by quinoxaline and thiophene, which are planar molecules and can organize in the space by mixed stacking or segregated stacking. In the first case, a quinoxaline ring forms a π -bond with a thiophene ring, the bond has a certain obliquity and can move in the space. In the second case, a quinoxaline ring forms a bond with another quinoxaline ring (and so for the thiophene) and the stacking is perfectly perpendicular to the chain, and there is no possible movement. When the spectrum of the solution is different from the spectrum of the film, the polymer has reached solubility in the solvent. This difference can be seen in the two curves on the left of the graphic: they have one peak and they are shifted to smaller wavelength.

Regarding ITIC-4F, the same solubility experiment was performed, testing its solubility in THF and chloroform, two interesting organic solvents for the aim of the work. Curves resulting from UV-visible spectrophotometry are reported in figure 3.9.

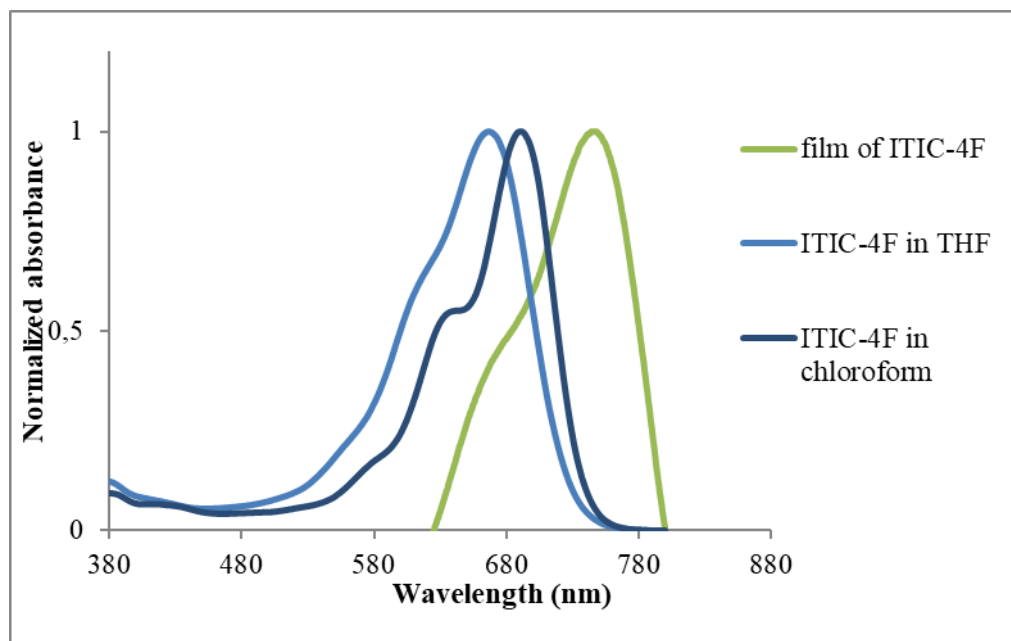


Figure 3.9: Normalized absorption spectra of ITIC-4F in $CHCl_3$, THF and in solid film.

It is possible to observe a left shift from the solid film spectrum to the spectra of the solutions. The molecule appears to be soluble in THF, which is the solvent that will be used in the nanoprecipitation procedure.

3.4. Nanoparticles elaboration

PTQ10 and ITIC-4F are going to be used to prepare nanoparticles which will lead to the production of laboratory-scale photovoltaic devices. The main purpose of these nanoprecipitation experiments is to obtain a sufficiently small dimension of the particles, in order to favor the interaction of the two photoactive substances, once they will be mixed; therefore, the focus is on obtaining the smallest possible diameter. The first experiments regard the preparation of nanoparticles containing only PTQ10, which is a much bigger molecule compared to ITIC-4F: it is probable that it will determine mainly the final size of nanoparticles. After reaching an optimal procedure and result for PTQ10 nanoparticles, composite nanoparticles will be prepared. As explained in detail in paragraph 2.12, solvent for PTQ10 is THF, and the nanoprecipitation is carried out using water and the surfactant Pluronic F127. In the following paragraphs, the correlation between the various parameters of the procedure and the size distribution of the nanoparticles obtained is shown.

The average diameters of the distributions are always calculated with the equation:

$$Dm = 2 \cdot \frac{\sum(Ri \cdot ni)}{\sum ni}$$

The dispersion values are calculated with the following equation:

$$\sigma = 2 \cdot \sqrt{\frac{\sum(Ri - Rm)^{2ni}}{\sum ni}}$$

3.4.1. Influence of the solubilization temperature of PTQ10 in THF

The solubility of PTQ10 in THF seemed difficult at ambient temperature: in fact, the polymer is in the form of thin but resistant foils, and the stirring was not sufficient to obtain a uniform solution. The solubilization was performed both at 45°C and 85°C. Since the T_{eb} of THF is 66°C, the heating must be done in a small Schlenk tube, in order to let the fluid evaporate, condensate and recirculate inside the Schlenk. Moreover, air was replaced completely with Argon. Results reported in table 3.2 and compared in figure 3.10 were obtained by preparing the nanoparticles following the same procedure, but using in the first case the solution solubilized at 45°C and in the other case the solution solubilized at 85°C in each couple of results, and changing the ratio between the THF solution and the aqueous solution.

Table 3.2: influence of solubilization temperature. Nanoprecipitation key parameters and DLS results.

Sample	Ratio (Vorg:Vaq)	T solubilization (°C)	T nanoprecip. (°C)	T evaporation (°C)	Average diameter (nm)	Dispersion (nm)
CC012	1 : 2	85	60	66	1121	3032
CC013		45			609	403
CC024	1 : 2	85			1453	198
CC028		45			2345	1367
CC025	1 : 4	85			1963	979
CC029		45			2585	2519
CC026	1 : 8	85			2148	633
CC030		45			1799	1704
CC027	1 : 16	85			1677	541
CC031		45			1091	734

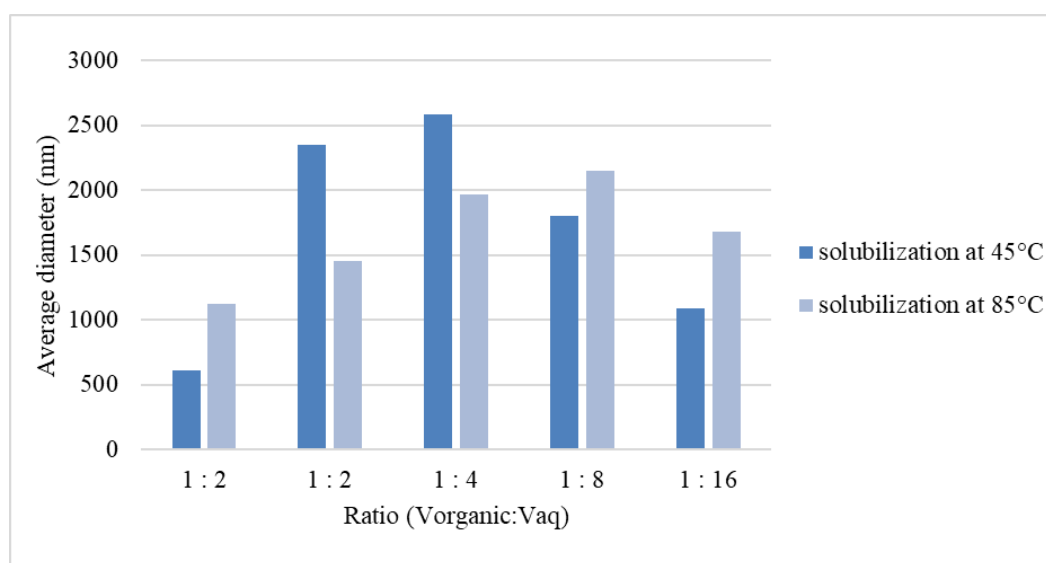


Figure 3.10: influence of solubilization temperature on nanoparticles size. Average diameter of particles in samples from CC012 to CC031.

Comparing how the average diameter of the nanoparticles changes as a function of the two different temperatures, it can be said that the results are devious. In fact, there seems to be no univocal relation between the two variables. Since no improvement or strong correlation is found, it can be concluded that the temperature of solubilization of the polymer in THF is not a determining parameter for the size of the nanoparticles. The solubilization at 45°C for one night appears to be sufficient; a higher temperature of solubilization is not necessary.

3.4.2. Influence of ratio between organic solvent and aqueous solution (Vorg:Vaq)

In order to find the optimal ratio between the volume of THF solution and the volume of H₂O with Pluronic F127 solution, a series of experiments were carried out. In the procedure, the ratio was changed from 1:2 to 1:16; the other parameters were maintained constant and the experiments were done using the solution solubilized at 45°C and at 85°C. Results are reported in table 3.3.

Table 3.3: influence of ratio between organic solvent and aqueous solution (Vorg:Vaq). Nanoprecipitation key parameters and DLS results.

Sample	Ratio (Vorg:Vaq)	T solubilization (°C)	T nanoprecipitation (°C)	T evaporation (°C)	Average diameter (nm)	Dispersion (nm)		
CC024	1 : 2	85	60	66	1453	198		
CC025	1 : 4				1963	979		
CC026	1 : 8				2148	633		
CC027	1 : 16				1677	541		
CC028	1 : 2	45					2345	1367
CC029	1 : 4				2585	2519		
CC030	1 : 8				1799	1704		
CC031	1 : 16				1091	734		

The correlation between the ratio and the average size of the particles can be observed in figures 3.11 and 3.12; there is firstly a slight growth and then a slight degrowth of the size. Of course, the ratios that contain more aqueous solution are less interesting and less desirable, because the polymeric nanoparticles suspension will be more diluted. It is possible to conclude that the ratio 1:2 is a favorable option, because this preparation provides the highest concentration of the polymer, and the size of the nanoparticles is not too disadvantaged and not too big.

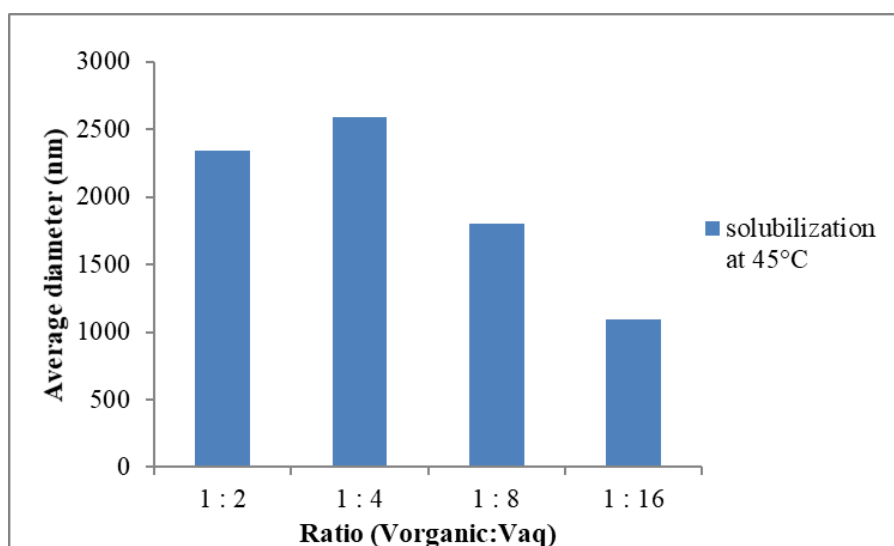


Figure 3.11: influence of ratio between organic solvent and aqueous solution (Vorg:Vaq). Average diameter of particles in samples from CC024 to CC027.

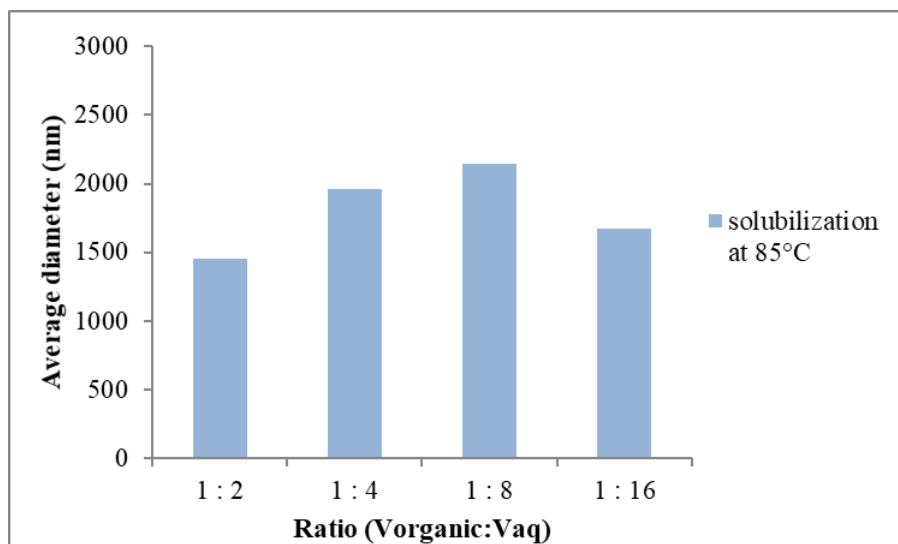


Figure 3.12: influence of ratio between organic solvent and aqueous solution (Vorg:Vaq). Average diameter of particles in samples from CC028 to CC031.

3.4.3. Influence of surfactant

To check the validity of the choice of the surfactant type and its concentration, nanoprecipitation experiments were carried out changing the concentration of Pluronic F127 firstly and replacing the Pluronic with the Sodium Dodecyl Sulfate (SDS) secondly. The SDS is another surfactant widely used in the preparation of nanoparticles with organic solvents.

Table 3.4: Influence of surfactant. Nanoprecipitation key parameters and DLS results of sample from CC041 to CC043.

Sample	Surfactant	Concentration (mg/ml)	Ratio (Vorg:Vaq)	T nanoprecip. (°C)	T evaporation (°C)	Average diameter (nm)	Dispersion (nm)
CC041	Pluronic F127	20	1 : 2	66	66	1475	108
CC042	Pluronic F127	10				>1 μ m	x
CC043	SDS	16				>1 μ m	x

The convenience of the utilization of Pluronic F127 20 mg/ml was confirmed. From table 3.4, it is possible to see that lowering the concentration from 20 mg/ml to 10 mg/ml led to the formation of big particles, visible to the naked eye, and unmeasurable with the DLS. The use of SDS 16 mg/ml led to the same outcome: much bigger particles compared to the initial experiment with Pluronic F127 20 mg/ml. For this reason, the concentration of Pluronic of 20 mg/ml was continued to be used for the following experiments.

After optimizing other parameters of the procedure for the formation of nanoparticles, the influence of the surfactant was investigated again. Table 3.5 contains parameters and results of experiments that have been done some weeks after table 3.4 (as the number of the samples can confirm) when other modifications, like the ultrasonication and the evaporation with Argon, were implemented, this is why the average diameter observable in table 3.5 is lower compared to the one in table 3.4.

Table 3.5: Influence of surfactant. Nanoprecipitation key parameters and DLS results of samples from CC093 to CC096.

Sample	Surfactant	Concentration (mg/ml)	T nanoprecip. (°C)	Evaporation	Ultrasonication	Av. diameter (nm)	Dispersion (nm)
CC093	Pluronic F127	18 mg/ml	Tamb	Argon	2 min	295	45
CC096	Pluronic F127	20 mg/ml				303	55
CC094	Pluronic F127	22 mg/ml				339	75

Looking at table 3.5 and at figure 3.13, it is noticeable that, in this range of concentrations, the size of the particles increases with the increase of surfactant concentration. The dispersion of the size distribution also increases in the same direction. The difference in size between the two lower concentrations is very slight, it is a difference of 8 nm (and the relative difference is 2.6% in percentage); in any case, it is possible to state that a concentration of 18 mg/ml appears to be more favorable for the obtainment of smaller particles, considering also the fact that an overall lower amount of surfactant to be removed in the dialysis step is an advantage for the final use of the nanoparticles.

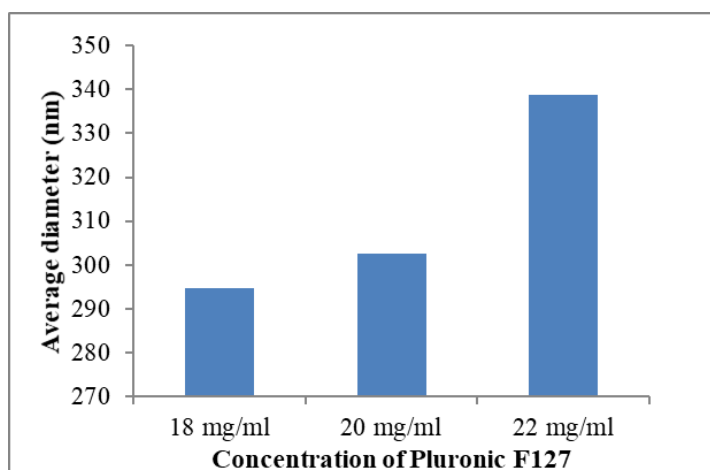


Figure 3.13a: Influence of surfactant. Average diameter of particles in samples from CC093 to CC096.

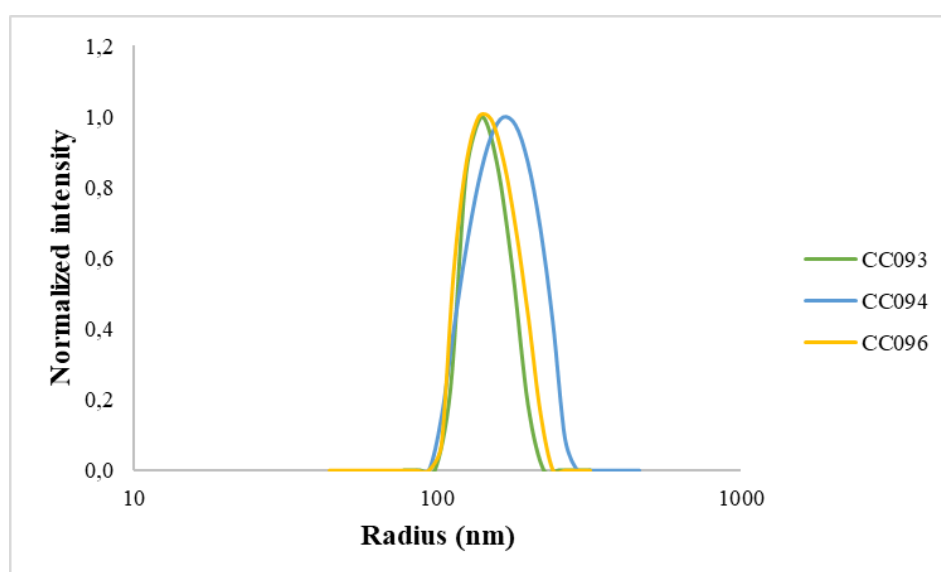


Figure 3.14b: Influence of surfactant. Size distribution curves from DLS results of samples from CC093 to CC096.

3.4.4. Influence of sonication

Sonication (and ultrasonication, which uses higher frequencies), are procedures often used in the preparation of nanoparticles with the nanoprecipitation and miniemulsion techniques. They consist in applying sound energy to the sample to agitate the particles, which helps in creating a suspension and in obtaining smaller particles.

In the experiments from CC038 to CC041, we tried to compare the effect of the sonicator on the nanoparticles in the samples, and we also tried a nanoprecipitation made by mixing the two solutions at a slower rate, dropwise.

Table 3.6: influence of sonication. Nanoprecipitation key parameters and DLS results of samples CC038 to CC041.

Sample	T nanoprecipitation (°C)	T evaporation (°C)	Average diameter (nm)	Dispersion (nm)	Notes
CC038	66	66	9263	15406	sonication bath before nanoprecipitation
CC039			5186	3851	nanoprecipitation drop by drop at 66°C
CC040			750	82	sonication bath after nanoprecipitation
CC041			1475	108	no sonication

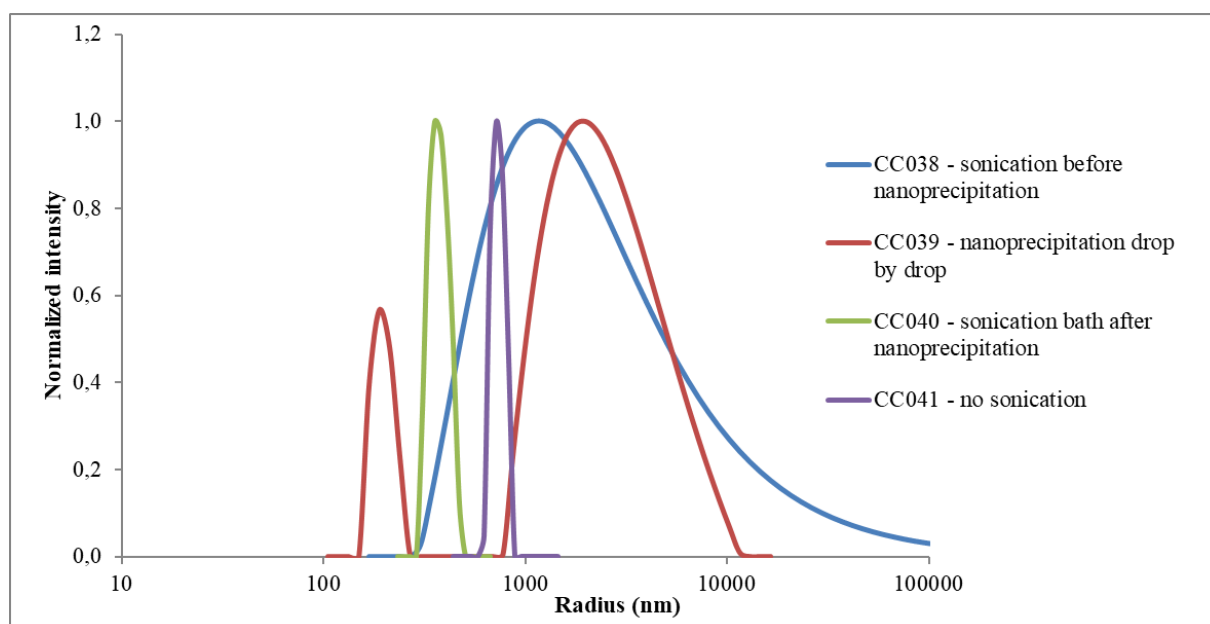


Figure 3.15: influence of sonication. Size distribution curves from DLS results of samples from CC038 to CC041.

In figure 3.14 it is possible to observe that the suspension of sample CC038, in which the sonicator was used just before the nanoprecipitation, has a bigger average diameter compared

to the one of sample CC041, in which the sonicator was not used; this suggests that applying the sonication step before proceeding with the nanoprecipitation has no positive effects. The opposite can be stated for sample CC040, in which sonication was used after nanoprecipitation. It has a smaller average diameter and the distribution of the particles population is narrower. Therefore, the energy given to the particles in the sonication step, after the nanoprecipitation, favors the formation of smaller particles. With respect to sample CC039, it was prepared by adding the THF solution to the aqueous solution slowly, 1 drop per second, it is evident that this procedure did not lead to a desirable distribution of the size of the nanoparticles. The rapid addition of one solution to the other remains a better option.

In the experiments from CC045 to CC049, reported in table 3.7, the effects of sonication were further examined, in some cases in similar condition, in order to confirm the previous results. This time the ultrasonication was investigated as well, in the procedure.

Table 3.7: influence of sonication and ultrasonication. Nanoprecipitation key parameters and DLS results of samples CC045 to CC049.

Sample	T nanoprecip. (°C)	T evaporation (°C)	Average diameter (nm)	Dispersion (nm)	Notes
CC045	Tamb	66	2839	1988	no sonication
CC046			2368	8363	sonication bath during nanoprecipitation
CC047			363	108	sonication bath during nanoprecipitation and then ultrasonication
CC048			2753	9126	sonication bath after nanoprecipitation
CC049			384	215	sonication bath after nanoprecipitation and then ultrasonication

It is very interesting, and very easy to notice from figure 3.15 that shows the results of the DLS, to observe that there are important differences between the sample with no sonication, the ones with sonication and the ones with ultrasonication. The sample we did not submit to sonication has a distribution shifted to the right, to higher values of radii, in the order of 1 μm ; the two samples CC046 and CC048, submitted only to sonication, have a peak shifted to the left, but a long tail showing the presence of big particles as well; the samples CC047 and CC049, which were submitted to sonication and subsequently to ultrasonication, have the peak shifted to the left, to smaller values of radii, in the order of 100 nm, and the distribution does not arrive to high values of radii. The ultrasonication is certainly an important parameter in the preparation of the nanoparticles, since it permits to form smaller particles, with a uniform distribution.

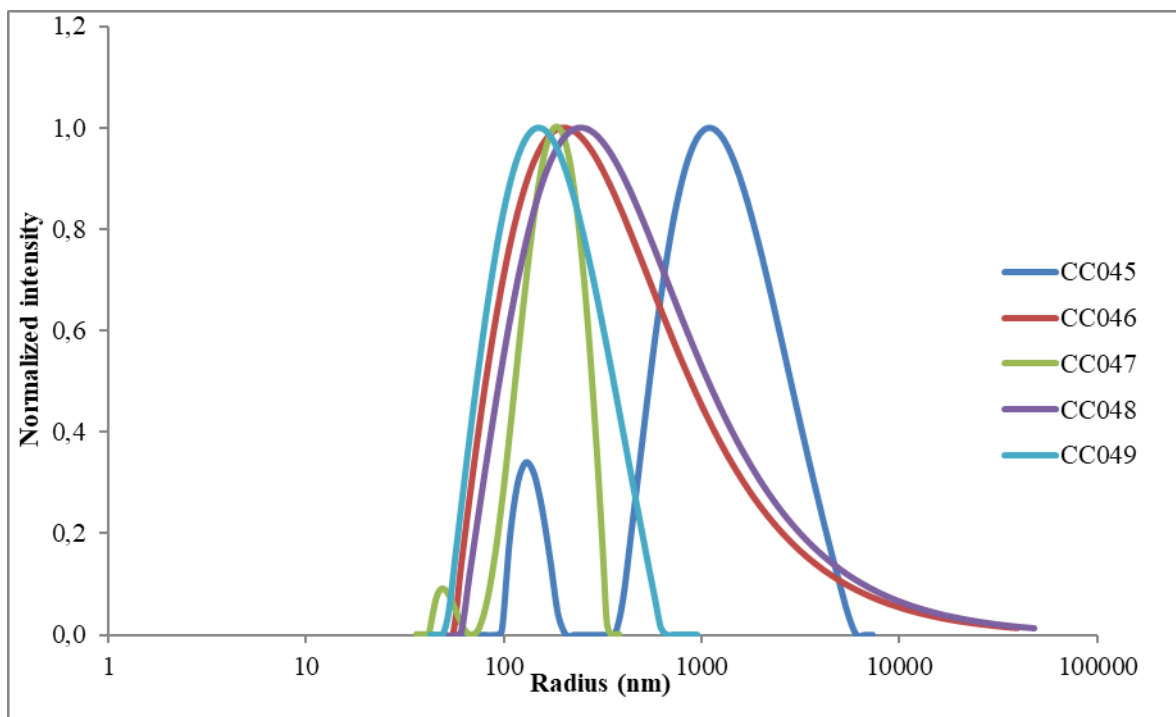


Figure 3.16: influence of sonication and ultrasonication. Size distribution curves from DLS results of samples CC045 to CC049.

3.4.5. Influence of temperature of nanoprecipitation

The most favorable temperature of the polymeric solution in THF and the aqueous phase at the moment of mixing them is a key variable. Until the moment the experiments were done at high temperatures, most of the time at 66°C: the effects of lowering the temperature to room temperature were then investigated. This had the advantage of making the procedure a bit simpler: the mix of the two solutions was done on the stirring plank instead of the sand bath. In table 3.8 are reported the results of two experiments made at room temperature and of two experiments made at approximately 66°C; the precise values of temperature, measured with a probe thermometer, are reported as well.

Table 3.8: influence of nanoprecipitation temperature. Nanoprecipitation key parameters and DLS results of samples CC045 to CC049.

Sample	T nanoprecip. (°C)	T nanoprecip. measured (°C)	Average diameter (nm)	Dispersion (nm)	Notes
CC050	Tamb	22,3	536	27	ultrasonication
CC051	Tamb	22,4	381	43	sonication bath during nanoprecipitation, ultrasonication
CC052	66°C	59	516	81	ultrasonication
CC053	66°C	59	529	21	sonication bath after nanoprecipitation, ultrasonication

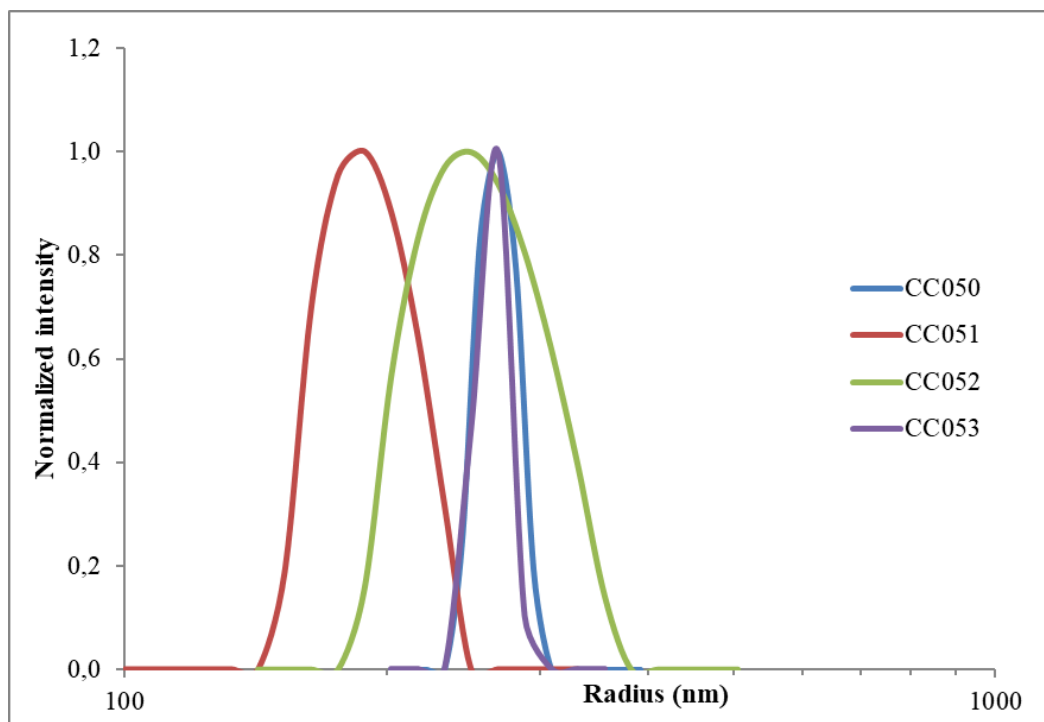


Figure 3.17: influence of nanoprecipitation temperature. Size distribution curves from DLS results of samples CC045 to CC049.

The conclusion is that performing the nanoprecipitation at 66°C is not a favorable condition: in fact, better results are obtained at room temperature. In particular, in experiment CC051 the sample was inside the sonication bath during the addition of one solution to the other, the fact that the sonication bath contains water at room temperature may have provided a refrigeration during the nanoprecipitation phenomenon (which is exothermic), and the effect on particles size seems positive: particles have an average diameter of 381 nm. In the following experiments, the nanoprecipitation is carried out with solutions at room temperature.

3.4.6. Influence of the evaporation procedure

The evaporation procedure can strongly affect the dimensions of the nanoparticles. In the previous samples, evaporation of THF was performed by heating the sample in a sand bath at the boiling temperature of THF ($T_{eb}=66^{\circ}\text{C}$), which was a quick and efficient method. As is reported in the publication by C. Xie², THF can be evaporated by blowing Argon in the vial, with a needle, in order to avoid heating the suspension. The aim of the experiments from CC055 to CC057 is to verify if the heat is cause of destabilization and aggregation of the nanoparticles, since the stability of Pluronic F127 (and so of the suspension) depends strongly on temperature.

Table 3.9: influence of evaporation procedure. Nanoprecipitation key parameters and DLS results of samples CC055 to CC057.

Sample	T nanoprecip. (°C)	Evaporation	Average diameter (nm)	Dispersion (nm)	Notes
CC055	Tamb	Argon	407	94	evaporation with Argon
CC056	Tamb	Argon	352	54	evaporation with Argon
CC057	Tamb	27°C	542	27	evaporation with heat (27°C)

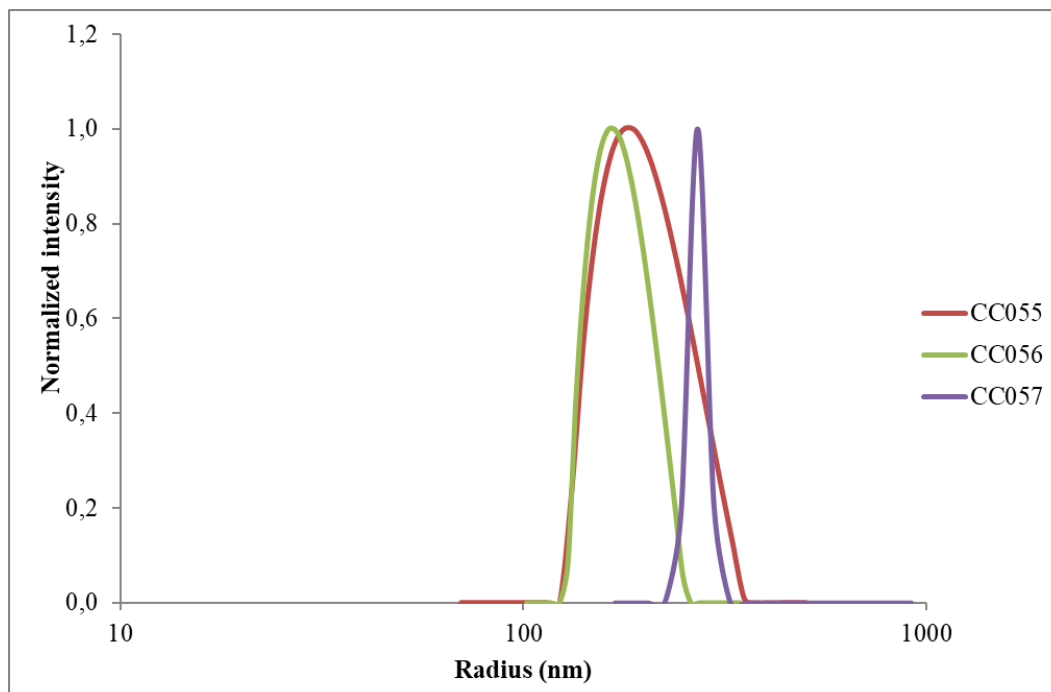


Figure 3.18: influence of evaporation procedure. Size distribution curves from DLS results of samples CC055 to CC057.

It is possible to observe from table 3.9 and the curves in figure 3.17 that the two experiments in which Argon was used led to the reach of an average diameter between 350 and 400 nm, a very interesting result. In the same set of experiments an attempt was also made to decrease the temperature of evaporation to 27°C, enlarging the evaporation time; overall, the average size of the particles formed did not show an improvement. In table 3.10, these results are compared with the previous, to appreciate the variation of the dimensions obtained with the two different methods.

Table 3.10: influence of evaporation procedure. Nanoprecipitation key parameters and DLS results of samples CC050 to CC057.

Sample	T nanoprecip. (°C)	Evaporation	Average diameter (nm)	Dispersion (nm)	Notes
CC050	Tamb	66°C	536	27	evaporation with heat (66°C)
CC052	66°C	66°C	516	81	evaporation with heat (66°C)
CC055	Tamb	Argon	407	94	evaporation with Argon
CC056	Tamb	Argon	352	54	evaporation with Argon
CC057	Tamb	27°C	542	27	evaporation with heat (27°C)

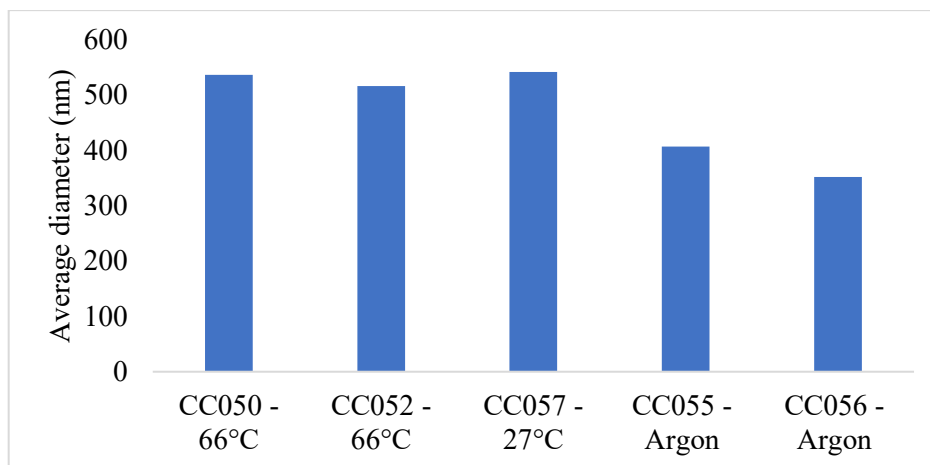


Figure 3.19: influence of evaporation procedure. Comparison among average diameter in samples CC050 to CC057.

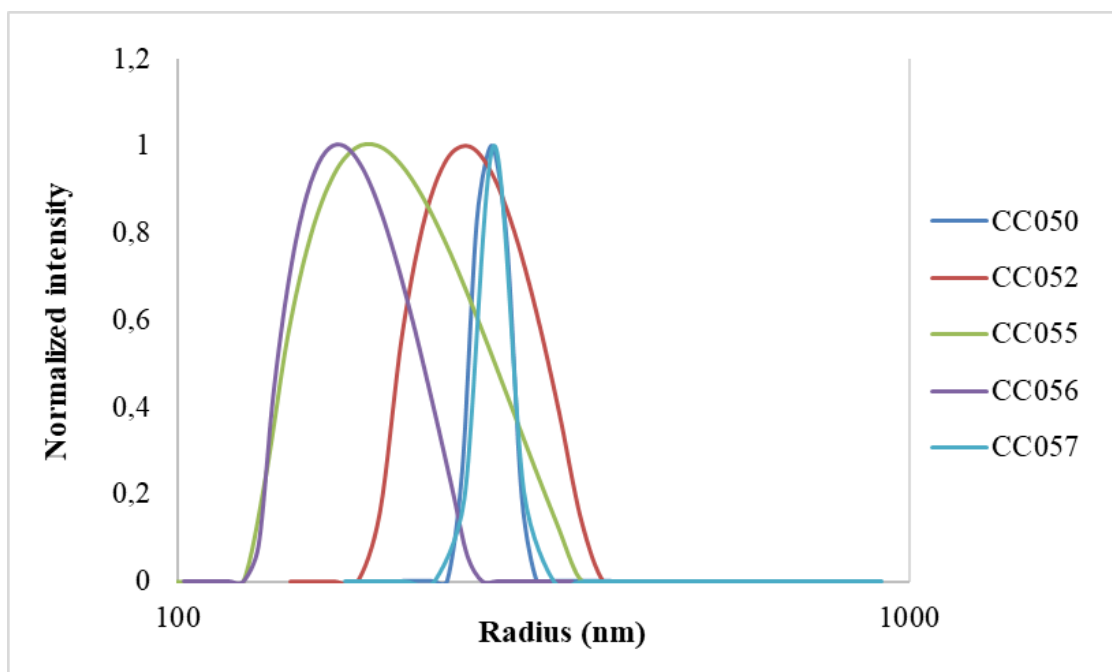


Figure 3.20: influence of evaporation procedure. Size distribution curves from DLS results of samples CC050 to CC057.

From the graphic in figure 3.19 it is possible to observe that samples CC055 and CC056, in which evaporation of THF was carried out without using heat, give a size distribution shifted to smaller values of radii. Thus, these are the most interesting results for the scope of the work, and the most practical procedure for evaporation is Argon blowing.

3.4.7. Influence of ultrasonication time

In the previous experiments the ultrasonication time was 1 minute for all the samples, at an amplitude of 40%, with 3 seconds ON and 2 seconds OFF. It is now worthwhile to analyze the effects of an increase of the ultrasonication time, keeping the other parameters constant. The experiments of nanoprecipitation were, in this case, performed using ITIC-4F, in order

to verify that the same procedure used for PTQ10 is valid also with this material, apart from studying the effects of an increase in ultrasonication time.

Table 3.11: influence of ultrasonication time. Nanoprecipitation key parameters and DLS results of samples CC058, CC059, CC070.

Sample	Molecule	Conc. (mg/ml)	T nanoprecip (°C)	Evaporation	Ultrasonication	Average diameter (nm)	Dispersion (nm)
CC058	ITIC-4F	1	Tamb	Argon	1 min	186	90
CC059					2 min	171	80
CC070					3 min	149	69

An increase in ultrasonication time appears to influence the size of the nanoparticles: the smallest particles are obtained with 3 minutes of ultrasounds; the standard dispersion of the population also decreases with the increasing of time. (Figure 3.20)

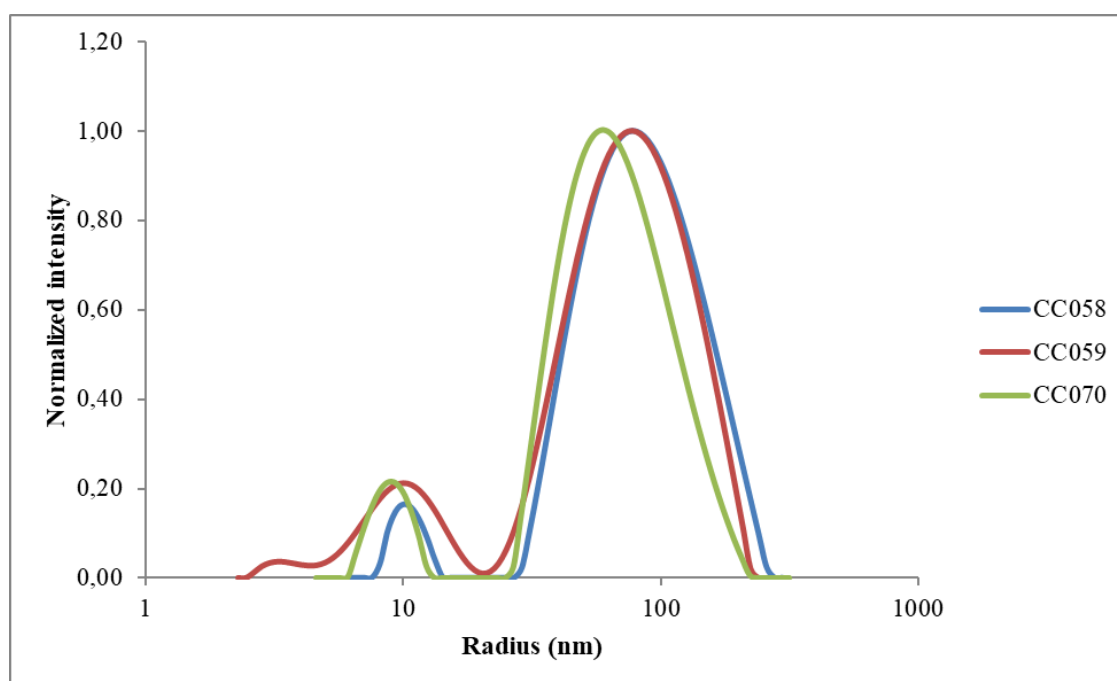


Figure 3.21: influence of ultrasonication time. Size distribution curves from DLS results.

3.4.8. Variation of nanoprecipitation temperature

The procedure for nanoprecipitation encloses now an ultrasonication step and evaporation with Argon and is done at room temperature. In experiments CC095 to CC097 the temperature of the two solvents mixed in nanoprecipitation was varied from 10°C to 30°C, a range close to ambient temperature, which was approximately 20°C. Table 3.12 shows the results of these experiments.

Table 3.12: variation of nanoprecipitation temperature. Nanoprecipitation key parameters and DLS results of samples from CC095 to CC097.

Sample	Molecule	T nanoprecip (°C)	Evaporation	Ultrasonication	Average diameter (nm)	Dispersion (nm)
CC095	PTQ10	10	Argon	2 min	288	27
CC096		20			303	55
CC097		30			339	139

A slight amelioration of the size was obtained decreasing the temperature to 10°C: the diameter of PTQ10 nanoparticles reaches 288 nm in this condition. With the decreasing of temperature in this range, there is a decreasing of particles size and of dispersion.

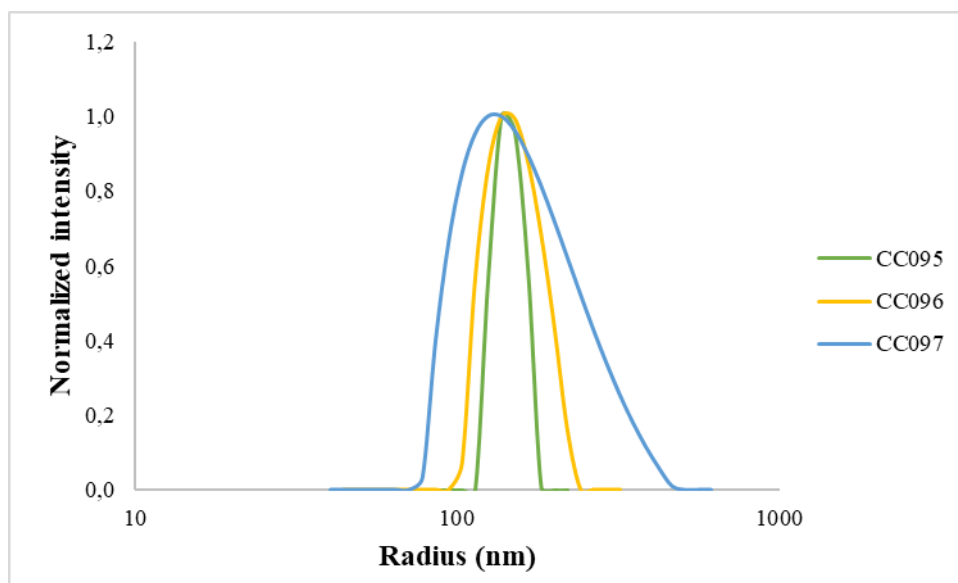


Figure 3.22: variation of nanoprecipitation temperature. Size distribution curves from DLS results.

3.5.Composite nanoparticles

After reaching a satisfying result for the preparation of PTQ10 nanoparticles, composite nanoparticles containing a donor and acceptor mixture in equal weight were prepared, using the best performing procedure until the moment. THF solution contains 0.5 mg/ml PTQ10 and 0.5 mg/ml ITIC-4F, making a total concentration of 1 mg/ml of active material. The experiment was performed two times, in the same conditions. Results are reported in table 3.14. With this procedure we prepared nanoparticles containing both the donor polymer and the acceptor molecule, as can be observed from table 3.13 and figure 3.21, the average diameter of the nanoparticles is 368 nm in one case and 409 nm in the other.

Table 3.13: Composite nanoparticles preparation. Nanoprecipitation key parameters and DLS results of samples CC060 and CC061.

Sample	Molecules	Total conc. (mg/ml)	T nanoprecip (°C)	Evaporation	Ultrasonication	Average diameter (nm)	Dispersion (nm)
CC060	PTQ10 + ITIC-4F	1	T amb	Argon	2 min	368	163
CC061						409	180

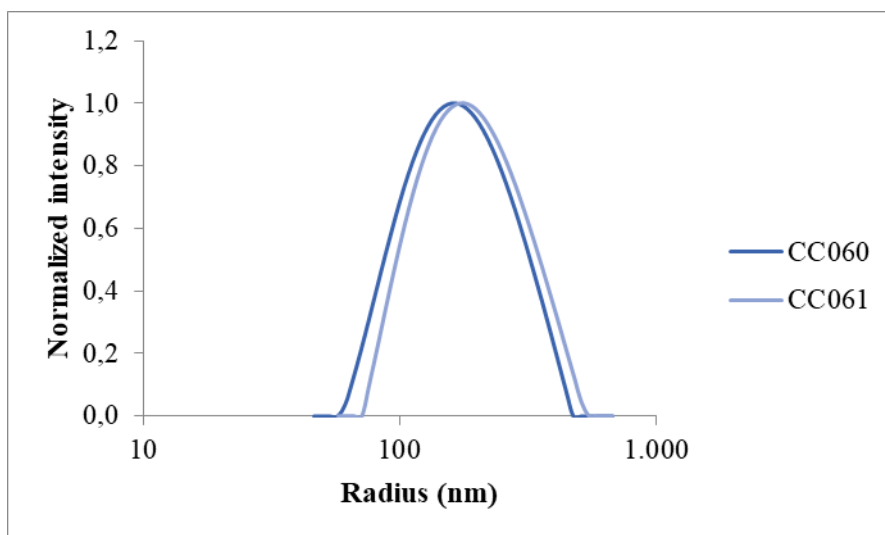


Figure 3.23: Composite nanoparticles preparation. Size distribution curves from DLS results of samples CC060 and CC061.

Subsequently, nanoparticles containing different ratios of the two molecules were prepared, with the same procedure. In table 3.14, the ratios and the concentrations are listed, together with the results of the DLS: average diameter and dispersion of the distribution. The size of the particles decreases with the rise of ITIC-4F concentration, with pure PTQ10 or ITIC-4F nanoparticles the diameter is the same obtained in the previous tests, when the two molecules are present in equal weight, which is the condition required for the active layer, the average diameter is 300 nm.

Table 3.14: Composite nanoparticles with different ratios of PTQ10:ITIC-4F. Nanoprecipitation key parameters and DLS results of samples from CC062 and CC070.

Sample	Ratio PTQ10:ITIC-4F	PTQ10 (mg/ml)	ITIC-4F (mg/ml)	Average diameter(nm)	Dispersion (nm)
CC062	1 : 0	1	0	598	410
CC063	8 : 2	0,8	0,2	503	349
CC064	7 : 3	0,7	0,3	333	102
CC065	6 : 4	0,6	0,4	330	86
CC066	5 : 5	0,5	0,5	300	70
CC067	4 : 6	0,4	0,6	322	176
CC068	3 : 7	0,3	0,7	268	93
CC069	2 : 8	0,2	0,8	244	114
CC070	0 : 1	0	1	149	69

The results of DLS are reported in figures 3.22 and 3.23.

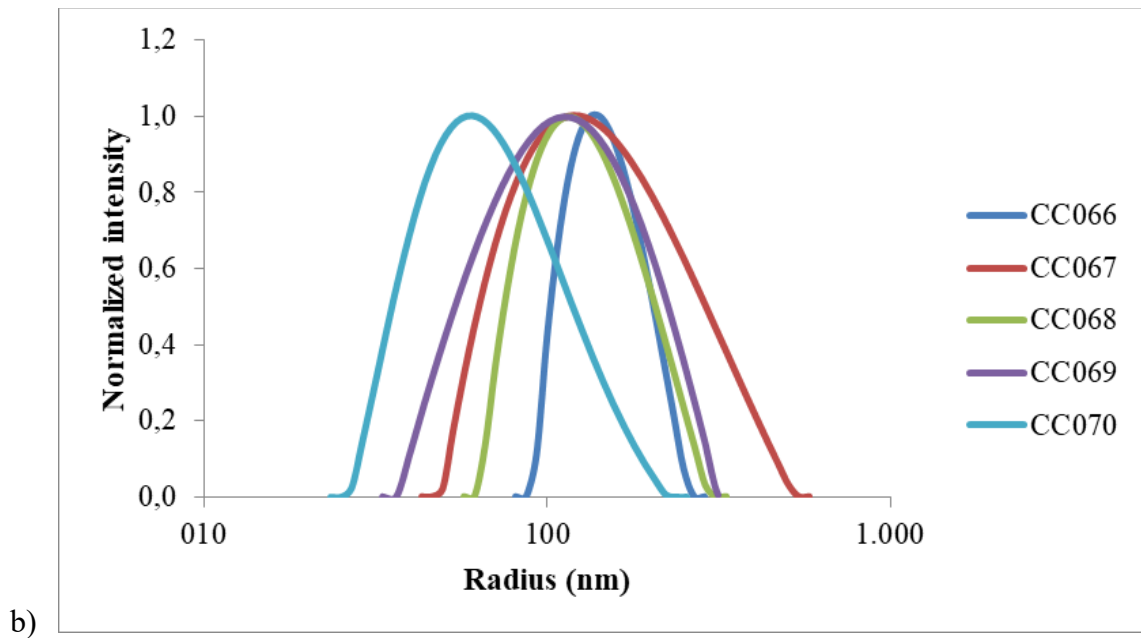
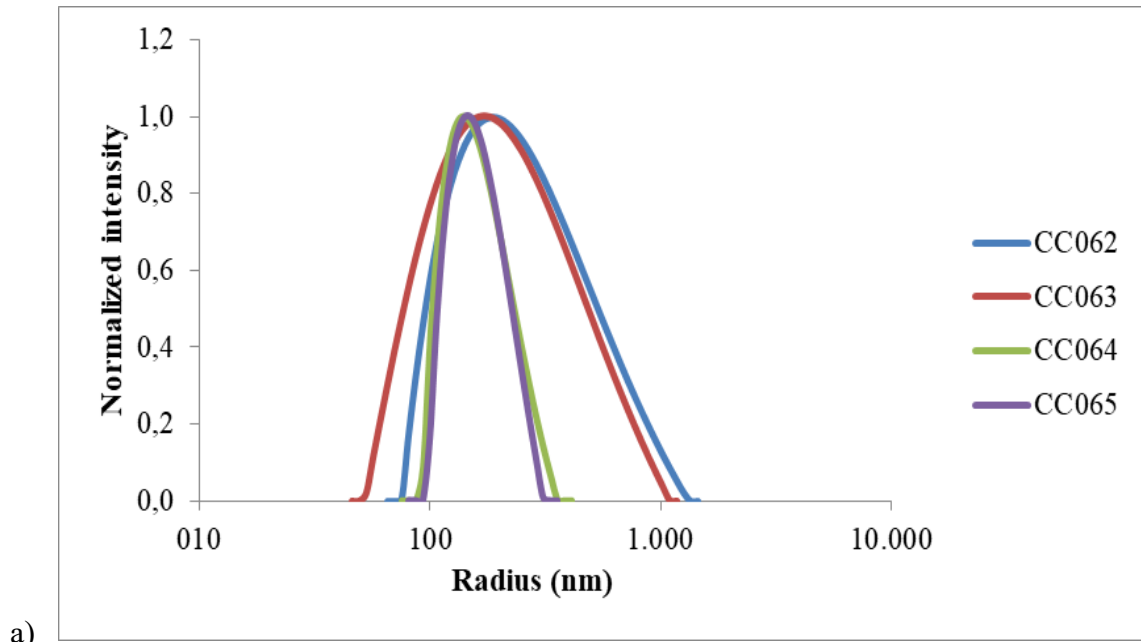


Figure 3.24 a) and b): size distribution curves from DLS results of samples from CC062 to CC070.

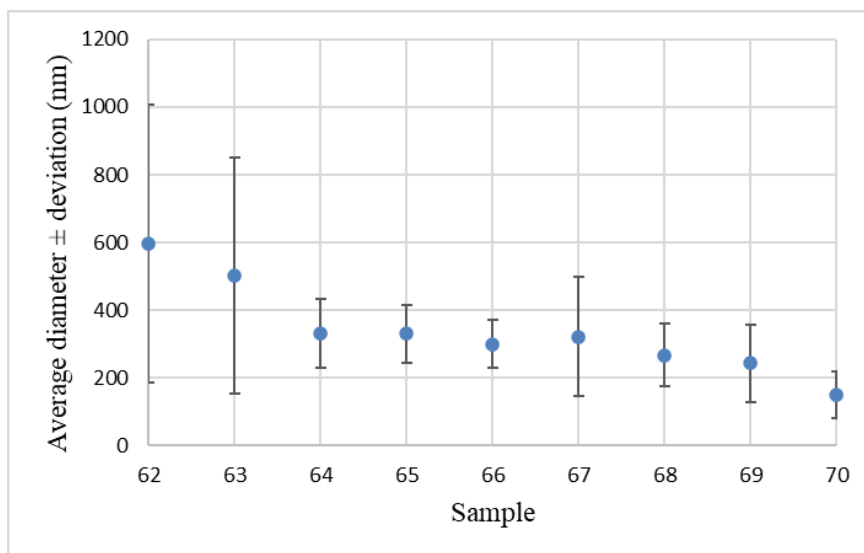


Figure 3.25: Average diameter and deviation of nanoparticles in samples from CC062 to CC070.

3.5.1. Stability of suspension

After three weeks from the preparation of the suspension CC061, the measurement of the dimension of the particles via DLS was repeated in order to study the stability of the suspension over time. The presence of surfactant Pluronic F127 should guarantee stability to the nanoparticles.

Table 3.15: DLS results of sample CC061 after three weeks.

Sample	Average diameter (nm)	Dispersion (nm)
CC061	409	180
CC061-after three weeks	326	110

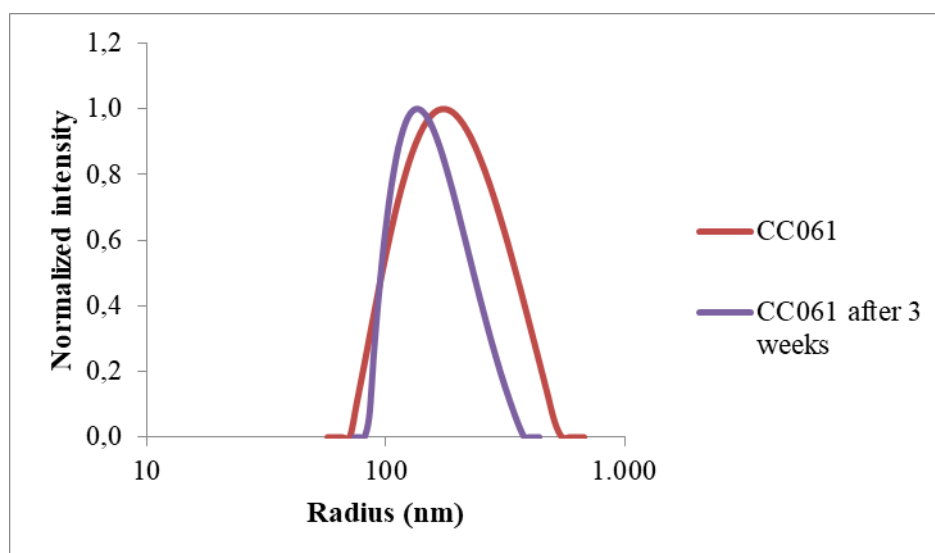


Figure 3.26: Size distribution curves from DLS results of sample CC061 after three weeks.

From the results showed in figure 3.24, it can be observed that the particles did not aggregate. There is no big difference in terms of average diameter and distribution, the little difference is attributable to statistical variations, the suspension with Pluronic is stable.

3.5.2. Stability of surfactant free suspension

Sample CC060, containing composite nanoparticles, was submitted to the process of surfactant removal; Pluronic F127 was removed by centrifuging the suspension with water in a filter. After this process, DLS measurement was repeated, to verify a change in particles dimension, if aggregation phenomena occurred.

Table 3.16: DLS results of sample CC060 without surfactant.

Sample	Average diameter (nm)	Dispersion (nm)
CC060	368	163
CC060-surfactant removed	364	179

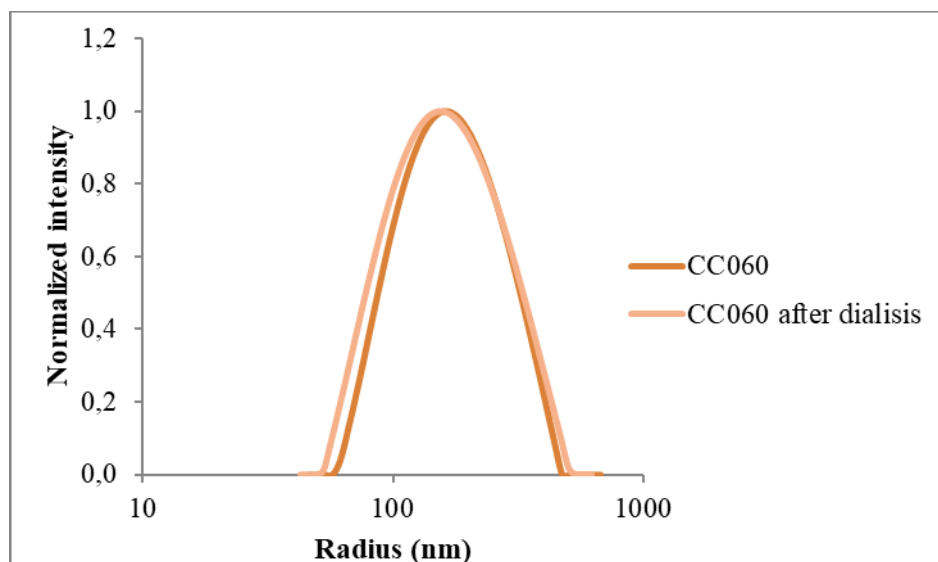


Figure 3.27: Size distribution curves from DLS results of sample CC060 with and without surfactant.

From the curves showed in figure 3.25, it can be observed that the particles did not aggregate. The two curves are almost equivalent; therefore, the surfactant-free suspension is stable.

3.5.3. Increase in concentration

Composite nanoparticles are going to be produced with the purpose of preparing a solid layer in an OPV device, for which a higher concentration of the two molecules present in the nanoparticles is needed. The suspension must be concentrated in all cases, so it is interesting to try to prepare a more concentrated initial solution.

Table 3.17: effect of increase in concentration. Nanoprecipitation key parameters and DLS results of sample CC072.

Sample	Molecules	Conc. (mg/ml)	T nanoprecip (°C)	Evaporation	Ultrasonication	Average diameter (nm)	Dispersion (nm)
CC072	PTQ10 + ITIC-4F	1mg/ml + 1mg/ml	Tamb	Argon	2 min	518	177

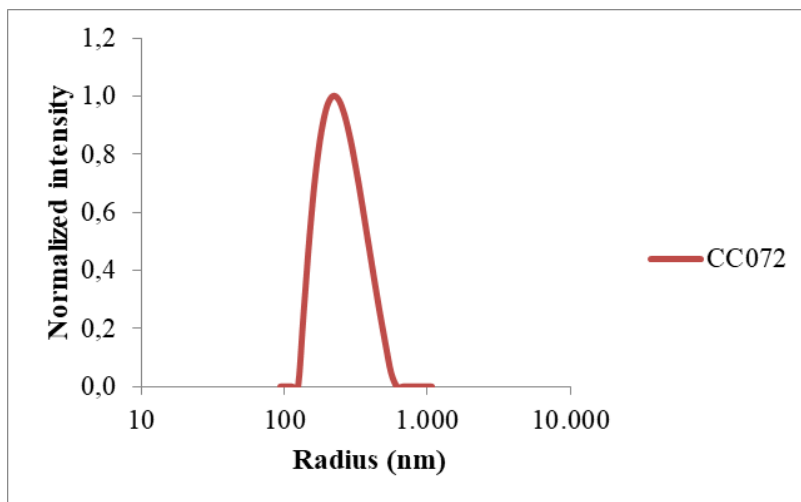


Figure 3.28: effect of increase in concentration. Size distribution curve from DLS results of sample CC072.

In this experiment, a total concentration of 2 mg/ml of PTQ10 and ITIC-4f in THF was used, the two materials having the same mass concentration. The obtained nanoparticles are bigger than in the others experiments with composite nanoparticles: the average diameter is 518 nm. This result implies that increasing the concentration of the molecules in THF solution has an impact on the size of nanoparticles; since the aim of this work is to prepare nanoparticles small enough, 1 mg/ml concentration is a better option, even if a quite low value.

3.6. Microscope images

Images obtained with Transmission Electron Microscope (TEM): composite nanoparticles of sample CC060 were observed with TEM, after removal of the surfactant, which would form a sort of film of Pluronic molecules, making the observing difficult. All samples were prepared with 0.05 mg/ml aqueous nanoparticles suspension on aluminum.

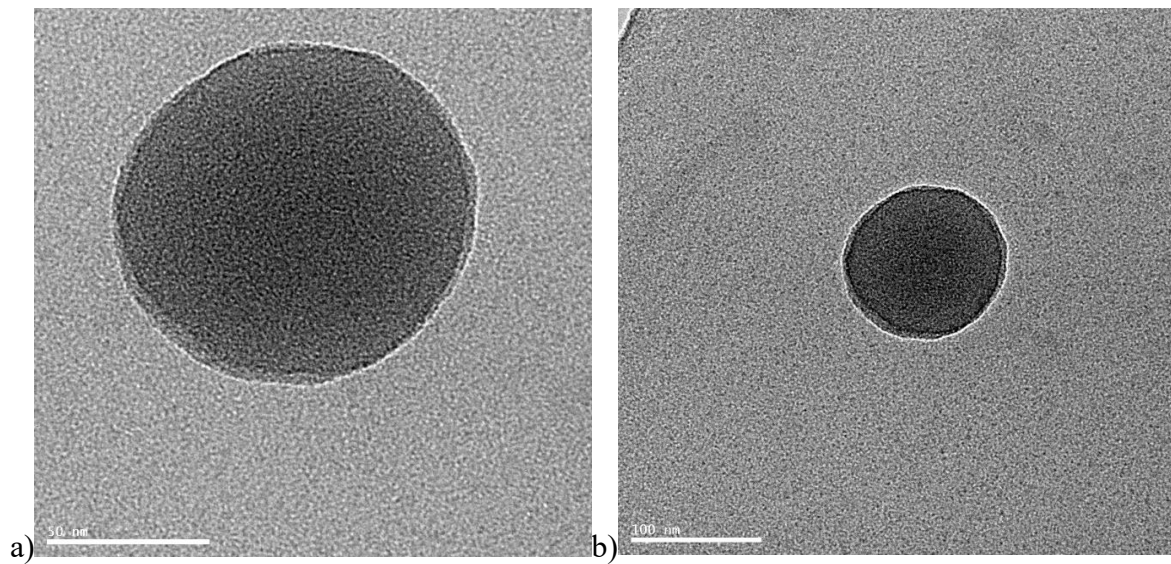


Figure 3.29a, b): TEM of dried PTQ10:ITIC-4F (1:1) nanoparticles. Round nanoparticle of 100 nm diameter, approximately.

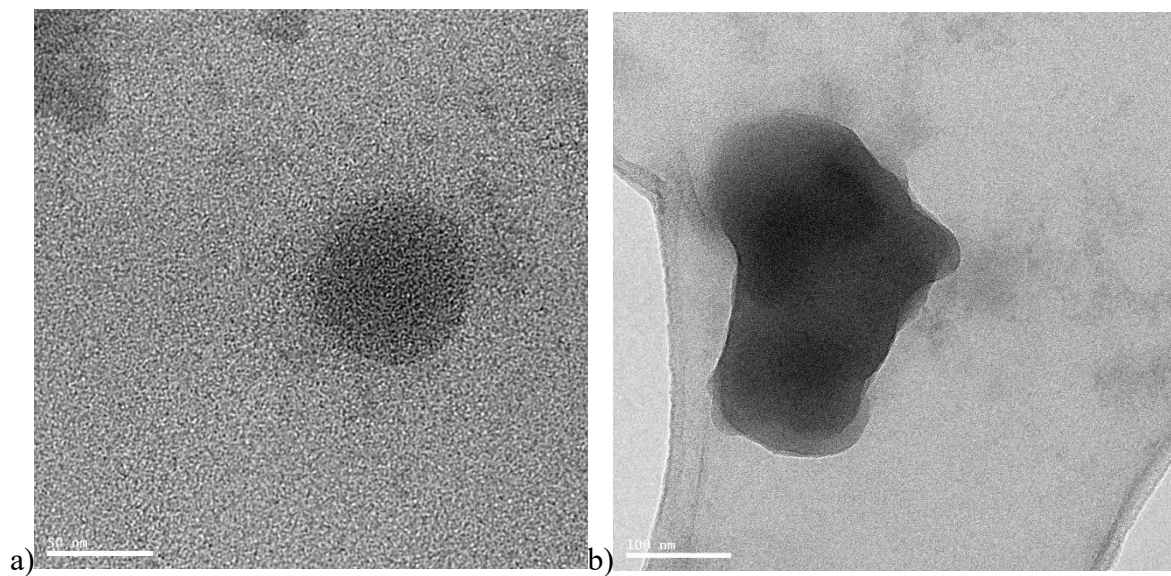


Figure 3.30: TEM of dried PTQ10:ITIC-4F (1:1) nanoparticles. a) small round nanoparticle b) flattened nanoparticle with irregular shape.

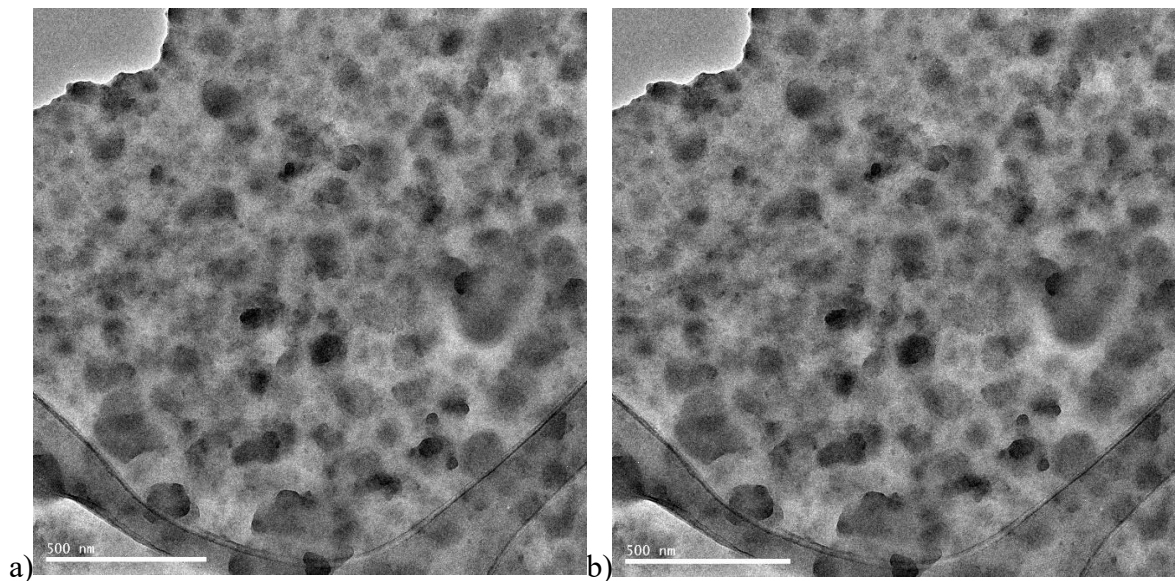


Figure 3.31a), b): TEM of dried PTQ10:ITIC-4F (1:1) nanoparticles. Cluster of nanoparticles.

Sample CC060 was also observed with Scanning Electron Microscope (SEM), thanks to which the external morphology of the nanoparticles is observable with more detail, together with the dimension.

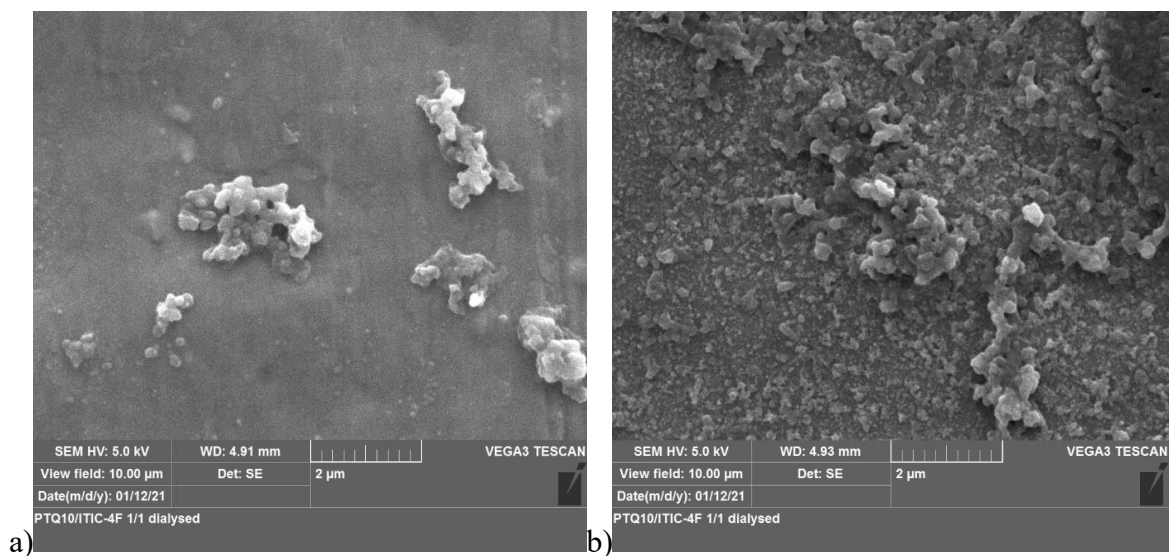


Figure 3.32: SEM of dried PTQ10:ITIC-4F (1:1) nanoparticles. View field, 10 μm.

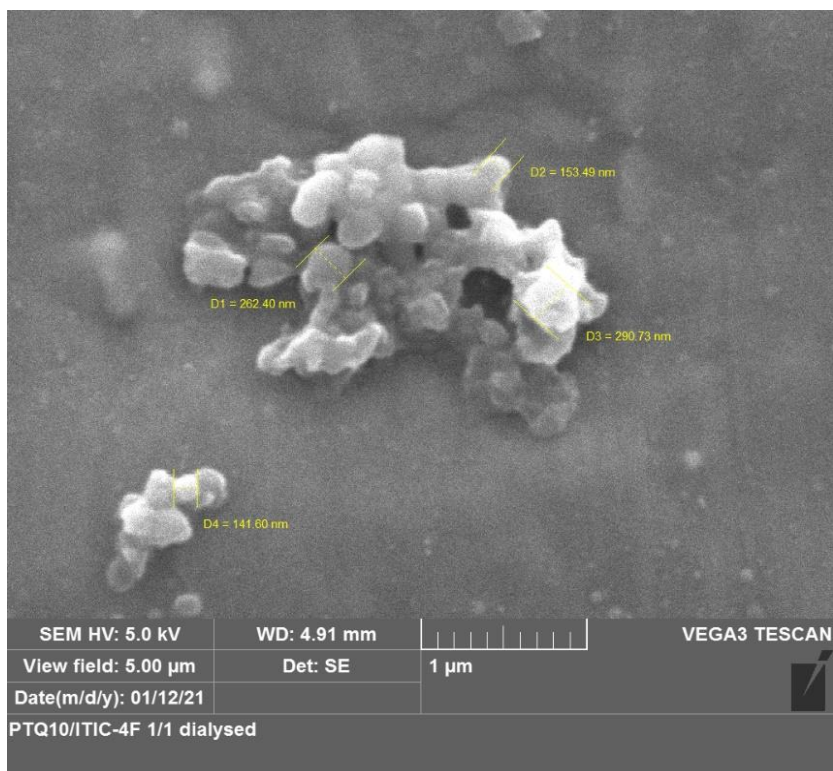


Figure 3.33: SEM of dried PTQ10:ITIC-4F (1:1) nanoparticles. View field, 5 μm.

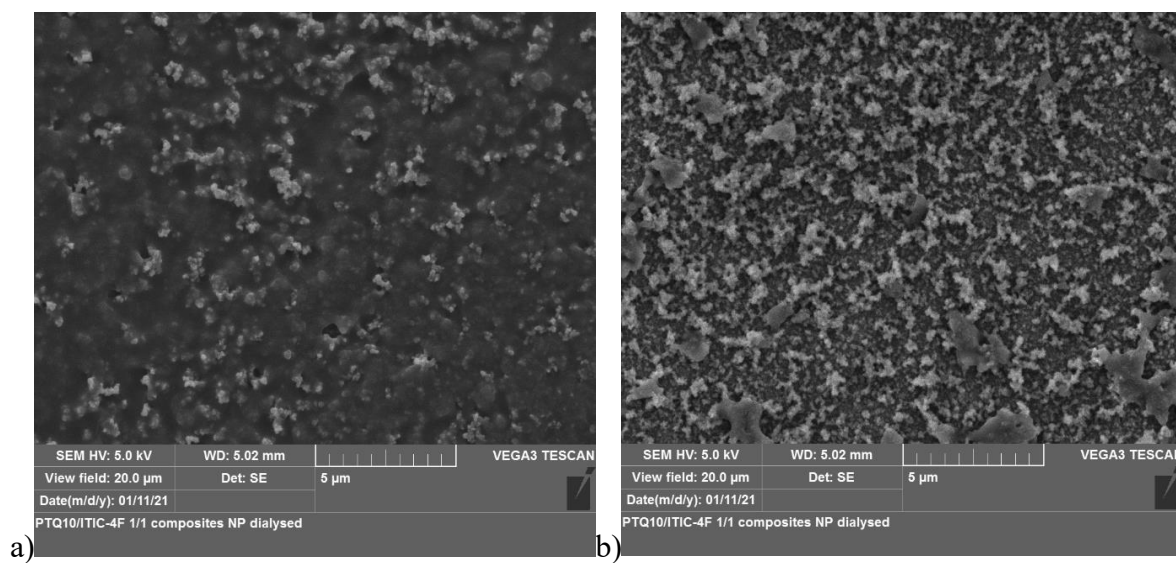


Figure:3.28a), b): SEM of dried PTQ10:ITIC-4F (1:1) nanoparticles. View field, 20 μm.

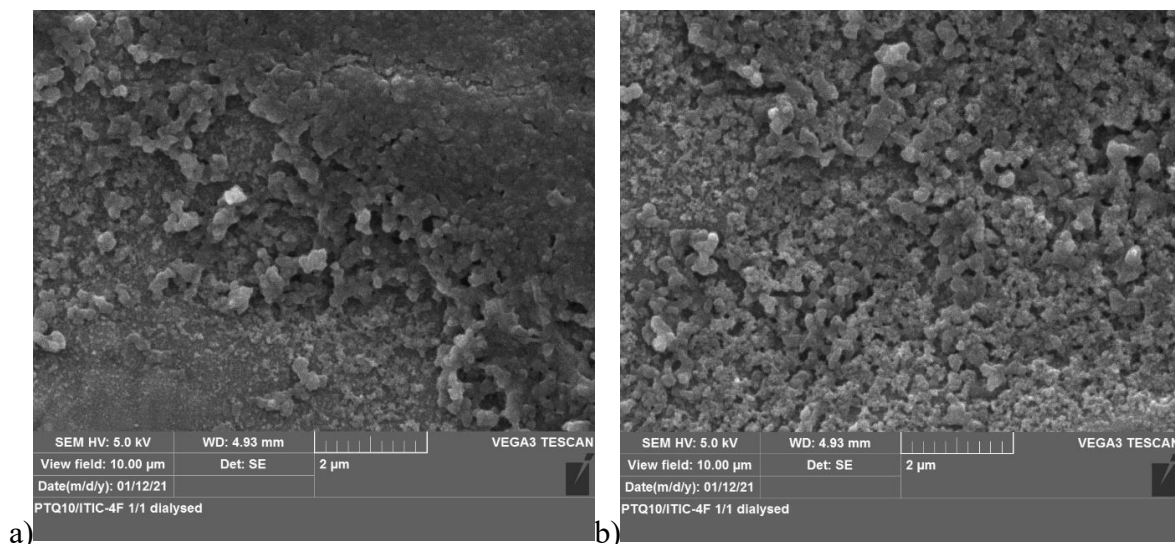


Figure 3.34: SEM of dried PTQ10:ITIC-4F (1:1) nanoparticles. View field, 10 μm .

3.7. Fluorescence

The fluorescence technique permits to verify the internal composition of the nanoparticles: while the techniques so far used (DLS, SEM, TEM) allowed to analyze the morphology of nanoparticles in terms of size and shape, they did not give information about the internal composition of the nanoparticles obtained via nanoprecipitation. It is known that a preparation of composite nanoparticles can lead to the obtainment of nanoparticles containing just one material (hence, the two types of molecules are in separated nanoparticles), to a Janus, core-shell or more complex morphology; these arrangements of the materials depend basically on the difference in the values of the two surface tensions. With fluorescence it is possible to determine the presence of both materials inside the same nanoparticles (even if this condition might not happen for all the nanoparticles obtained in the suspension) thanks to the fact that transfer energy phenomena only occur when the different species are at a distance inferior to 20 nm, i.e. inside a same nanoparticle.

Before analyzing the samples with the fluorescence technique, the UV-visible spectra of the two substances present in the nanoparticles must be analyzed. The normalized intensity curves of the suspension with just PTQ10 or ITIC-4F show 2 peaks (figure 3.33), as it is supposed to be for a water suspension of the substances; the highest peak for PTQ10 is at 605 nm and for ITIC-4F is at 736 nm. These two different wavelength values allow to determine the range of excitation and emission in the fluorescence analysis and to interpret the results. There is a perceivable difference in the intensity of the two curves, this is due to the fact that the absorptivity, the constant present in the Beer-Lambert equation, is different in the two species.

$$A = \epsilon cl$$

Beer-Lambert equation, where A is the absorbance, ϵ is the molar attenuation coefficient or absorptivity of the attenuating species, l is the optical path length in cm, c is the concentration of the species.

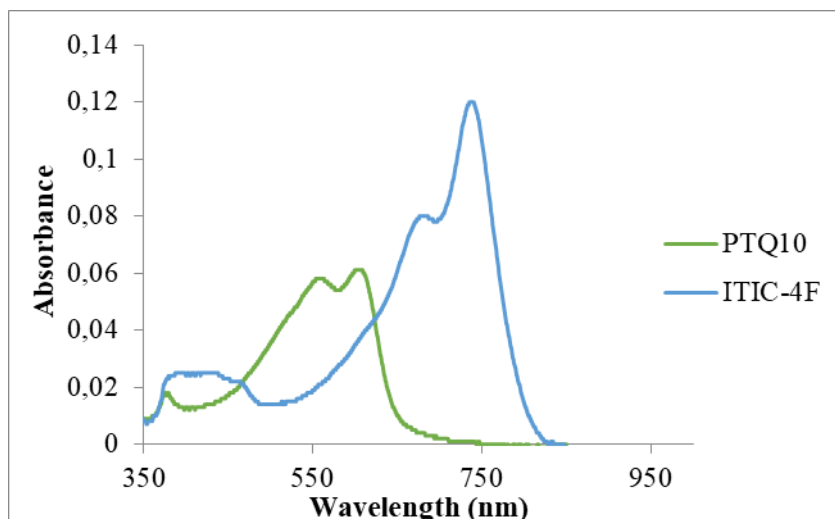


Figure 3.35: UV-visible spectra of PTQ10, ITIC-4F, 350 nm to 800 nm wavelength.

In figure 3.34 are reported the fluorescence results for suspensions containing a mix of PTQ10 or ITIC-4F nanoparticles: the nanoparticles are obtained by performing nanoprecipitation separately and then mixing the obtained suspensions with different ratios, therefore, each nanoparticle contains just one specie. In this experiment no transfer phenomena occur, because the distance between the two materials is of the order of the nanoparticle's diameter. As the presence of PTQ10 decreases, the emission curves decrease, this is because the emission of PTQ10 is prominent, while the emission of ITIC-4F is very small. The height of the curves is proportional to the ratio between the two species. However, the proportion is not exact, this is due to little imprecisions in the concentration of the two types of nanoparticles.

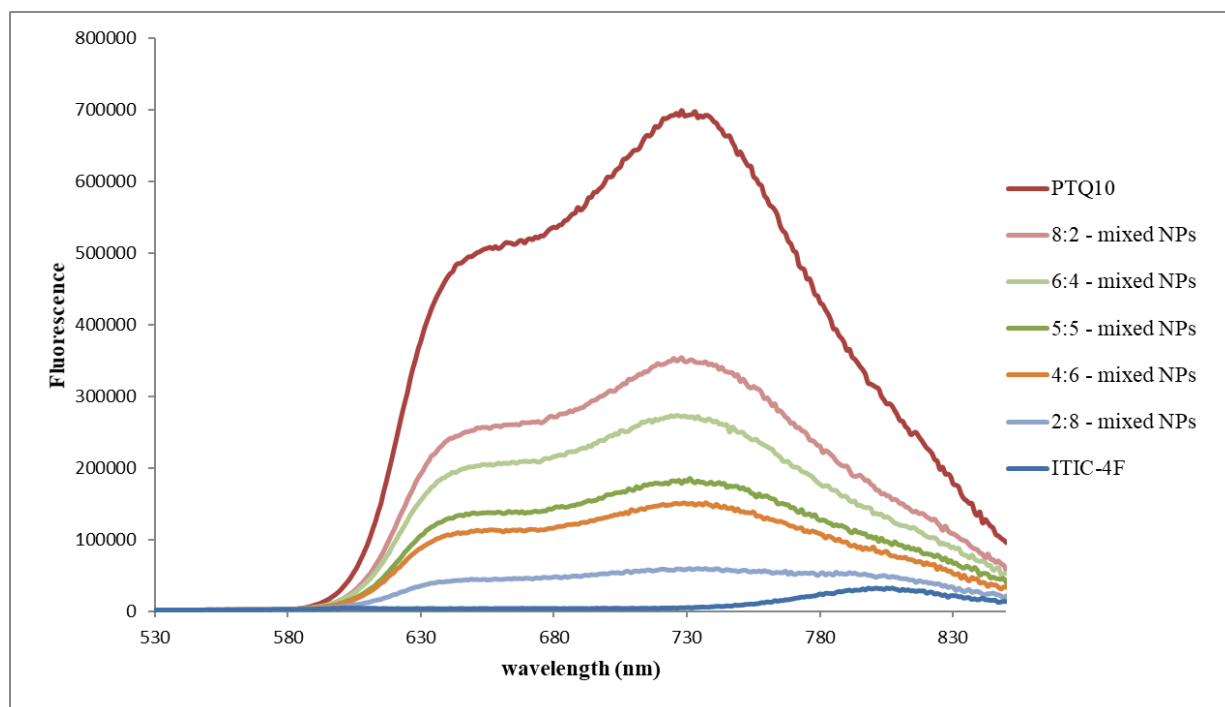


Figure 3.36: fluorescence curves. Samples are nanoparticle suspension of PTQ10 and ITIC-4F, mixed with different ratios.

In figure 3.35 it is possible to observe a much more significant quench. The peak at 730 nm, visible in pure PTQ10 nanoparticles, quenches for the curves of composite nanoparticles, these curves have a higher peak at 800 nm, because of the fact that energy is transferred to ITIC-4F, that fluoresce more, while PTQ10 fluoresce less. This is due to FRET phenomenon: energy absorbed from PTQ10 does not convert into an emission in PTQ10 wavelength range, because energy is spontaneously transferred to ITIC-4F if the two materials are sufficiently close, therefore, ITIC-4F emission is observed even when using PTQ10 excitation wavelength. This variation in the peak is enhanced as the concentration of ITIC-4F increases and the one of PTQ10 decreases.

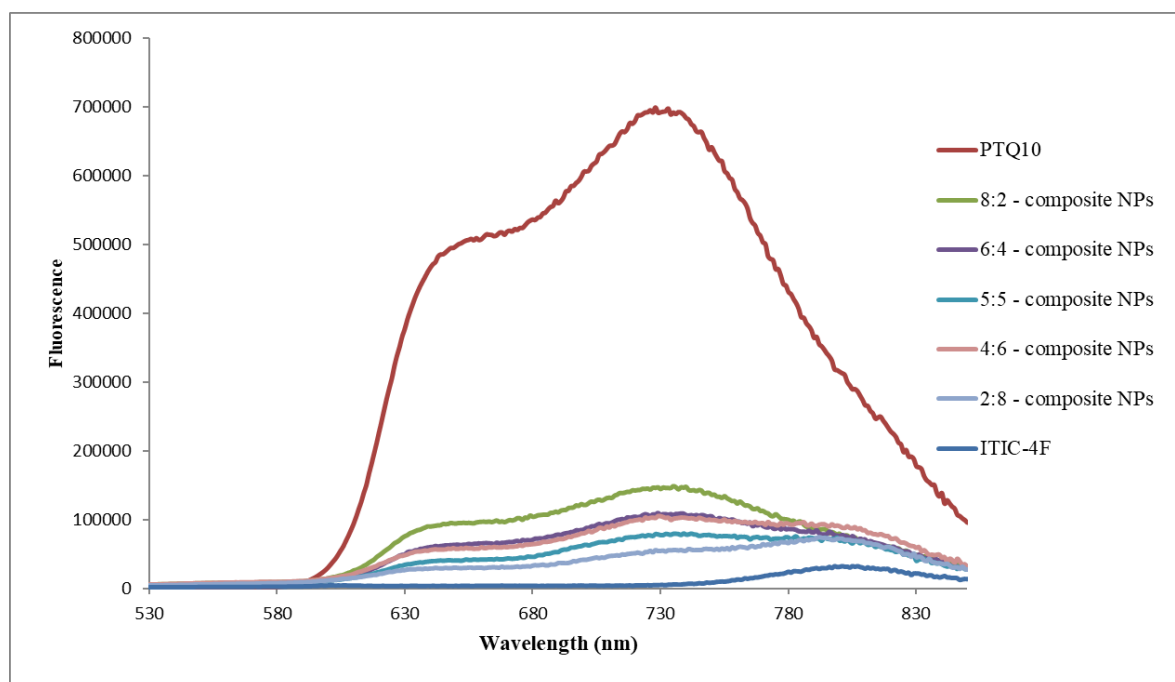


Figure 3.37: fluorescence curves. Samples are composite nanoparticle suspension of PTQ10 and ITIC-4F, obtained using different ratios of the two species.

FRET is observed to occur when there is significant spectral overlap between the donor and acceptor and a short distance between them. The efficiency is higher when the donor and acceptor are in close proximity (figure 3.36a). Acceptor emission is observed even when using the donor excitation wavelength. A larger distance between the donor and acceptor results in inefficient energy transfer (figure 3.36b), in this case, donor excitation results simply in donor emission. The donor-acceptor distance scenarios can be observed in the ratio of donor emission to acceptor emission.¹⁶

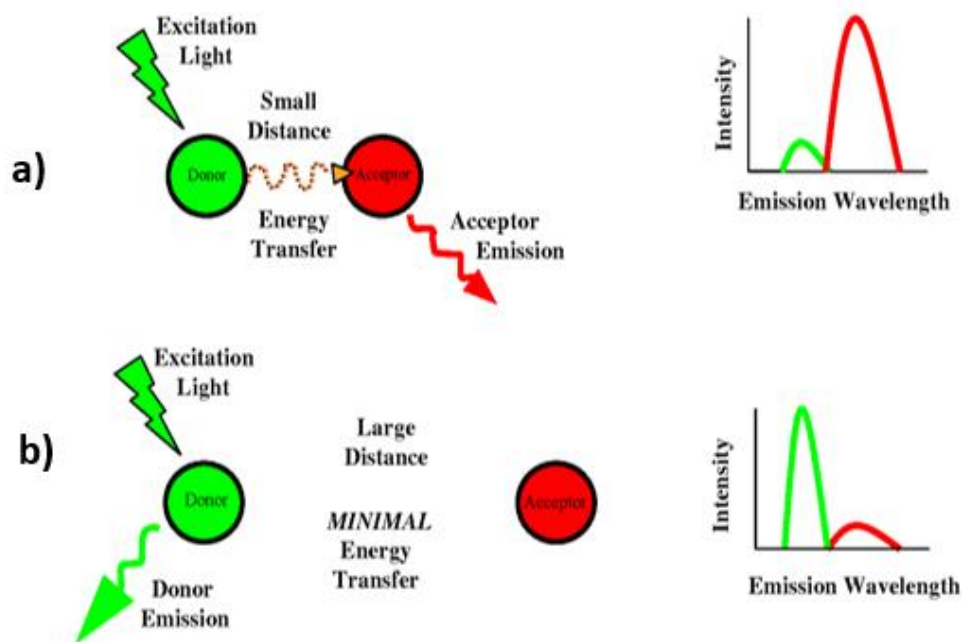


Figure 3.38: FRET effect schematization.¹⁶

3.8.Surfactant removal

Surfactant Pluronic F127 was used for nanoprecipitation and, consequently, nanoparticles in suspension are covered with surfactant molecules, which is a drawback for the preparation of the active layer. The aim is to remove it, maintaining the suspension stable, for this, a centrifugation at 0°C is performed. At this temperature the removal of Pluronic is easier for the surfactant properties. In the first experiment, suspension CC047 was transferred into centrifuge filter VIVASPIN with a polyethersulfone (PES) membrane. The sample was centrifuged at 8000 rpm, 15 minutes, at 0°C. After every step, the surface tension of the permeate was analyzed, in order to see the amount of surfactant removed in every step. The results are not satisfying; in fact, surface tension values are about 60 mN/m, far from the value of surface tension of pure water (figure 3.37). Also, in step 2 and 3 the permeate solution was slightly purple, instead of being completely transparent, which means a small amount of particles crossed the membrane.

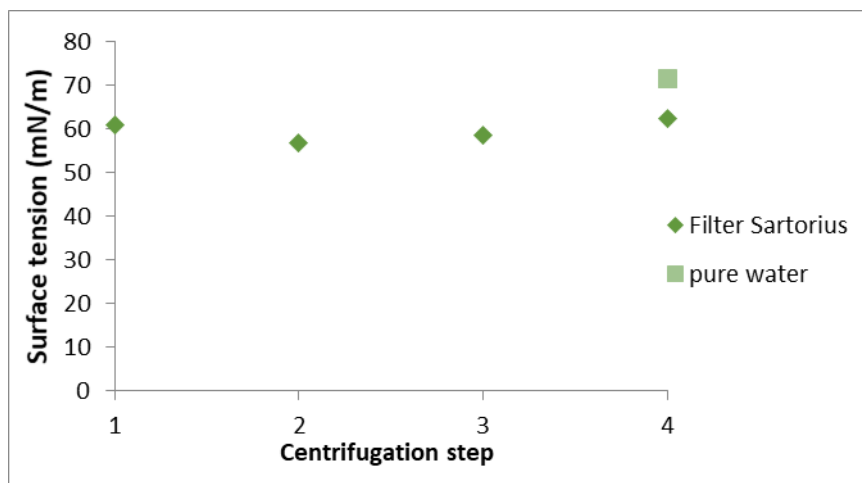


Figure 3.39: surface tension of permeate solution. Sample CC047, filter Sartorius.

The retentate was transferred to filter Amicon Ultra-15 with cellulose filter and centrifuged at 3500 rpm, 10 minutes, at 0°C. At the end of centrifugation almost all the liquid appeared to have crossed the membrane, the suspension had dried and formed solid aggregates. In this case, the centrifugation did not permit to maintain the suspension stable, but the removal of the surfactant was accomplished, as can be seen from the values of surface tension of the permeate in figure 3.38. Therefore, filter Amicon Ultra-15 will be used for the removal of surfactant.

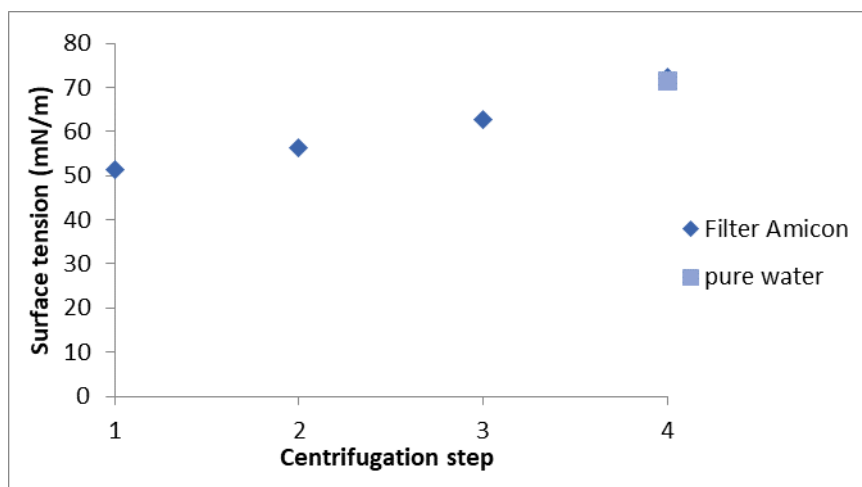


Figure 3.40: surface tension of permeate solution. Sample CC047, filter Amicon.

The experiment was repeated with suspension CC060, to corroborate the result and to find centrifugation conditions that keep the suspension stable, without formation of aggregates, and to observe the surfactant free nanoparticles at microscope. In figure 3.39 it can be seen that the removal of surfactant was completed in five centrifugations; the optimal conditions for centrifugation are: 2500 rpm, 10 minutes, 0°C, after every step 8 ml of pure water were added.

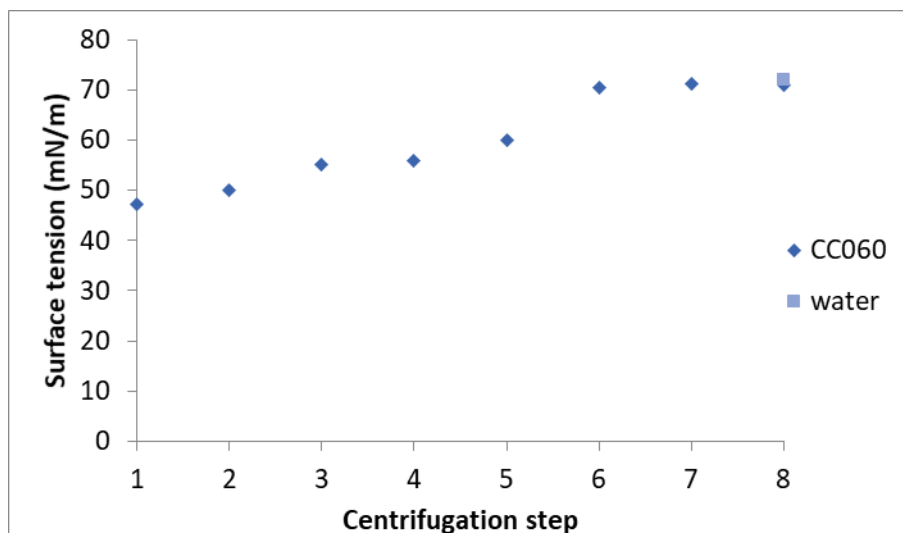


Figure 3.41: surface tension of permeate solution. Sample CC060, filter Amicon.

Table 3.18: centrifugation conditions and surface tension, sample CC060.

Centrifugation step	Rotational velocity (rpm)	Time (min)	T (°C)	Volume permeate (ml)	Surface tension (mN/m)
1	2500	10	0	5	47,21
2	2700			7,17	57,07
3	2600			8,1	55,22
4	2500			7,5	55,82
5	2500			7,6	59,93
6	2500			8	70,37
7	2500			7,6	71,28
8	2500			7,57	70,86

Finally, removal of surfactant was performed to obtain a concentrated suspension for the active layer deposition. Instead of centrifuging one sample containing 2 ml of suspension, 20 samples, totaling 40 ml, were mixed and transferred into 3 centrifuge filters, since the total content of surfactant was higher, a bigger number of centrifugations were required. Only some steps were analyzed, measuring the surface tension of the permeate (Table 3.19), after 19 centrifugations, the values approached the surface tension of pure water (72 mN/m) and the points on the graphic stopped increasing (Figure 3.33), meaning that Pluronic removal had been completed.

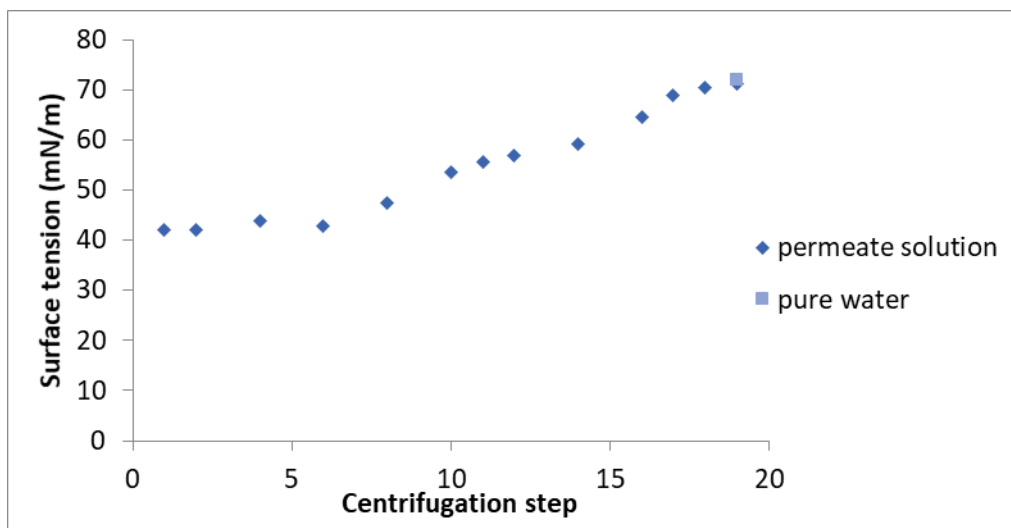


Figure 3.42: surface tension of permeate solution. Samples CC073 to CC092, filter Amicon.

3.9. Active layer thickness measurement

The layer deposition through spin-coating and the addition of Aluminum electrodes through evaporation of Al led to the obtainment of nine laboratory-scale OPV cells. The cells and their internal structure scheme are showed in figure 3.41.

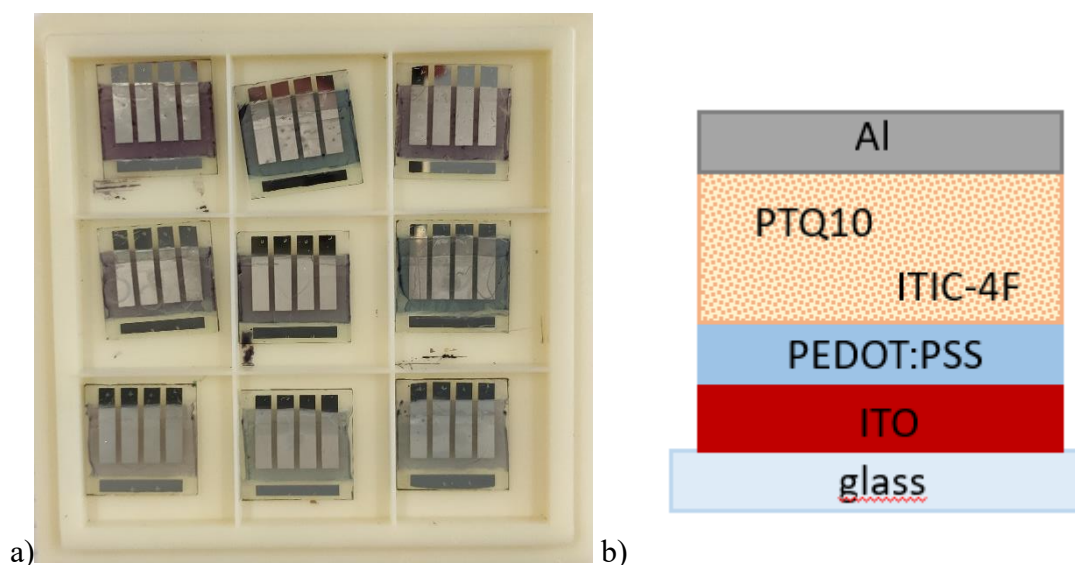


Figure 3.43: a) photo of OPV cells from PV1 to PV9. b) scheme of OPV layers.

The thickness of the nanostructured layer was measured through profilometry. In table 3.19 it is possible to compare the results of thickness for all the devices: in the central columns there are the results of the single measurements, while in the last column an average of the three measurement is shown. The average thickness of a single layer is approximately 200 nm, while the average thickness of a double layer presents values close to 400 nm, and the average thickness of a triple layer is about 600 nm. A higher thickness is correlated to a bigger capacity of electron absorption; therefore, double and triple layer devices should give better results in terms of efficiency.

Table 3.19: thickness of active layer in cells from PV1 to PV9.

Cell name	Number of layers	Annealing	Thickness 1	Thickness 2	Thickness 3	Average thickness
			(nm)			
PV1	1	100°C/10 min	279	203	196	226
PV2	1		214	226	224	235
PV3	1	100°C/10 min 130°C/10 min	156	173	159	163
PV4	2		392	401	359	384
PV5	2		380	372	355	368
PV6	2	100°C/10 min	463	452	461	459
PV7	2	100°C/10 min 130°C/10 min	405	404	424	411
PV8	2		321	332	310	321
PV9	3	100°C/10 min 130°C/10 min	582	589	566	577

In figure 3.41 it is possible to observe in detail the surface profile of the active layer of cell PV1. The peaks and the valleys are owed to some imprecisions in the deposition and aggregates in the suspension, that lead to small irregularities of the layer. In general, these irregularities are negative for the efficiency of the cell and must be avoided as much as possible. In figures 3.42 and 3.43 we can observe the profile, and thus the thickness, of the active layers of devices PV4 and PV9: the graphics show an example of double layer and triple layer thickness.

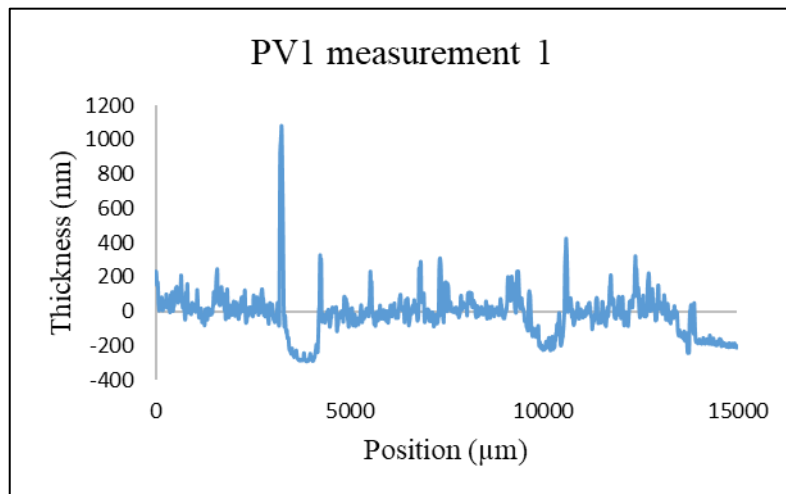


Figure 3.44: thickness measurement PV1.

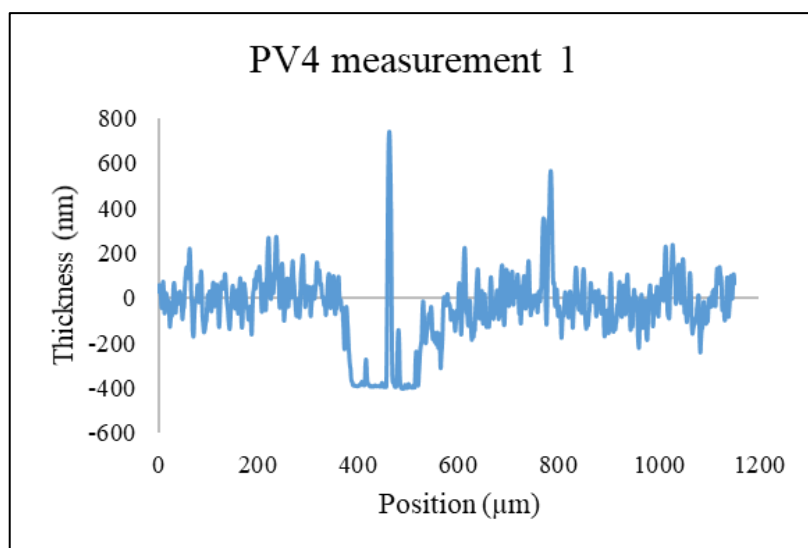


Figure 3.45: thickness measurement PV4.

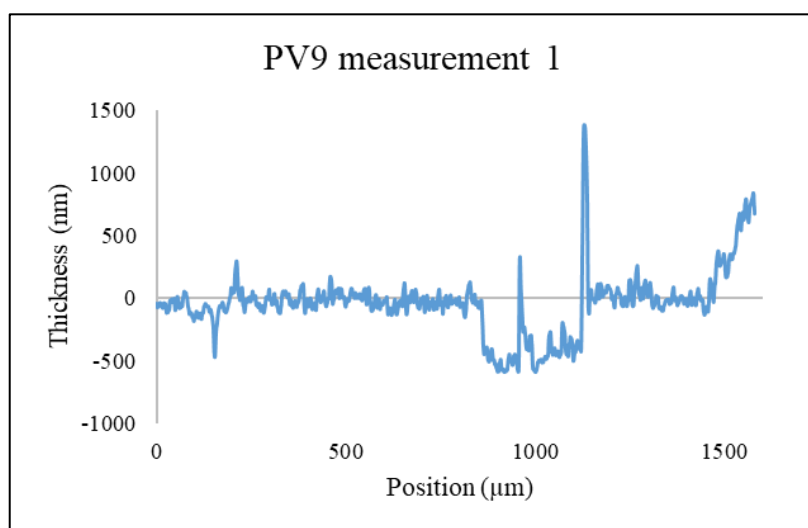


Figure 3.46: thickness measurement PV9.

3.10. OPV devices efficiency measurement

The PCE (power conversion efficiency) of the photovoltaic cells produced was measured simulating sun light in a Nitrogen protected atmosphere. Cells from PV1 to PV9 were positioned in a circuit, exposed to light with a controlled power and connected to a device measuring electric parameters. Tension (V_m), current (I_m), short circuit current density (J_{sc}), power (P_m) and efficiency were measured, all the values are reported in table 3.20. From the table it is possible to observe that efficiency tends to increase with the thickness of the active layer: the lowest efficiencies were obtained in single layer devices (PV1-PV3), while the highest efficiency refers to the triple layer device PV9. Moreover, a pre-annealing step seems to be favorable: devices PV3, PV5 and PV7 were submitted to heat at 100°C for 10 minutes before deposition of the electrodes, and they show a higher efficiency. In any case, efficiency measured in the devices has a low value, ranging from $10^{-8}\%$ to $10^{-4}\%$.

Table 3.20: OPV cells efficiency measurement, before annealing. Note that devices PV3, PV5, PV7 were pre-annealed.

Before annealing								
Device	Vm (volts)	Im (A)	Cell area (cm ²)	P light (mW/cm ²)	Jsc (mA/cm ²)	Pm (mW)	Shape factor	Efficiency(%)
PV1	8,01E-02	6,50E-05	0,12	100	1,03E-03	5,21E-09	30,85	4,34E-05
PV2	-4,58E-05	6,64E-05	0,12	100	7,43E-05	-3,04E-12	-58,50	-2,53E-08
PV3	1,00E-01	1,86E-04	0,12	100	3,07E-03	1,86E-08	20,79	1,55E-04
PV4	7,01E-02	6,42E-05	0,12	100	9,25E-04	4,50E-09	22,02	3,75E-05
PV5	9,01E-02	1,29E-04	0,12	100	3,48E-03	1,16E-08	10,52	9,67E-05
PV6	8,01E-02	1,22E-04	0,12	100	2,83E-03	9,76E-09	11,45	8,14E-05
PV7	1,10E-01	1,76E-04	0,12	100	6,34E-03	1,94E-08	7,75	1,61E-04
PV9	1,80E-01	2,43E-04	0,12	100	5,78E-03	4,38E-08	12,38	3,65E-04

After the first measurement, another annealing step was performed to the devices which presented the best efficiencies; since the pre-annealing showed a slight improvement of performance, the same conditions (100°C/10 min) were applied again to devices 1, 3, 6, 7, 9. Results are reported in table 3.21. This time, annealing did not show a positive effect, in fact, efficiencies lowered after annealing.

Table 3.21: OPV cells efficiency measurement, after first annealing.

After first annealing								
Device	Vm (volts)	I (A)	Cell area (cm ²)	P light (mW/cm ²)	Jsc (mA/cm ²)	Pm (mW)	Shape factor	Efficiency(%)
PV1	-3,97E-05	-1,02E-04	0,12	100	1,51E-03	4,048E-12	-0,6254	3,37E-08
PV3	5,01E-02	1,42E-04	0,12	100	1,37E-03	7,098E-09	43,02	5,92E-05
PV6	-1,01E-02	1,82E-03	0,12	100	1,98E-03	-1,832E-08	76,9	-1,53E-04
PV7	1,01E-02	7,31E-05	0,12	100	8,33E-05	7,363E-10	890,3	6,14E-06
PV9	-1,01E-02	1,01E-04	0,12	100	4,11E-04	-1,019E-09	74,38	-8,49E-06

A second annealing was performed to devices 3, 7, 9, this time with a temperature of 130°C for 10 minutes. Again, no improvement was perceived, as can be observed in table 3.22. In the conditions of these experiments, annealing did not bring an improvement of OPV's performance.

Table 3.22: OPV cells efficiency measurement, after second annealing.

After second annealing								
Device	Vm (volts)	Im (A)	Cell area (cm ²)	P light (mW/cm ²)	Jsc (mA/cm ²)	Pm (mW)	Shape factor	Efficiency(%)
PV3	8,01E-02	1,34E-04	0,12	100	1,68E-03	1,08E-08	29,98	8,97E-05
PV7	3,01E-02	5,28E-05	0,12	100	8,44E-05	1,59E-09	602,90	1,32E-05
PV9	-1,01E-02	7,76E-05	0,12	100	1,61E-04	-7,80E-10	101,10	-6,50E-06

Curves of current and current density as a function of the tension are reported for device PV9, which presented the highest efficiency, they are shown in figures 3.47 and 3.48.

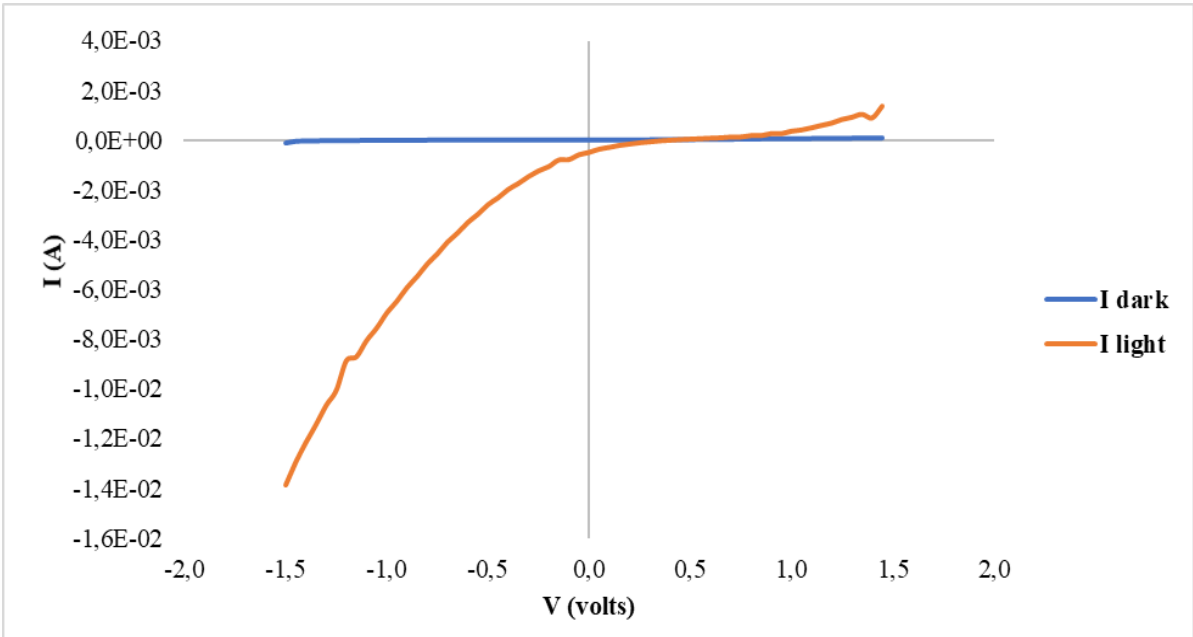


Figure 3.47: current measurement, device PV9.

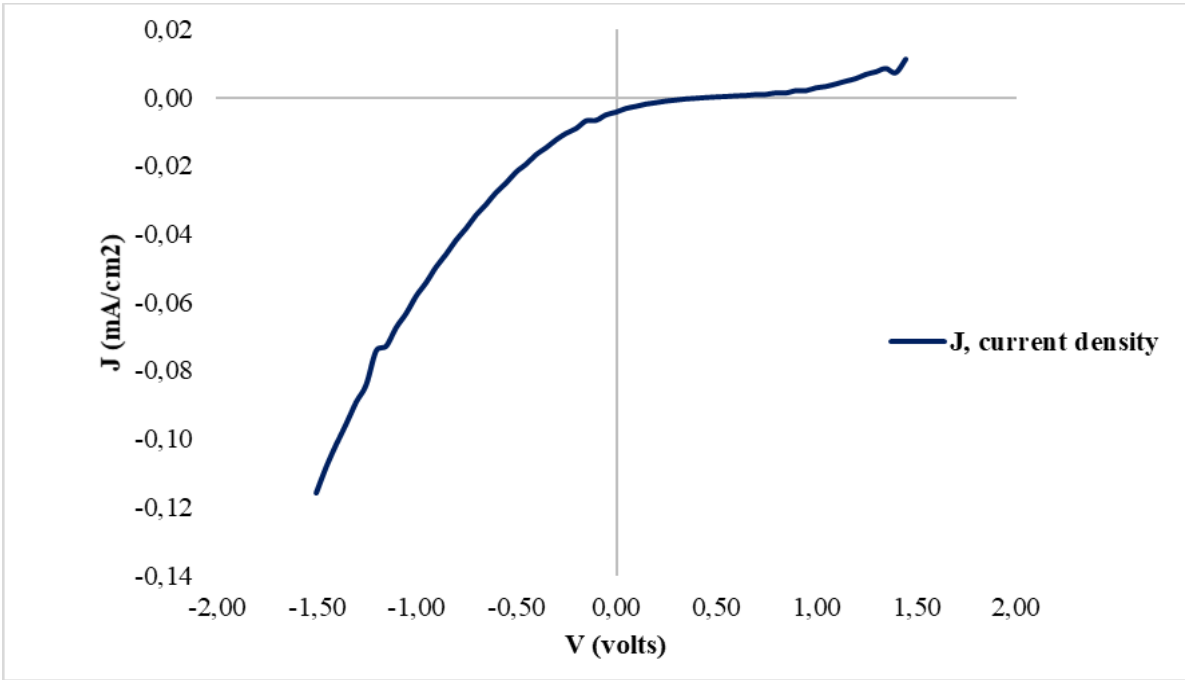


Figure 3.48: current density measurement, device PV9.

4. Conclusions

In this study, the elaboration of composite nanoparticles of PTQ10 and ITIC-4F was performed using the innovative technique of nanoprecipitation in water.

Polymer PTQ10 was synthesized using affordable materials and with a satisfactory yield, attesting the possibility of producing a promising donor polymer with a cost-effective synthesis.

Many issues were faced in the preparation of a water suspension of small particles containing PTQ10 and ITIC-4F. The procedure initially employed gave big particles, visible at naked eye and worthless for the preparation of a nanostructured layer. A big improvement was reached with the introduction of an ultrasonication step, which significantly decreased the size of the particles in suspension. Another important advance was obtained regulating the temperature at which the nanoprecipitation takes place, with a spontaneous formation of surfactant-covered nanoparticles: at the beginning high temperatures have been tested, in a second moment nanoprecipitation was attempted at ambient temperature, which gave better results in terms of particles size. Ultimately, procedure for evaporation of the solvent (THF) was examined: the employment of heat turned out to be disadvantageous for the stability of the particles, while evaporation through the blowing of an inert gas allowed the obtainment of small and stable nanoparticles.

Finally, the production of a concentrated surfactant-free suspension of composite nanoparticles was accomplished, therefore, the possibility of elaborating polymeric nanoparticles in aqueous dispersion was confirmed. The size of the particles obtained should enable the preparation of a worthwhile nanostructured active layer for OPV cells.

In conclusion, a series of OPV cells were prepared through spin-coating deposition of active layer and their efficiencies were measured. The outcome was not satisfactory as expected, as the measured efficiency is of the order of $10^{-4}\%$. A purpose for future works is the reaching of efficiencies of 1% or higher, testing different methods for the preparation of the active layer, modifying the thickness, optimizing the deposition technique, or trying to add an annealing or pre-annealing step.

5. List of abbreviations and symbols

BHJ, bulk hetero junction

CHCl₃, Chloroform

C_{mc}, critical micellization concentration

C_{mt}, critical micellization temperature

DMF, N, N-DiMethylFormamide

HOMO, Highest Occupied Molecular Orbital

ITIC-4F, 3,9-bis(2-methylene-((3-(1,1-dicyanomethylene)-6,7-difluoro)-indanone))-5,5,11,11-tetrakis(4-hexylphenyl)-dithieno[2,3-d:2',3'-d']-s-indaceno[1,2-b:5,6-b']dithiophene

ITO Indium Tin Oxide

LUMO, Lowest Unoccupied Molecular Orbital

M_n, Number-average molecular weight

M_w, Weight-average molecular weight

M_p, Peak molecular weight

NPs, nanoparticles

o-DCB, orto-dichlorobenzene

OPV, organic photovoltaic

OLED, Organic Light Emitting Diode

OSC, Organic Semiconductor

PCE, power conversion efficiency

PEDOT, Poly(3,4-EthyleneDiOxyThiophene)

PSS, PolyStyrene Sulfonate

PTQ-10, poly [(thiophene)-alt-(6,7-difluoro-2-(2-hexyldecyloxy)quinoxaline)]

SEC, Size Exclusion Chromatography

SDS, Sodium Dodecyl Sulfate

THF, TetraHydroFuran

UV-Vis, Ultra Violet-Visible

6. Bibliography

1. Sun, C. *et al.* A low cost and high performance polymer donor material for polymer solar cells. *Nat. Commun.* **9**, (2018).
2. Xie, C. *et al.* Overcoming efficiency and stability limits in water-processing nanoparticulate organic photovoltaics by minimizing microstructure defects. *Nat. Commun.* **9**, (2018).
3. Xie, C. *et al.* Robot-Based High-Throughput Engineering of Alcoholic Polymer: Fullerene Nanoparticle Inks for an Eco-Friendly Processing of Organic Solar Cells. *ACS Appl. Mater. Interfaces* **10**, 23225–23234 (2018).
4. Cui, Y. *et al.* Fine-Tuned Photoactive and Interconnection Layers for Achieving over 13% Efficiency in a Fullerene-Free Tandem Organic Solar Cell. *J. Am. Chem. Soc.* **139**, 7302–7309 (2017).
5. Rammal, M., Lévêque, P., Schlatter, G., Leclerc, N. & Hébraud, A. Recent advances in the green processing of organic photovoltaic devices from nanoparticle dispersions. *Materials Chemistry Frontiers* vol. 4 2904–2931 (2020).
6. Bardagot, O. Semi-conducteurs organiques de type n pour la conversion d' énergie N-type organic semiconductors for energy conversion. PhD thesis (2016).
7. Liu, Q. *et al.* 18% Efficiency organic solar cells. *Sci. Bull.* **65**, 272–275 (2020).
8. Zhang, Q., Kelly, M. A., Bauer, N. & You, W. The Curious Case of Fluorination of Conjugated Polymers for Solar Cells. *Acc. Chem. Res.* **50**, 2401–2409 (2017).
9. Bronstein, H. *et al.* Effect of Fluorination on the Properties of a Donor–Acceptor Copolymer for Use in Photovoltaic Cells and Transistors. *Chem. Mater.* **25**, 277–285 (2013).
10. Landfester, K. The generation of nanoparticles in miniemulsions. *Adv. Mater.* **13**, 765–768 (2001).
11. Gärtner, S. *et al.* Relating Structure to Efficiency in Surfactant-Free Polymer/Fullerene Nanoparticle-Based Organic Solar Cells. *ACS Appl. Mater. Interfaces* **9**, 42986–42995 (2017).
12. Salatin, S. *et al.* Development of a nanoprecipitation method for the entrapment of a very water soluble drug into Eudragit RL nanoparticles. *Res. Pharm. Sci.* **12**, 1–14 (2017).
13. Betancourt, T. Targetable Biodegradable Nanoparticles for Delivery of Chemotherapeutic and Imaging Agents to Ovarian Cancer. *Philosophy* (2007).
14. Bohorquez, M., Koch, C., Trygstad, T. & Pandit, N. A study of the temperature-dependent micellization of pluronic F127. *J. Colloid Interface Sci.* **216**, 34–40 (1999).
15. Li, Y. *et al.* Novel low-bandgap oligothiophene-based donor-acceptor alternating conjugated copolymers: Synthesis, properties, and photovoltaic applications. *J. Polym. Sci. Part A Polym. Chem.* **48**, 2765–2776 (2010).
16. Merckx, R. *et al.* Förster resonance energy transfer in fluorophore labeled poly(2-ethyl-2-oxazoline)s. *J. Mater. Chem. C* **8**, 14125–14137 (2020).